STREAMING POTENTIAL MEASUREMENTS IN SULFIDE RICH TAILINGS

by:
Bassam El Husseini

Department of Mining, Metals and Materials Engineering
McGill University, Montreal

October 2008

A thesis submitted to McGill University in partial fulfillment of the requirements of the degree of Doctor of Philosophy

Your file Votre référence
ISBN: 978-0-494-66646-3
Our file Notre référence
ISBN: 978-0-494-66646-3

ABSTRACT

In general, tailings dams are expected to seep. Anomalous seepage, especially when induced by internal erosion, is a major concern for owners and operators. The long established techniques for monitoring water seepage provide sparse information which may not be sufficient to detect and map the seepage path. Hence, there exists a great need for non-invasive techniques that would be sensitive to changing seepage conditions. The non-invasive nature of the techniques is particularly important because drilling and other penetrating (invasive) investigation methods are normally avoided.

Non-invasive techniques such as self-potential and high-resolution resistivity have been significantly improved in the past decade and have been successfully used for water retention dam investigation and monitoring. The main difficulty in the use of these techniques in monitoring sulfide rich tailings dams is the presence of electrochemical potentials that renders the interpretation of the acquired self-potential data difficult.

Numerical modelling is one of the latest methods in interpreting self-potential anomalies induced by liquid flow. But, in order to model streaming potentials several parameters need to be measured or estimated; (1) the hydraulic driving force and the hydraulic conductivity are required to solve for the hydraulic pressure distribution; (2) the cross-coupling conductivity distribution is needed to calculate the conduction current source parameter; and (3) the resistivity distribution is needed to determine the resulting potential distribution.

The zeta-potential and the resistivity of three pyrite rich tailings from the Abitibi region in Quebec were measured over the pH range 2 to 5 in different KCl aqueous solutions for the purpose of estimating the magnitude of electrokinetic effect induced by mine water seepage and the electrical resistivity variation induced by particle migration. The experimental and theoretical results obtained in the present study are pertinent to the interpretation of self-potential data. The zeta-potential was found to vary from -27 to -2 mV and the resistivity of the tailings was found to increase when fine particles are eroded.

RÉSUMÉ

Les barrages de résidus miniers sont généralement conçus pour fuir. Tout écoulement anormal, surtout celui relié à l'érosion interne, est une cause de soucis aux propriétaires et aux exploitants. Les méthodes usuelles d'auscultation des débits infiltrations donnent des résultats disparates et insuffisants pour détecter et définir les chemins d'écoulement. D'où la nécessité d'une méthode non-intrusive sensible aux changements du débit d'infiltration. La nécessite d'une méthode non-intrusive est particulièrement importante dû au fait que les méthodes destructives, tel que les forages, ne sont pas recommandées.

Durant les dix dernière années les méthodes non-intrusives tel que la polarisation-spontanée et les mesures de résistivité se sont grandement améliorées et elles ont été utilisées avec succès pour l'auscultation de barrage de rétention d'eau. L'utilisation de ces techniques d'auscultation pour les barrages de résidus miniers présente certaines difficultés d'interprétation, notamment dû à la présence du potentiel électrochimique.

La modélisation numérique du potentiel d'électro-filtration est une des méthodes les plus récentes pour l'interprétation des anomalies de polarisation-spontanées induites par l'écoulement. Toutefois pour modéliser le potentiel d'électro-filtration plusieurs paramètres doivent être mesurés ou estimés: (1) la force et la conductivité hydraulique sont nécessaires pour déterminer la distribution de la pression hydraulique dans le modèle; (2) le coefficient de couplage du flux est requit pour calculer la source du courant de conduction; et (3) finalement la distribution de la résistivité est requise pour obtenir la distribution du potentiel résultant.

Le potentiel zeta et la résistivité de trois rejets miniers provenant de la région de l'Abitibi ont été mesurés pour un pH variant entre 2 et 5 dans différentes solutions électrolytiques. Le but est d'estimer l'ordre de grandeur du potentiel d'électro-filtration induit par l'écoulement et la variation de la résistivité induite par la migration des particules. Les résultats expérimentaux et théoriques obtenus lors de cette étude sont pertinents pour l'interprétation des relevés de polarisation spontanée. Les résultats montrent que le potentiel zeta varie entre -27 et -2 mV et que la résistivité des rejets augmente avec la diminution du pourcentage des particules fines.

ACKNOWLEDGEMENTS

I wish to express my appreciation and sincere thanks Professor Ferri Hassani and Prof. Moe Monayez for supervising this thesis, for their helpful comments and suggestions and for the much needed financial support provided during the first few years of this research.

I also wish to express my gratitude to my fellow graduate students, to the faculty and staff of the Mining Department for their support through many hours of discussion.

I would like to thank Professor T. Van de Ven and Dr. J. Petlicki from the Pulp and Paper Research Center for allowing me to use their facilities, without which the majority of this work would have been extremely laborious.

Finally I wish to express my sincere gratitude to my parents, sisters and friends for their unlimited supply of moral support and continuous encouragement during many difficult times

TABLE OF CONTENTS

LIST OF TABLES

LIST OF FIGURES

LIST OF SYMBOLS

A	*positive sending electrode*
a	*spacing between electrodes*
A_a	*cross-sectional area*
A_c	*constant equal to 0.29 – 0.5*
a_c	*constant that depends on the type of soil*
AE	*acoustic emission*
AM	*distance between A and M*
AN	*distance between A and N*
B	*negative receiving electrode*
BM	*distance between B and M*
BN	*distance between B and N*
C	*arbitrary constant*
c_i	*number of charged particles*
C_k	*coefficient of gradation*
C_s	*streaming potential coefficient*
C_U	*uniformity coefficient*
CVI	*colloid vibration current*
CVP	*colloid vibration potential*
D_{10}	*particle diameter with 10 % finer by weight*
D_{30}	*particle diameter with 30 % finer by weight*
D_{60}	*particle diameter with 60 % finer by weight*
dL	*conductor's length*
D_R	*specific weight of the solids*
dV	*potential difference*
E	*electric field (V/m)*
e	*void ratio*
EDL	*electric double layer*
ESA	*electrokinetic sonic amplitude*
f	*resonant frequency*
g	*standard gravity (9.81 m/s^2)*
G_S	*specific gravity*
H	*Helmholtz plane*
H_h	*hydraulic head*
I	*electric current*
i	*type of charged particles*
i_{cond}	*conduction current per unit area*
i_{conv}	*convective current per unit area*
I_n	*compensation current*
I_s	*surface current*
i_{total}	*total current ($i_{total} = i_{conv} + i_{cond}$)*
J	*current density (A/m^2)*
J_i	*flow density of type i*
K	*hydraulic conductivity*

k	*intrinsic permeability*
L	*length / distance*
L_{11}	*relates the fluid flow to a pressure gradient and becomes the hydraulic conductivity (K)*
L_{12}	*cross-coupling conductivity that relate the liquid flow to a potential gradient (electro-osmosis phenomenon)*
L_{21}	*cross-coupling conductivity that relate the current flow to pressure gradient (stream-potential phenomenon)*
L_{22}	*relates the current flow to a potential gradient and becomes the bulk conductivity (σ_b)*
L_{ij}	*coupling coefficient (relating the flow of type i to a force of type j)*
m	*empirical parameter equal to two (m=2)*
M	*positive potential electrode*
m_c	*constant that depends on the type of soil*
N	*negative potential electrode*
n	*spacing factor*
n_p	*porosity*
$P_{No\ D}$	*percentage by weight at size D*
$P_{No\ d}$	*percentage by weight at size d*
Q	*fluid flux*
Q_a	*liquid flow density (volume / unit area)*
r	*distance from the electric source to electrode*
R	*resistance*
r_A	*distance from source to positive electrode*
r_B	*distance from source to negative electrode*
r_p	*pore radius*
s	*conductor's cross-section area*
S	*slipping plane*
SP	*streaming potential*
S_S	*specific surface*
t	*time*
v	*Darcy's velocity (Q/A_a)*
V	*voltage*
V_i	*instantaneous voltage*
V_l	*voltage at the lower part of ore body*
VMS	*volcanogenic massive sulphide*
V_o	*potential drop in ore body*
V_s	*streaming potential*
V_u	*voltage at the upper part of ore body*
X_i	*gradient of type j*
XRD	*X-ray diffraction*
XRF	*X-ray fluorescence*
z_i	*charge*
ΔH	*hydraulic head*
$\Delta\phi$	*electric potential gradient*
ΔP	*pressure difference / hydrodynamic pressure*

ΔV	*potential difference / potential gradient*
$\Delta\xi$	*pressure potential gradient*
α	*empirical parameter equal to one (α=1)*
ε	*dielectric constant of the fluid / permittivity of solution*
ε_0	*vacuum permittivity / dielectric constant of vacuum*
ε_r	*relative dielectric constant of the liquid*
ϕ	*fraction filled with the fluid*
η	*viscosity of the fluid*
ρ	*resistivity*
ρ_B	*electrical resistivity of saturated soil*
ρ_f	*electrical resistivity of pore fluid*
ρ_s	*density of solids*
ρ_w	*density of water / fluid*
σ	*electrical conductivity*
σ_f	*bulk conductivity of the liquid*
σ_s	*specific surface conductance*
τ	*decaying time envelope*
ζ	*zeta-potential*

CHAPTER : 1 INTRODUCTION

1.1. A GLOBAL PERSPECTIVE ON SEEPAGE INDUCED PROBLEMS IN EMBANKMENT DAMS

Embankment dams (earthfill and rockfill) and tailings dams are expected to seep. Dam designs include drainage systems to collect and discharge seepage water into the downstream channel. Sometimes seepage occurs in an unplanned manner, either exceeding the capacity of the drainage system, or along a path not considered in the design. This unplanned and excessive seepage, especially when induced by internal erosion, may threaten the structural integrity of the dam. In both cases there is a great need for a methodology to detect, measure, and map seepage paths.

Measurements in dams are carried out either for continuous monitoring or for special examinations. Different methods for the monitoring and examination of dams are reported in the literature. The different methods are classified as: (1) built-in methods (these methods measure crest, slope and internal movements, seepage water from drainage systems, and pore water pressure), (2) borehole methods (these methods measure pore water pressure using standpipes or water temperature), and (3) non-destructive methods (these methods measure mainly resistivity and self-potential).

The long established techniques of using built-in (weirs and piezometers) and borehole (piezometers) methods to monitor water seepage in embankment dams are excellent for conditions existing at the specific location of the piezometer or for measuring the total seepage from a predetermined section of the embankment dam. However, when one wants detailed information between piezometers or the location of the seepage path there are adverse factors that arise from adding new instrumentation. These include the relatively high cost for borings which are not usually recommended due to the risk of hydraulically fracturing the core; the presence of gravel, boulders or rockfill; and a lack of time. Thus there exists a need for non-destructive methods for monitoring seepage and seepage paths in embankment dams.

1.2. CHARACTERISTICS OF TAILINGS DAMS

Tailings are the residues of the milling process used to extract minerals from mined ore. Extracted minerals often represent a small percentage of the ore, so the majority of the mined materials end up as finely ground slurry. Tailings usually contain heavy metals and other substances at concentration levels that are toxic for the environment.

There are basically two types of structures used to retain tailings in surface impoundments: water-retention type dams and raised embankments.

- Water-retention type dams are constructed to their full height prior to the disposal of the tailings in the impoundment. In some cases, in order to reduce the initial investment, the construction of these structures is scheduled over the life of the mine. They are usually constructed using borrow material. Water retention type dams design and construction are similar to embankment dams used for water storage. These structures are widely used by the mining industry in Quebec (Aubertin et. al, 2002).

- Raised embankments are designed and constructed in stages over the life of the mine. They are usually constructed using a certain fraction of the tailings and mined waste rock. Construction of the raised embankments begins with a starter dike, sized for several years of mill tailings production. Consequent raises are made so as to match the elevation of rising tailings. There are three methods for the construction of raised embankments; upstream, downstream and centerline methods. They are named after the direction in which the embankment crest moves, as it is raised, with regards to the started dike.

Tailings dams are important hydraulic structures, impounding millions of tons of toxic water, mill effluents and slimes. These structures can present a considerable threat, especially in cases of improper handling and management (ICOLD 2001). Recent accidents such as Nchanga Chingola 2006 (Zambia), Bangs Lake 2005 (Mississippi, USA), Pinchi Lake 2004 (British Colombia, Canada), Reiverview 2004 (Florida, USA) and well publicised incidents like Baia Mare 2000 (Romania), Aznalcollar 1998 (Spain),

Omai 1995 (Guyana) and Stava 1985 (Italy) resulted in major environmental disasters and in some cases caused the loss of human life (WISE 2006).

Upstream tailings dams account for 58 to 67% of all tailings dams failures with 19% of these failures related to water forces such as overtopping or internal erosion (Davies 2000; data from USCOLD 1994; UNEP 1996 and WISE 2006). On the other hand, in water retention dams piping through the embankment, the foundation, or from the embankment into the foundation accounts for 30 to 50 % of all failures (Foster et al. 2000; ICOLD 1983, 1995). Hence it is important to continuously monitor the water level in the pond, the phreatic surface in the dam and the structural integrity of tailings dams especially under extreme meteorological conditions.

1.3. PARAMETER CHANGES INDUCED BY INTERNAL EROSION

Internal erosion or piping refers to a process in which fine particles are transported away from the core, the embankment or the foundation. This process results in an increase in seepage flow and an expansion of the seepage area. Piping is defined as a progressive backward erosion; (1) a seepage channel is initiated at the downstream interface of the affected area (for example between the core and the downstream filter or the foundation and the downstream shell), and (2) erosion progresses in the opposite direction of the seepage flow. Particle migration is mainly controlled by colloidal, hydrodynamic and geometric conditions. In the absence of adequate downstream filters (Terzaghi 1922; Vaughan & Soares 1982; Sherard et al. 1984 a, b; Sherard & Dunnigan 1985; Kenny et al. 1985; Kenny & Lau 1985; USBR 1994; USSCS 1994; ICOLD 1994) fine particles (usually clay and silt fractions) begin to migrate with the flow when the hydraulic gradient or the flow velocity exceeds a certain threshold (Bartsh 1995). Eventually, the continuous loss of fines leads to the collapse of the soil structure and material from above or upstream replaces the lost material. This process results in the formation of sinkholes at the surface. Such problems have been documented and examined at the WAC Bennett Dam in British Colombia (Stewart 2000). In the worst case scenario, seepage may result in the creation of a direct channel connecting the reservoir to the downstream face. Just such problem has been documented and examined following the failure of the Omai Tailings Dam (Vick 1996, 1997; Haile 1997).

The early development of piping in dams is a complex process about which little is known, and the process of particle migration is slow and can go on for a long period of time before it is detected or the consequences are observable (Johansson, 1997). Upon discovery, the impact on the function of the dam may already be severe. Standard monitoring systems can only observe the phenomenon in its final stages. For example, seepage collection and measuring systems show an increase in leakage combined with murky water followed by a sudden decrease in leakage. Such events are interpreted as an internal erosion phenomenon followed by self-healing of the embankment (Sherard 1989; Reddi 2004; Kakuturu & Reddi 2006 a, b). The occurrence of sinkholes induced by the cycle of internal erosion and self-healing reaching the surface may take years. It is

important to note that the appearance of sinkholes in embankments is not always associated with internal erosion (Boncompain 1989).

Internal erosion affects a limited number of non-intrusively measurable parameters such as density, seepage rate, hydraulic conductivity, temperature, seismic velocity, dielectricity and resistivity. The relative sensitivity of these parameters to changes in the porosity (internal erosion results in a increase in porosity due to the loss of fine particles) were initially studied by Johansson et al. (1997). They concluded (Figure 1-1) that the material dependent parameters (density and dielectricity) are less sensitive to changes in porosity than flow dependent parameters (hydraulic conductivity and temperature), and that accuracy and resolution should also be considered when evaluating the potential of a method since sensitivity alone is insufficient to evaluate the potential properly.

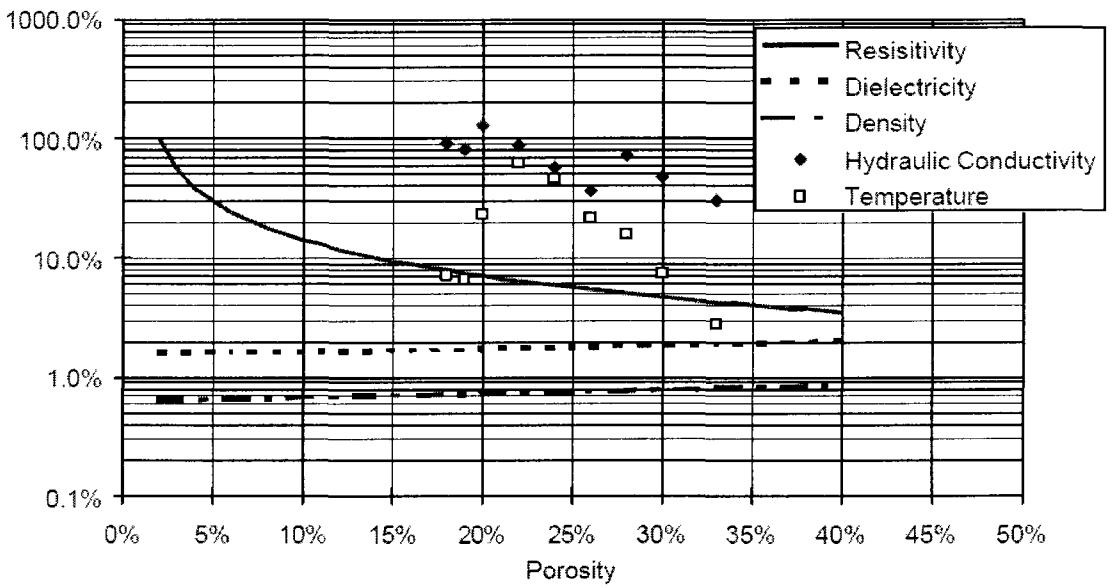

Figure 1-1: Relative change of various parameters with changes in porosity. (After Johansson 1997)

1.4. APPLICATION OF SELF-POTENTIAL AND RESISTIVITY METHODS TO SEEPAGE MAPPING AND MONITORING

Self-potential and resistivity are two electrical geophysical techniques used to map and monitor seepage in embankment dams. It is important to point out that self-potential, or more precisely the streaming potential phenomenon, is the only geophysical method that responds directly to seepage flow.

When submerged in a liquid, most particles develop an electrical double layer, with negative ions bound to the surface of the particles. The liquid layer (charged with positive ions) surrounding each particle is divided in two parts; an inner region (or Stern layer) where the ions are strongly bound to the particle and an outer (or diffuse) region where they are less firmly associated. Within the diffuse region there is a theoretical boundary known as the slipping plane, which constitutes the boundary between the stationary phase (closest to the particle) and the mobile liquid phase. The potential at this boundary is known as the zeta-potential. Details of the formation and properties of the electric double layer are given in chapter 3 and in many references such as MacInnes (1961), Mitchel (1976), Morgan (1989), and Morgan et al. (1989).

The self-potential method measures changes in the electrical potential induced by the fluid flow through the porous medium. Figure 1-2 illustrates a conceptual model of the streaming current and conduction current paths in the dam body and soil structure. The height difference between the pond water level and the exit point (downstream) of the seepage channel is the hydraulic potential that drives the fluid through. The flow carries with it excess positive charges from the diffuse portion of the electric double layer, creating an electric streaming current through the seepage channel. The electric potential difference created by the accumulation of positive charges downstream in turn drives a conduction current back through the seepage channel, the dam body and the fluid body based on their respective resistivity. Therefore, the conduction current is measurable at any point within the embankment using the self-potential method.

The Helmholtz-Smoluchowski equation (Eq. 1-1) gives the relationship between the pressure gradient driving the flow and the streaming potential. This relationship is

further explained in chapter 3. From the Helmholtz-Smoluchowski equation, it is obvious that the streaming potential current is directly proportional to the electrical resistivity of the pore fluid and the pressure difference driving the flow. Hence the importance of conducting resistivity surveys as part of a self-potential field investigation.

$$\Delta V = \left(\frac{\rho \varepsilon \zeta}{4 \pi \eta} \right) . \Delta P = C_s . \Delta P \qquad \textbf{(Eq. 1-1)}$$

where:

ΔV	:	*streaming potential*
ρ_f	:	*electrical resistivity of pore fluid*
ε	:	*dielectric constant of the pore fluid*
ζ	:	*zeta-potential*
η	:	*viscosity of pore fluid*
ΔP	:	*pressure difference driving the seepage flow*
C_S	:	*streaming potential cross-coupling coefficient*

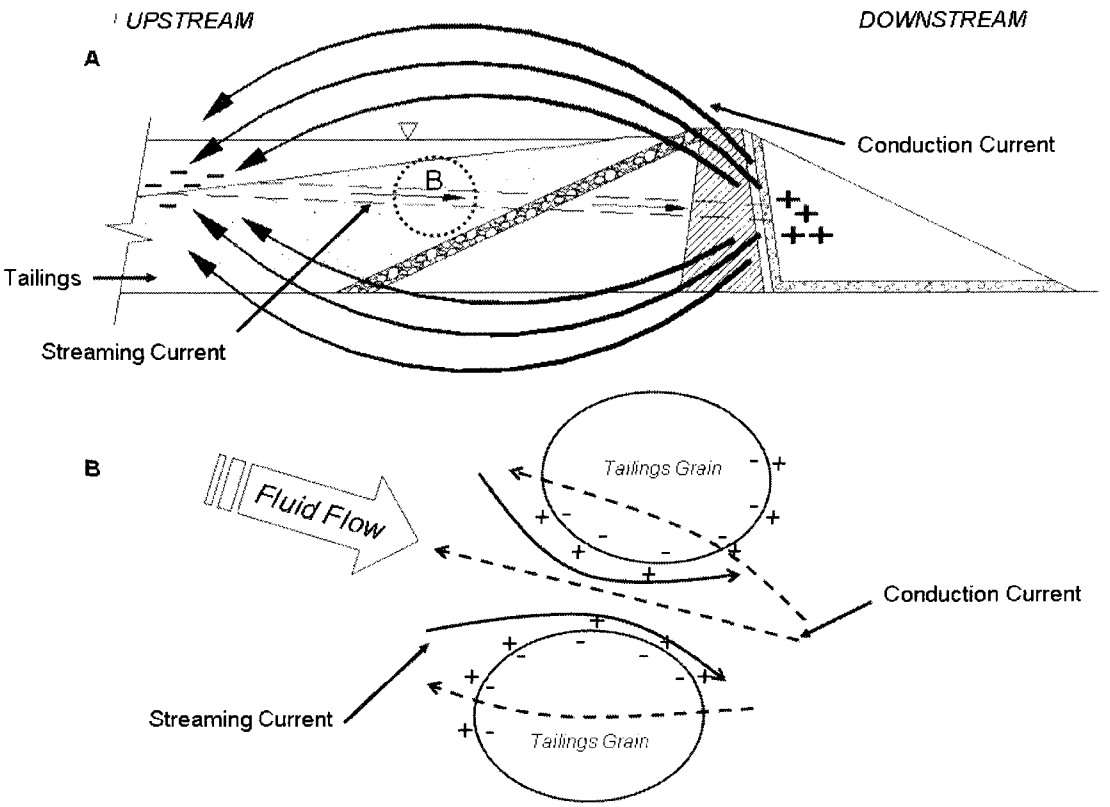

Figure 1-2: Schematic representation of fluid flow through a seepage zone in a dam structure (example of a water retention type dam).

1.5. PROBLEM DEFINITION

The methods presented in this research are the self-potential (SP) and resistivity methods. The fact that water flowing through a porous medium induces an electrical field has been known for a while. Such evidence has been observed in the vicinity of dams, reservoirs or lakes, or in different geologic settings such as volcanoes, and tectonically active or geothermal and karst areas. On the other hand, a quantitative relationship between the flow and the electric field is usually assumed rather than observed because detailed measurements of the electric and hydraulic parameters are rarely available.

The self-potential (SP) is generated by a number of processes. In field situations, SP may arise from: (i) sedimentation potential (ii) electrochemical potential, or (iii) streaming or electrofiltation potential. SP anomalies are often assumed to result primarily from streaming potential because sedimentation and electrochemical potentials are supposed to be considerably smaller than the electrofiltration potential and in some cases non existent, which may not be true in the case of sulfide rich tailings.

Tailings are usually transported to the impoundment site in a slurry form and they are discharged either by spigotting, single point discharge or by cycloning. In either case the coarse particles will settle on the beach near the discharge point while the fines will settle in the pond. The sedimentation potential induced by the settlement of the fine particles in the pond is an important source when measuring SP anomalies in the vicinity of tailings facilities.

The sulfide rich tailings are known to oxidise in the presence of oxygen and water. The rate of oxidation is affected among others by the oxygen content, chemistry, pH, and temperature of the pond water. The electrochemical potential induced by the oxidation of the tailings is an additional source of noise when measuring SP anomalies in the vicinity of tailings facilities.

The differential motion between the fluid and the solid, in a saturated porous medium, induces electrokinetic phenomena or in other words a streaming potential. The

streaming potential induced by water seepage may be an additional source when measuring SP anomalies in the vicinity of tailings facilities.

In order to interpret the SP anomalies in tailings dams the origin of the potential has to be understood. The anomaly could be due to one or a combination of the potentials mentioned previously. The streaming, electrochemical and sedimentation potential depend on the in-situ conditions in the tailings pond; they are strongly affected by temperature, pH and the age of the tailings.

1.6. SCOPE AND OBJECTIVES

The present research was instigated by a lack of information on the cross-coupling parameter associating the hydraulic gradient within the tailings dam to the electrical current flow. The primary objectives of this research are to:

- develop a clear understanding of the streaming potential in sulfide rich tailings and to further the knowledge of the influence of the tailings' geophysical parameters and fluid properties on the cross-coupling coefficient (Figure 1-3);
- estimate the magnitude of the zeta-potential induced by water flow through sulfide rich tailings;
- determine the variation of the zeta-potential with respect to the pH and conductivity of the pond water; and
- study the effect of loss of fine particles on the resistivity of the sulfide rich tailings.

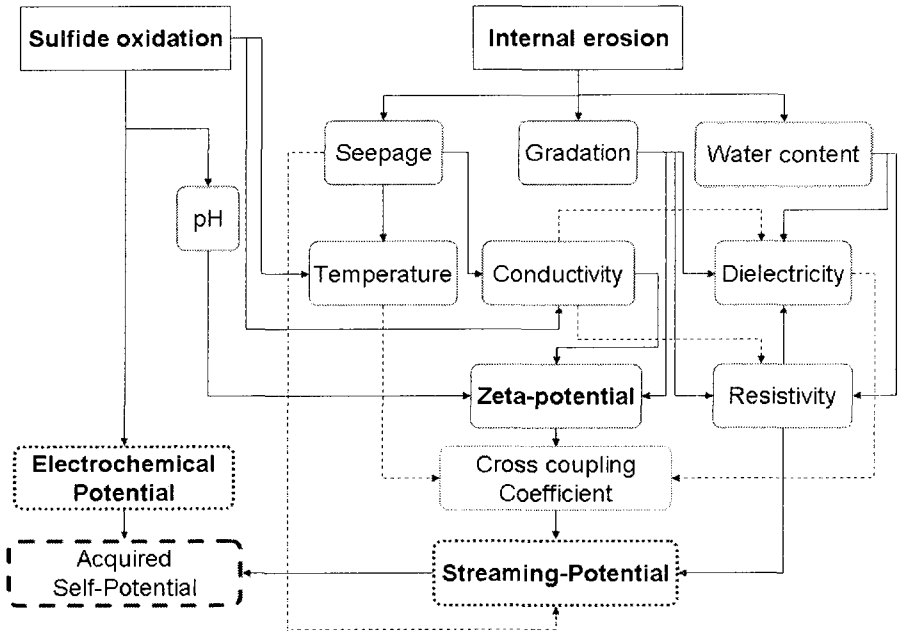

Figure 1-3: Sulfide oxidation and internal erosion's major influences on the zeta-potential and resistivity.

1.7. METHODOLOGY

In order to fulfill the objectives of the present research and to determine the relationship between the streaming potential in sulfide rich tailings and seepage induced by particle migration, a comprehensive and fundamental experimental study is performed.

To achieve this understanding, the effect of tailings chemistry and the loss of fines on resistivity and SP readings need to be investigated. Chemical reactions within the tailings induce an additional effect to the electric potential created during the transport of charged particles in a fluid rendering the SP data un-exploitable in the absence of a baseline reference.

The main parameters that influence resistivity and SP readings are the tailings resistivity and zeta-potential changes due to the loss of fine particles. In turn, pH and electrolyte concentration in the fluid affect both the resistivity and zeta-potential.

To understand these complex relationships, a testing program is designed, for three representative sulfide rich tailings from three different base metal mines from the Abitibi region in Quebec, to determine the magnitude and variation of the resistivity induced by the loss of fine particles and the zeta-potential's dependence on pH and electrolyte concentration variations. The following steps are carried out in the laboratory investigation:

1. *Tailings characterisation*: The following physical and mineralogical tests are carried out on the three tailings samples, to ensure a statistically representative result each test is repeated at least three time (with the exception of SEM and petrographic analysis) :
   - Particle size analysis: the particle size distribution is determined by sieving for coarse fraction of the tailings while the gradation of the fine fraction is determined using a Cyclosizer (Warman International) and a light scattering particle size analyser (Horiba LA-920);

- Specific gravity: the specific gravity is determined according to the ASTM D854-06 standard;
- Particle shape and surface texture: the particle shape and surface texture are determined using SEM (scanning electron microscopy) photographs;
- Petrographic analysis: detailed mineralogical composition of the tailings is determined using petrographic microscopy on polished thin sections;
- X-Ray fluorescence: elemental composition of the tailings;
- X-Ray diffraction: the mineralogical composition of the tailings is validated using the XRD technique with a semi-quantitative analysis.

2. *Resistivity testing:* The electrical resistivity is determined using a laboratory built apparatus. Using this apparatus the electrical resistivity variations with the loss of fine particles (particles less than 0.075 mm) is measured as a function of different concentrations (10^{-3}, 10^{-2} and 10^{-1} mol/l) of KCl aqueous solutions, Table 1-1 lists the experiments used to measure the resistivity variation. To ensure a statistically representative result each test is repeated at least three times.

Table 1-1: Outline of resistivity testing experimental program.

Electrolyte Concentration	**Particle size distribution**		
	Full Gradation	Particles retained on 0.075 mm	Particles Passing 0.075 mm
DIW*	LA+ Mine Tailings LV+ Mine Tailings BH+ Mine Tailings		
KCL 10^{-1} mol/l			
KCL 10^{-2} mol/l			
KCL 10^{-3} mol/l			

* Deionised water
\+ LA, LV and BH are the acronym for the different mines

3. *Zeta-potential measurements*: Due to the fine gradation of the tailings and the resulting low permeability, the ζ-potential is determined using two different methods: *(i)* streaming potential; and *(ii)* electroacoustic spectroscopy. Using these methods the ζ-potentials variations with pH of the electrolyte solution (within a pH range of 2–5) is measured as a function of different concentrations (10^{-3}, 10^{-2} and 10^{-1} mol/l) of KCl aqueous solutions. Table 1-2 lists the experiments used to measure the zeta-potential variation with pH and electrolyte concentration. To ensure statistically representative results each test is repeated at least three times, it is important to note that the result of each test is an average of ten potential measurements.

Table 1-2: Outline of zeta-potential measurements experimental program.

Electrolyte Concentration	**Streaming Potential (SP)**				**Electroacoustic Spectroscopy (CVI)**			
	pH				pH			
	2	3	4	5	2	3	4	5
KCL 10^{-1} mol/l	LA^{+} Mine Tailings LV^{+} Mine Tailings BH^{+} Mine Tailings							
KCL 10^{-2} mol/l								
KCL 10^{-3} mol/l								
$^{+}$ LA, LV and BH are the acronym for the different mines								

CHAPTER : 2 NON-INTRUSIVE METHODS FOR SEEPAGE DETECTION, MAPPING AND MONITORING IN EMBANKMENT DAMS

2.1. INTRODUCTION

Embankment dams, for example earthfill, rockfill, as well as tailings dams, are expected to seep. Dam designs include drainage systems to collect and discharge seepage water into the downstream channel. Sometimes seepage occurs in an unplanned manner, either by exceeding the capacity of the drainage system or along a seepage path not considered in the seepage design. This unplanned and excessive seepage may threaten the structural integrity of the dam causing internal erosion which is one of the major causes of dam failures (Foster et al. 2000a and b).

Different methods for monitoring water seepage in embankment dams are reported in the literature, these methods are classified as built-in, borehole and non-intrusive methods. The built-in (weirs and piezometers) and borehole (piezometers or observation wells) methods provide a sparse sampling of the subsurface hydrogeologic conditions. In many cases, these methods provide insufficient data for the detection and mapping of internal erosion problems. The proximity of the standard instrumentation (piezometers or observation wells) to the eroded zone determines their sensitivity to changing seepage conditions. Increased seepage induced by erosion problems may be detected and measured at the drainage collection weirs, but this information does not give any indication on the source or seepage path.

Geophysical methods were primarily developed for resource exploration. Their use in geotechnical and hydrogeological investigations has increased significantly in recent years. These methods are either used at the surface or down the hole in existing observation wells. A number of the employed geophysical methods are sensitive to changes in soil and fluid properties. These non-intrusive methods play an important role in detecting, mapping and monitoring the changes in seepage with time. To generate a

more comprehensive image of the subsurface, the information gathered by geophysical methods should be used in conjunction with standard monitoring methods.

There exist a limited number of non-intrusive methods for the detection, mapping and monitoring of seepage in embankment dams. These methods are mainly acoustic emission, temperature, resistivity, and self-potential measurements. The results of numerous research projects (Johansson 2007) indicate that for internal erosion detection, flow dependent methods are more sensitive than material dependent parameters. A comprehensive study done Johansson et al. in 1995 concluded that of all possible non-destructive methods, temperature, resistivity and self-potential are the most suitable for the study of seepage and the resulting internal erosion. Never-the-less, all of these methods have been used with relative success in detecting anomalous seepage through embankment dams. A review of these different methods with an emphasis on the self-potential method is presented below.

2.2. ACOUSTIC EMISSION MONITORING

The use and detection of sound or noise to assess material stability was first employed in the mining industry in the early 1930s. Researchers from the US and Canada studied the instability of mine roof, face and rock pillar in order to predict failure. They referred to the acquired sounds as "microseismic activity" and the individual noises as "microseisms" (Koerner 1976). A total change in application area occurred in the 1950s with the monitoring of sounds produced in metals. The initial studies in metals (steel, copper, aluminum, lead and zinc) were done by Kaiser (Kaiser 1950), who named the technique "acoustic emission" monitoring. The acoustic range is 20Hz to 20 000 Hz. In the past two decades there have been no publications on the use of acoustic emission monitoring of seepage.

Several attempts by the author using state of the art hydrophones, signal amplifiers and signal processing techniques to measure the acoustic emissions induced by clear and turbid water flow in coarse and fine grained soils and in different laboratory controlled setups resulted in failure. The major problems encountered were the amount of noise acquired with the signal which rendered the data un-exploitable and the repeatability of the results. The major portion of the noise turned out to be induced by high voltage cables running through the test area, this problem was resolved by placing the complete test setup within a grounded Faraday cage. The following brief review of the AE principles and their use for seepage monitoring is presented for completion.

2.2.1. PRINCIPLES OF ACOUSTIC EMISSION

Acoustic emission (AE) can be defined as an acoustic wave generated by a material when subjected to an external stimulus. The basic difference between acoustic emission and ultrasonics, is that acoustic emission is generated within the material itself, whereas in ultrasonics the wave is generated by a transducer and introduced into the material. In AE the operator has no control over the wave generating mechanism but can only subject the material to conditions which will induce AE.

AE signals have been classified into different types; the (a) continuous type and (b) the bust type. The difference between these two different types resides in the average repetition rate. Above a certain value the length of the bursts exceeds the time interval between them; this results in the superimposition of different bursts giving the appearance of a continuous emission (Raj and Jha 1994).

2.2.1.1 Acoustic wave

The only link between the source and the AE signal received by the transducer is the acoustic wave. The majority of the complexity in the signals is generated as the wave travels through the medium. In order to understand the AE signal, knowledge of the acoustic wave is required (Beatti 1983). The AE wave form of a resonant transducer is most appropriately modeled as a decaying sinusoidal wave:

$$V = V_i.\sin(2\pi ft).\exp\left(-t/\tau\right) \qquad \textbf{(Eq. 2-1)}$$

where V is the resultant voltage, t is time, V_i is the instantaneous voltage, f is the resonant frequency and τ is the decaying time envelope.

2.2.1.2 Acquisition and signal processing

The transducer is a device which generates an electrical signal when it is stimulated by acoustic emission waves. Most transducers used in AE systems are piezoelectric crystals and have been developed for high sensitivity at frequencies in the range of 1 Hz – 2 MHz. The transducer is the most critical component of any acoustic emission system. If any meaningful source characterisation is to be carried out, the response of this device should be extremely satisfactory.

The basic idea behind acoustic emission signal processing is to extract relevant information and to gain some information about the nature and location of the source. Signal processing is a perennial problem of AE research. The arrival of powerful acquisition hardware and analysis software introduced a number of activities that resulted in a flurry of tools that permit effective and efficient extraction of information from the

AE signal. Nevertheless, one of the major factors limiting our ability to extract information from AE signals is the adverse effect of noise, which in some cases could be reduced by the use of signal enhancement techniques.

2.2.2. ACOUSTIC EMISSION MONITORING OF SEEPAGE

2.2.2.1 Laboratory testing

As discussed in the introduction, internal erosion and piping are a significant cause of failure and accidents affecting embankment dams. In order to simulate this phenomenon in the laboratory, both clear and turbid water were passed through a column of soil at various flow rates (Koerner et al. 1981). A hydrophone inserted in the soil column (Figure 2-1) acquired the acoustic wave. In the case of clear water, flow rates of approximately 45 ml/s are required for acoustic emission detection (the hydrophone sensitivity used is 10.5 V/psi or). For turbid water, the minimum detectable flow rate is approximately 10 ml/s (using the same hydrophone). The acoustic emission behaviour appeared to increase exponentially as a function of flow rate (Figure 2-1).

2.2.2.2 Field testing

Acoustic emission monitoring has been used to monitor a limited number of small embankment dams (five in total). The available data on most of these tests is very scarce. A selected case history of acoustic emission monitoring is presented below.

Seepage Monitoring Within Cased Borings – A seepage problem under a small earth dam of 3.6m height and approximately 370m length was detected (Koerner 1976). A series of borings were made along the axis of the dam and flow rate tests were done. The results indicated that the section between borings B3 and B4 seems most likely to be the area of concern (Figure 2-2).

Since borings were accessible and acceptable for this embankment dam, acoustic emission monitoring was also attempted. The plastic casing used in the borings could not

conduct emissions and therefore was not suitable as a wave-guide. As an alternative, a heavy steel cable was inserted down the hole to the bottom where seepage was most probably occurring. Acoustic emission count rates were recorded, and the AE counts per minute are plotted on Figure 2-2. The obvious correlation between seepage and AE counts per minute in the B3 – B4 zone is to be noted. The actual mechanism causing the emissions is not known. Koerner (1976) assumed that the emissions could be due to the erratic flow of water against and around the casing.

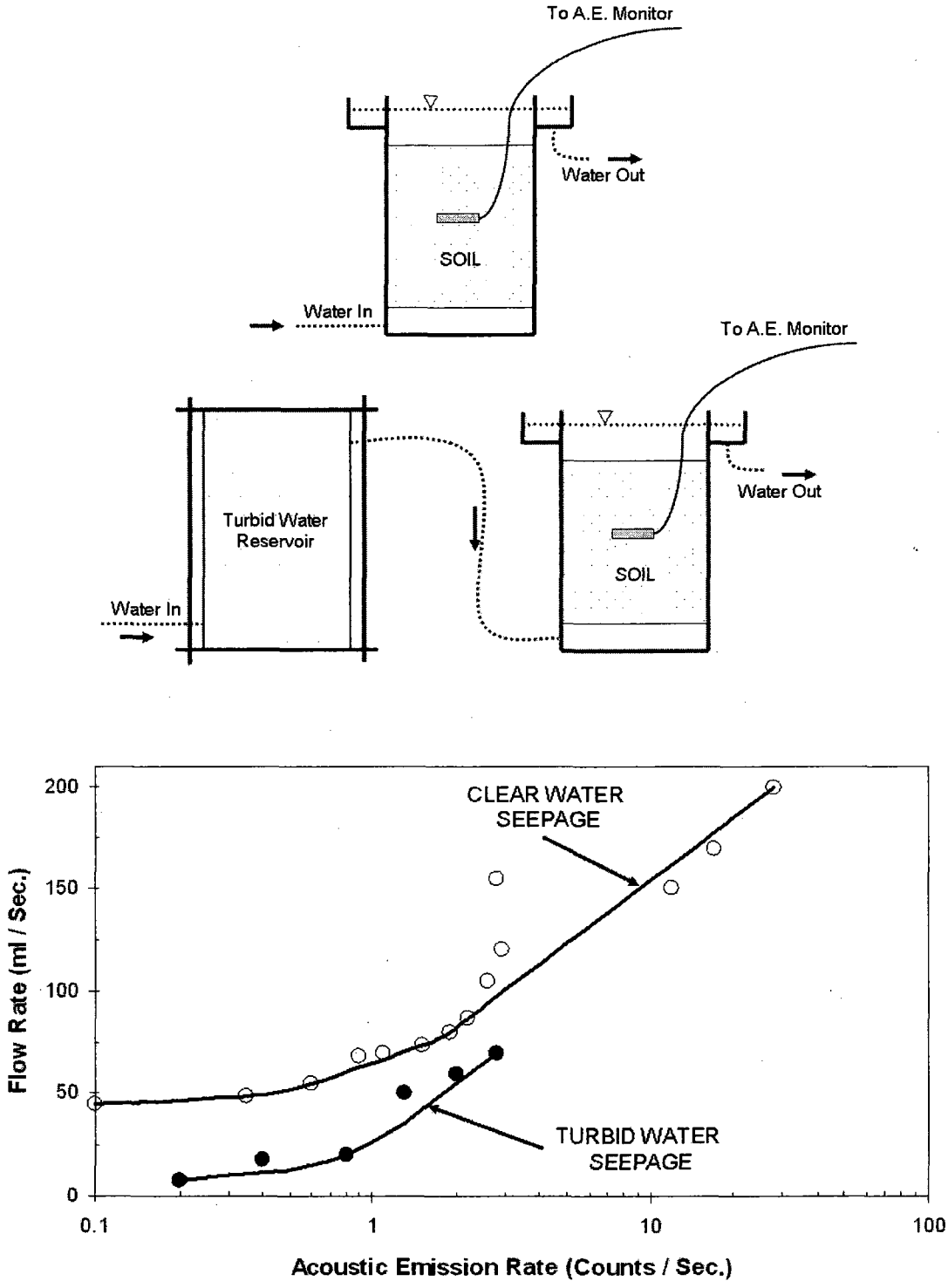

Figure 2-1: Schematic diagram of clear and turbid water seepage test and resulting flow versus AE rate (After Koerner 1981).

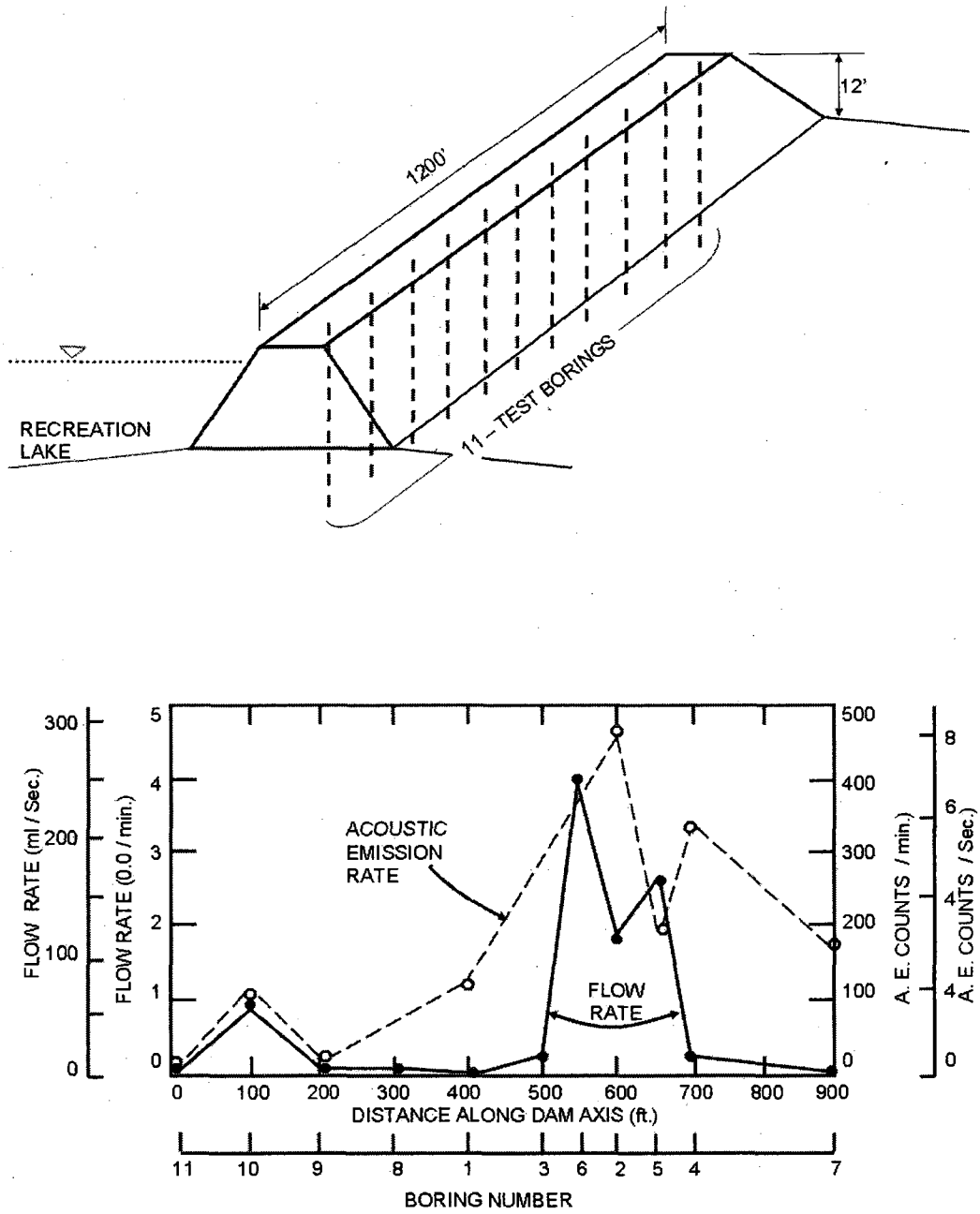

Figure 2-2: Results of seepage study using AE and flow rate measurements (After Koerner 1976).

2.3. SELF-POTENTIAL MEASUREMENTS

Streaming potential measurements along a seepage flow path generate an electric flow in the ground that produces self-potential (SP) variations at the surface. The self-potential or more precisely the streaming potential phenomena is the only geophysical (non-intrusive) method that responds directly to seepage flow. Other non-intrusive methods respond to secondary physical property changes associated with particle migration or changes in seepage conditions (porosity, density, temperature, degree of saturation, ...). The methods used to calculate the induced SP variations were discussed by Nourbehecht (1963), Sill (1983), Wurmstich and Morgan (1994), Sasitharan et al. (2001), and Sheffer and Howie (2001) and are further examined in chapter 3.

Usually, negative SP values are acquired above areas of seepage inflow (the upstream portion of a subsurface flow path) while positive SP values are acquired above areas of seepage outflow (the downstream portion of a subsurface flow path) (Bogoslovsky and Ogilvy 1970b). Typical SP patterns associated with different anomalies are shown in Figure 2-3. Examples of SP measurements conducted under controller conditions at model dams are given by Sasitharan et al. (2001), Armbruster et al. (1989), Wurmstich (1995) and Wurmstich et al. (1991). Examples of SP survey results at embankment dam sites are presented in Wilt and Corwin (1989), Corwin (1989), Corwin (1990a), and Bogoslovsky and Ogilvy (1970a, 1970b, 1973).

The self-potential method is based on measuring the naturally occurring electrical potentials that are present between any two points in the earth. These potentials are made of two portions, one constant and unidirectional and the other fluctuating. The relatively steady part of the potentials is the result of various electrochemical processes occurring in the ground, including streaming potentials. The time-varying potentials are due to magnetotellurics; i.e. fluctuations in the earth's magnetic field.

Usually SP values vary from a few tenths of a millivolt to several tens of millivolts, although values of several hundred millivolts have been observed. Such large anomalies

are often obtained over electrically conductive mineral deposits, in areas of considerable topographic variation, in geothermal areas and in areas with high groundwater flow rates.

The self-potential method was first documented by Fox in 1830 for the investigation of sulphide deposits (Telford et al. 1976, Parasnis 1997, and Sharma 1997). However, widespread use of this method did not occur until after the introduction of non-polarizing electrodes by Schlumberger in 1922 (Telford et al. 1976). Since then, the major environmental and engineering application of the SP method has been the investigation of subsurface water movements. Specific uses include the mapping of seepage flow through retaining structures such as dams, dikes and reservoir floors (Ogilvy et al. 1969, Bogoslovsky and Oglivy 1970a, b, 1973, Haines 1978, Bogoslovsky et al. 1979, Gex 1980, Fitterman 1983, Hardley 1983,Godfrey 1984, Black and Corwin 1984, Butler 1984, Corwin and Butler 1989, Al-Saigh 1994, Panthulu 2000, Titow 2000, Sheffer 2001, Sasitharan et al. 2001, Sheffer 2002, Dahlin et al. 2004, Rozycki 2006, and Johansson 2007); and the mapping of flow patterns in the vicinity of landslides, sinkholes, wells, shafts, volcanos, tunnels and faults (Bogoslovsky and Ogilvy 1972, 1977, Erchul and Slifer 1987, Beck 1988, Lange and Kilty 1991, Kilty and Lange 1991, Stewart and Parker 1992, Birch 1993, Lange and Barner 1995, Aubert and Atangana 1996, Wanfang et al. 1999, Fagerlund and Heinson 2003). The self-potential method has also been used extensively in mineral explorations and geothermal investigations.

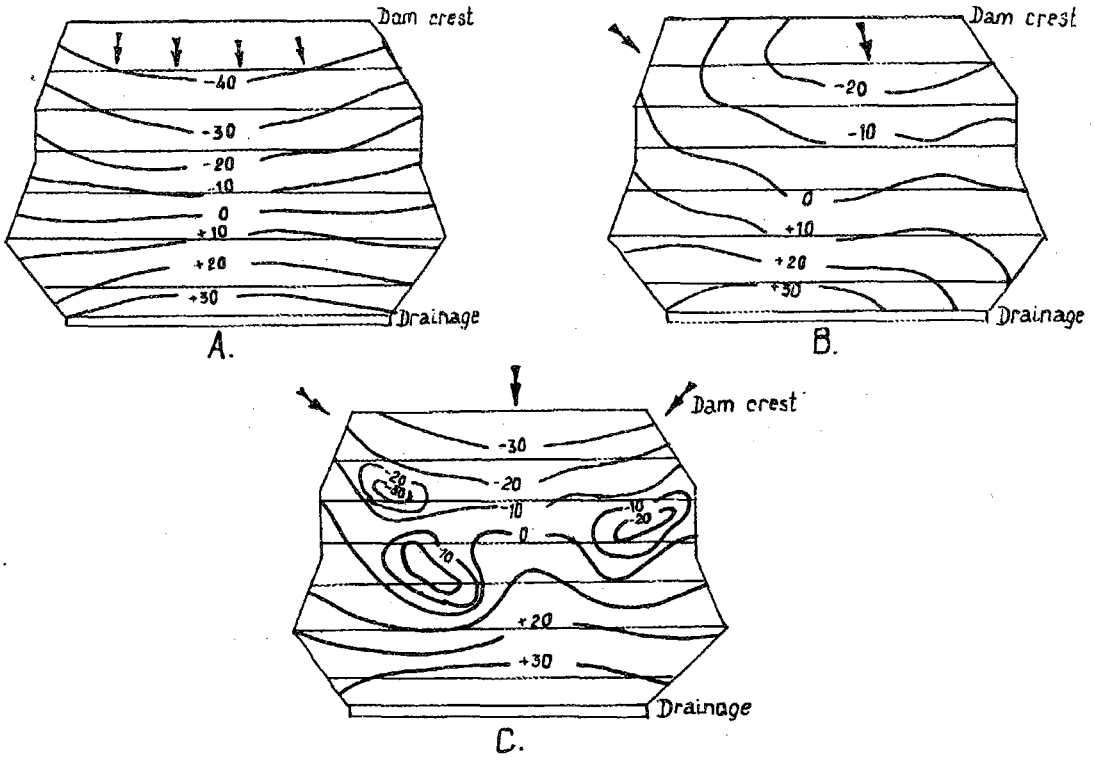

Figure 2-3: Distribution of natural electrical potential on the downstream slope depending on the type of seepage. (A) Frontal seepage. (B) Frontal and roundabout seepage (around the right flank of the dam). (C) Frontal and roundabout seepage when there are heterogeneous materials in the dam supporting mass (After Bogoslovsky and Ogilvy 1970b).

2.3.1. THE ORIGIN OF SELF-POTENTIALS

Self-potentials are induced by numerous processes which are still not fully understood (Sharma 1997). The main mechanisms are briefly described below. For a more detailed description the reader can refer to Telford et al. 1976, Parasnis 1997, and Sharma 1997.

2.3.1.1 Electrofiltration or Streaming Potentials

Electrofiltration or streaming potentials result from electric currents that are generated whenever a liquid flows through a porous medium. This phenomenon was first observed in capillary tubes by Quincke in 1859. A theoretical model for these effects in capillaries was later developed by Helmholtz in 1878. The Helmholtz model is still in use to this day and was shown to be equally valid for a liquid flow through a porous medium.

The basic theory of electrofiltration is that when an electrolyte solution moves with respect to a solid it is in contact with, it carries with it charged particles that are attached to the charged surface of the solid, creating an electric convection current. This current will cause the mobile charges to deplete upstream and accumulate downstream, creating an electric potential difference. This potential difference is the streaming potential, which in turn will drive a conduction current back through the body of the fluid. In steady state these two currents will balance each other.

The magnitude of the streaming potential depends on the resistance of the return current path; therefore if the solid is a conductive material, part of the conduction current will pass through it, reducing the streaming potential. Consequently the subsurface resistivity distribution will play an important role in determining the magnitude of streaming potential anomalies.

Streaming potentials are of great engineering interest since they provide information directly related to subsurface flows. Other geophysical methods, such as resistivity, only provide secondary information about the effects of subsurface flows,

such as porosity, density, and degree of saturation; however this information can be of great assistance when interpreting SP measurements.

Of the various electro-chemical mechanisms that produce self-potentials, the streaming potential phenomenon is obviously the most important for subsurface water flow investigations. But in order to distinguish true streaming potential anomalies when interpreting SP measurements, an awareness of all of the possible self-potential generating electrochemical mechanisms is required.

Streaming potentials are further discussed in Chapter 3 with other electrokinetic phenomena.

2.3.1.2 Diffusion or Electrochemical Potentials

Theoretically, if a surplus of a certain type of ion were to exist in a particular underground area then diffusion forces would act to restore a homogenous distribution. The migration of the ions in the direction of the concentration gradient would create an electric convection current, which would in turn drive an electric conduction current in the reverse direction. This conduction current creates an electric potential drop that is the measured diffusion potential anomaly. The convection current can be calculated for a known concentration gradient; however conditions are much more complicated in nature where several different types of ion contribute to the creation of the diffusion current.

It is suggested that concentration differences in groundwater may contribute to the background potentials encountered in most SP investigations; yet their influence can be very difficult to determine and no appropriate explanation exists for why diffusion potentials persist over time. The phenomenon is not fully understood but it is suggested that concentration differences are regenerated by redox reactions involving oxygen from the atmosphere.

2.3.1.3 Mineralization Potentials

Mineral potentials are the most common cause of SP anomalies; they occur above all types of electrically conducting mineral bodies. Self-potential values caused by mineral bodies are typically greater than those associated with streaming potentials. SP anomalies caused by mineralization potentials are relatively strong, ranging from 100 mV to 1000 mV. They usually occur over pyrite, chalcopyrite, pyrrhotite, magnetite and graphite deposits.

The origin of these anomalies is not completely understood. Early explanations attributed the anomaly to the oxidation of the mineral body above the water table, but such a theory does not explain graphite. Later, Sato and Mooney (1960) proposed a more acceptable theory of mineralisation and developed a new model where electrons are lost in the lower portion of the ore body and gained in the upper part by a number of chemical reaction pairs and the ore body acts only as an electron conductor. The different electrochemical reactions at the upper and lower parts of the ore body create potential drops across the mineral-electrolyte interface that can be solved by assuming a chemical equilibrium. A noticeable problem with this method is that no current flow can exist under chemical equilibrium, thus no SP anomaly would be registered. The voltages at the interface are not only dependant on the chemical reactions, but also on current flow, which is determined by the subsurface resistivity distribution.

Kilty (1984) used non-equilibrium thermodynamic equations to expand the Sato and Mooney theory. According to his theory there are four separate voltages to consider: the potential drop in the ore body (V_o), the potential drop in the ground and the interface voltages at the upper (V_u) and lower (V_l) parts of the ore body. The voltages can be written as $IR = V_u - V_l - V_o$ where I is the current flow and R is the resistance of the current path outside of the ore body. The mineral potential value is a part of the potential drop IR.

SP anomalies caused by mineralization potentials can be very difficult to predict due to the complexity of the interactions between the electric current, the electro-

chemical interface reactions and the subsurface resistivity distribution. The SP method has been widely used in mining exploration and mineral prospecting investigations (Parasnis 1997, Sharma 1997, Telford et al. 1976).

2.3.1.4 Other Sources of SP Potentials

There are other sources of SP potentials which may influence the normal distribution of self-potential. These sources include, but are not limited to sedimentation, adsorption, thermoelectric, vegetation and precipitation potentials.

a. Sedimentation Potentials

Sedimentation potentials are the result of the same mechanism that creates streaming or electrofiltation potentials. In this case solid particles move with respect to the liquid that is stationary. Sedimentation potentials could occur where there are standing water bodies with a high concentration of suspended solids; tailings ponds for example. Sedimentation potentials are further discussed in the following Chapter along with the other electrokinetic phenomena.

b. Adsorption Potentials

Self-potential anomalies induced by ion adsorption are known to take place above quartz and pegmatite granite bodies; they are generally in the order of +20 to +40 mV. The anomaly has been attributed to the adsorption of positive and negative ions on the surface of these bodies (Parasnis 1997), but the details of the electrochemical mechanism are not clear.

c. Thermoelectric Potentials

Temperature gradients are known to generate self-potential anomalies. Moderately large anomalies can be observed in the vicinity of geothermal areas. They are assumed to be caused by a combination of both electrokinetic and thermoelectric coupling (Corwin

and Hoover 1979). The electrokinetic potentials are created when geothermal sources induce convection of the groundwater. The thermoelectric potential is not fully understood, but it is believed to be due to the differential diffusion rates of both ions in the groundwater and electrons and ions in the soil and rock. The thermoelectric coupling effect is usually expressed as a ratio between the temperature gradient and the resulting electric potential gradient. This ratio which is called the thermoelectric coupling coefficient has been shown to lie between -0.1 and 1.36 mV/°C for a variety of rock types (Nourbehecht 1963).

d. Vegetation Potentials

The presence of ground vegetation can lead to fake potential anomalies, potentially attributed to its effect on soil moisture content. It is even possible that diffusion or electrochemical potentials occur around the roots. Erntson and Sherer state that vegetation effects can be seen as short wavelength SP anomalies with amplitudes of up to 150 mV (Erntson and Sherer 1986). It has been observed that densely vegetated areas tend to give positive SP values compared to barren areas.

e. Precipitation Potentials

Precipitation will give rise to false SP anomalies due to streaming potentials. The measured potentials will misrepresent the normal ground conditions. Reflection should be made when taking measurements in heavy rainfall or snowmelt.

2.3.2. FIELD PROCEDURE

Self-potential data acquisition methods are not as developed as those for other geophysical methods. There is great room for improvements and the application of new ideas. The acquisition of good-quality SP data for dam investigation is challenging. The magnitude of self-potential anomalies associated with water flow is usually smaller than those associated with geothermal activity or mineral explorations, and the presence of man-made structures or buried objects in the vicinity of the study area can create a significant amount of noise. Consequently it is very important to take great care when acquiring and interpreting SP data.

Because SP is a passive technique (like gravity or magnetics), there is no way of changing source parameters to vary depth of investigation or to help distinguish noise from signal. Smoothening and filtering techniques can be applied to enhance the quality of the acquired SP data. However, it is recommended that one identify and remove error and noise from the acquired measurements as much as possible before using such techniques.

2.3.2.1 Survey Equipment

SP measurements are somewhat simple to perform. They require a pair of non-polarizing electrodes, although there are cases of simple metal rods (stainless steel or copper-clad steel) performing adequately (Butler et al. 1990, Parasnis 1997, Koester et al. 1984, Johansson et al. 2003). They also require a high impedance voltmeter, and the cables to connect them. It is important to note that complete SP equipment sets are usually assembled by the user since they are not readily available from commercial sources.

a. Electrodes

There are three different applications for the self-potential electrode; onshore, offshore and long-term SP measurements. To some extent, the requirements for these

electrodes differ. For onshore measurements, the electrodes must be rugged, easy to store and they must quickly recover from polarisation induced by external sources such as resistance measurements, changes in soil chemistry and temperature. For offshore measurements, the electrodes must be submersible (at least to the required depth of the survey), have minimal electrolyte leakage, and be compatible with water chemistry. For long-term monitoring, the electrodes must have minimal electrolyte leakage, be compatible with the soil in which they are installed, and show minimal drift with time.

Electrodes in the form of metal rods have been used with relative success. Self-potential surveys have been made using simple stainless steel rods (Parasnis 1997, Johansson et al. 2000a, b, c and 2003) and copper-clad steel (Koster et al. 1984, Corwin 1989a). On the other hand, the data acquired from using these electrodes is not acceptable for streaming potential measurements. When metal rods are used the electrochemical reactions that occur where the metal meets the ground moisture creates potentials, called redox potentials. These may surpass the electrofiltration potential. The magnitude of the redox potential is difficult to determine as several different reactions are involved, depending on properties of both the electrode and the electrolyte solution (Timm and Möller 2001).

Non-polarizing electrodes have been found to give much more reproducible data (Parasnis 1997, Sharam 1997, Corwin and Butler 1989). These electrodes (Figure 2-4) consist of a metal element immersed in a solution of a salt of the same metal, with a porous junction forming the boundary between the solution and the soil (Ives and Janz 1961). Examples of these electrodes include copper-copper sulphate ($Cu\text{-}CuSO_4$), silver-silver chloride (Ag-AgCl), lead-lead chloride ($Pb\text{-}PbCl_2$), zinc-zinc sulphate ($Zn\text{-}ZnSO_4$) and cadmium-cadmium chloride ($Cd\text{-}CdCl_2$).

The most commonly used non-polarizing electrodes in SP surveys are of $Cu\text{-}CuSO_4$ or Ag-AgCl type, and their response to environmental variations is well documented (Ewing 1939, Ives and Janz 1961, Corwin and Conti 1973, Petiau and Dupis 1980). It has been shown that the measured potential of these electrodes increases with increasing soil moisture content as well as with increasing temperature. Corwin (1989b) reported an

effect of 0.3 to 1 mV per percentage change in moisture content, and Kassel et al. (1989) described an effect of 0.5 to 1 mV per degree of temperature change in the electrode's metal solution.

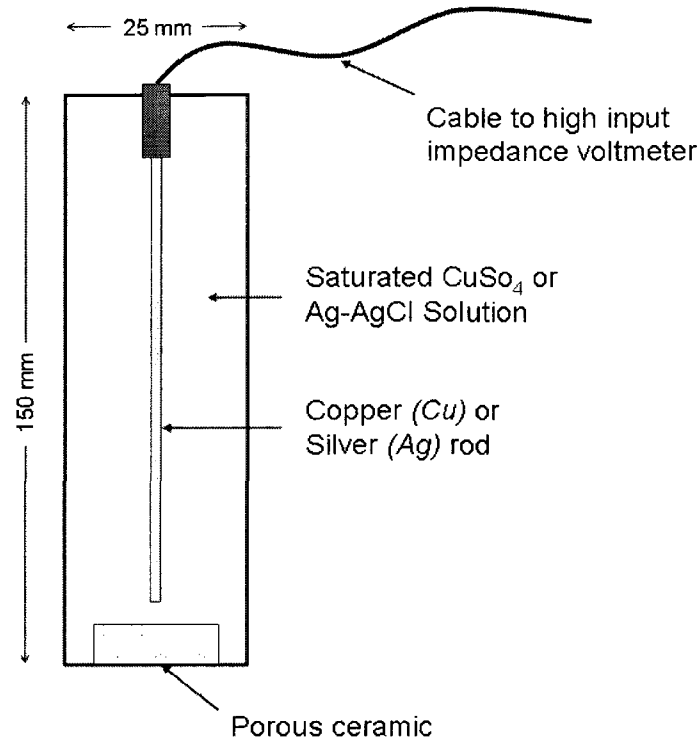

Figure 2-4: Schematic cross-section of a typical non-polarizing electrode.

b. Self-Potential Measuring Instrument

The most important requirements for the voltmeter used for SP field measurements are: resolution, range, input impedance and suitability for field use. A resolution of 0.1 mV is adequate for SP field measurements, and a range of +/- 10 VDC will cover even very large anomalies. The voltmeter should have relatively high input impedance, at least 10^8 ohms, in order to prevent drawing considerable current from the ground, which would disturb the potential distribution and cause polarization of the electrodes.

2.3.2.2 Survey Configurations

A self-potential survey is conducted by mapping the electric potential field between a randomly selected base station and a series of points on the surface. The results are presented in the form of isocontours and/or profiles of the measured electric field. There are three basic techniques used in SP surveys: gradient, absolute, and multiple-electrode methods.

a. Gradient Survey Configuration

For the gradient method, also called the dipole, leapfrog, or fixed-electrode configuration (Parasnis 1997, Sharam 1997, Telford et al. 1976), a dipole with a constant electrode separation is moved along the survey line, with the trailing electrode occupying the station of the previous leading electrode (Figure 2-5 a). If the electrode separation length is not too large then the ratio of the potential difference to length measures the potential gradient. The absolute potential can be obtained by summing the potential differences along the profile; however the value obtained would contain the accumulated noise from each individual measurement. This can be reduced somewhat by 'leapfrogging', where the forward electrode becomes the rear electrode for the next measurement and only the rear electrode ever moves forward. Care must be taken in recording the polarity of each measurement when using this technique.

Gradient surveys are usually performed by a team consisting of a two-person field party, while the fixed-base surveys (described below) can be performed by a single operator. For the fixed-base survey method a recorder installed at a strategic location within the survey area is used to monitor SP time variation (electrode drift). Later inspection of this record will help indicate which readings were affected by time variation. Techniques for quantitative correction of electrode drift on gradient SP measurements have not yet been developed.

The major advantage of the gradient configuration is the use of relatively short connecting cables minimising the risk of cable damage, and the relative speed of the

survey since there is no need to cross the survey line to reel in the wire. However, it is important to note that the gradient configuration is extremely sensitive to "false anomalies" by cumulative error. These errors are mainly due to electrode / soil contact, electrode polarization, and time-varying potentials. The effects of electrode polarization can be reduced by "leapfrogging" as previously mentioned, but the other errors are more difficult to quantify and correct. These errors add-up for each measured SP value, and because the measured values are summed in the data reduction process, the errors can build up to a significant level. Hence, the gradient configuration should only be used when site conditions prevent the use of the fixed-base configuration.

b. Fixed-Base Survey Configuration

The fixed-base measurement method, also called the total field or potential method (Parasnis 1997, Sharam 1997, Telford et al. 1976), involves a stationary electrode and a roving electrode, connected by long cable reels. The stationary or reference electrode is usually placed outside of the study area in a spot where the SP values are expected to remain constant. The stationary electrode is then connected to the negative terminal of the voltmeter and the mobile electrode to the positive terminal. Successive measurements are made between the reference and the mobile electrode moving to the different survey stations 1, 2, 3, ... n (Figure 2-5 b). This method provides the absolute potential difference between the measurement points in the survey area and the stationary reference electrode.

When logistical considerations (cable length, topography, potential damage to the cable by traffic, etc.) require the use of more than one reference station, additional reference stations are established and carefully tied to the main base station. In-order-to provide the best quality of data, the number of auxiliary stations should be minimised since tie-in errors accumulate with each additional station.

The major advantage of the fixed-base configuration compared with the gradient configuration is the lower level of cumulative error and the relative ease in which one can estimate the magnitude of electrode polarization and time-varying errors and remove

these errors from the fixed-base measurements. Therefore, the reproducibility of data obtained using the fixed-base configuration is generally considered better than that for the gradient configuration.

c. Multiple-Electrode Survey Configuration

A multiple-electrode survey configuration is similar to a long-term SP monitoring setup (Koester et al. 1984). The electrodes installed at the different measuring stations are connected to a base station terminal through a multi-conductor cable. Measurements are made between a reference electrode and the measuring electrode using a multi-channel data acquisition system. Using these permanently installed electrodes, measurements can also be made using a gradient and/or fixed-base procedure.

The advantage of this survey configuration is the ease with which repeated measurements are made to check for time variations, and applying different data processing techniques. For the fixed-base configuration, cumulative error is minimised by the used of a single reference station. Another advantage is the ability to monitor electrode drift and to take measurements after values stabilize.

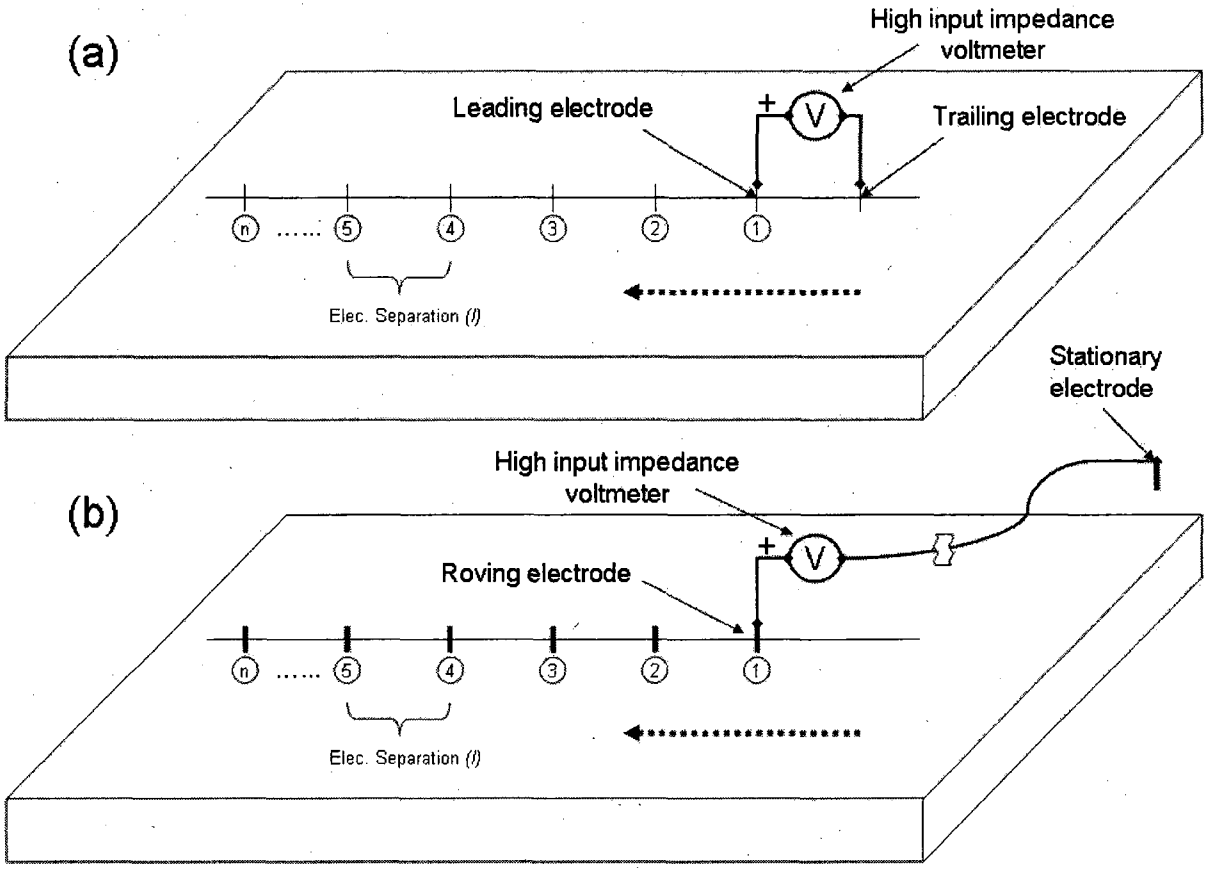

Figure 2-5: Electrode arrangement for self-potential surveys. (a) Gradient configuration uses two mobile electrodes with a constant electrode separation. (b) Fixed-base configuration uses a stationary electrode at a remote location and a moving measuring electrode along the survey line.

2.3.2.3 Potential Sources of Noise and Error in SP Measurements

Self-potential measurements conducted at dam sites should display a fairly low signal to noise ratio. Large amplitude and hard to detect errors can be induced by instrument problems or incorrect field procedures. Before any effort is put into interpreting SP measurements in term of seepage detection, mapping and monitoring, it is important to identify noise and error in the acquired data and to curtail their effects.

As previously mentioned, standardised data quality control, field procedures and hardware have not been fully established for the self-potential method. Hence, this section discusses the most commonly reported sources of SP noise and error. One useful method for separating seepage and non-seepage induced anomalies is by repeated SP measurement at different reservoir elevations. Seepage induced anomalies would be expected to increase with increasing head (reservoir elevation); while non-seepage induced anomalies are rather unaffected. A simple procedure for eliminating unwanted noise is by subtracting low-pool data values from high-pool values. Profiles and contours of SP measurements filtered using this procedure, are much more indicative of a potential seepage problem than a single survey.

The potential sources of noise and errors in SP measurements on embankment dams can be divided into three major categories; topographic effects, buried metal, and ground conditions.

a. Topographic Effects

Topographic effects play an important role in SP measurements on dams, due to the geometry of the embankment. It is important to recognise these effects and ensure they are not misinterpreted as seepage induced anomalies. Topographic effects are thought to be caused by the down-slope movement of subsurface water. They tend to generate SP contours parallel to the elevation contours. The largest topographic effects are usually encountered in areas having volcanic geology, highly porous soils or rocks, large

topographic changes, and high rainfall producing an abundant supply of fresh near-surface ground water (Corwin and Hoover 1979, Vagshal and Belyaev 2001).

SP contours running parallel to the dam axis are also created by the downstream movement of the steady state seepage through the embankment. Without any additional information, it is practically impossible to determine the contribution of either the topographic effects or the uniform seepage to the observed SP anomaly. Additional information could be acquired by repeated SP survey at different reservoir elevations (as previously discussed). The SP effect of steady state seepage is expected to increase with an increase in the reservoir elevation. On the other hand, topographic effects may vary seasonally, since they are somehow related to precipitation patterns, they are not expected to depend on reservoir elevation.

b. Buried Metal

Electrochemical reactions between soil and buried or partially buried metal sources (casings, pipes, debris, rebars, light pole ...) can generate large potential fields. These anomalies are generated by an oxidation-reduction mechanism similar to that of mineral deposits (Sato and Mooney 1960). Buried metal sources are very common at dam sites; hence, it is important to record their location along the survey line. A simple magnetic or electromagnetic survey can help reveal buried metal sources that not visible from the surface.

c. Ground Conditions

Changes in soil properties or conditions such as moisture content, chemistry, temperature, or vegetation cover can produce a significant SP variation. The response of the most commonly used electrodes (copper-copper sulphate and silver-silver chloride) to environmental variation is documented among others in Ives and Janz (1961), Ewing (1939), Petiau and Dupis (1980), and Corwin and Conti (1973).

Corwin (1989 b) examined the effect of varying the soil moisture content while holding other parameters constant. He concluded that the soil moisture variation can

represent a significant source of noise, since positive changes up to a few tens of millivolts are measured when soil moisture increases from dry to saturated. Thus, SP measurements taken during or shortly after precipitations or during snow melt may be affected by changes in soil moisture.

Non-polarizing electrode design (liquid junction) tends to contain any response to electrochemical variations within the soil. Nevertheless, changes in the chemical composition or ionic strength of the soil moisture can still affect the acquired SP data. The SP data quality is strongly affected by the total ionic content of the soil moisture. Fresh soil moisture may have very low electrical conductivity reducing the electrode's contact with the earth. This will result in a very high electrode contact resistance, unstable readings, poor reproducibility and very high noise levels. Such conditions are usually encountered in areas of heavy rainfall or snow melt, where fresh water washes most of the mobile ions from the near-surface soil moisture. One way to identify this condition is to conduct a resistivity survey. A high near-surface resistivity combined with a difficulty in forcing the current into the soil confirms the presence of such conditions.

The direct effect of soil temperature on SP measurements is negligible. Differences in temperature at the measuring depths of a few centimetres are not enough to cause significant thermoelectric potential differences (Perrier et al. 1997). Conversely, the electrode's potential is strongly affected by its electrolyte temperature. Care should be taken to maintain constant electrode temperature, by keeping the electrodes out of the sun and from contact with hot or cold soil for a prolonged duration.

Changes in the vegetation cover may indicate corresponding changes of soil properties or subsurface hydrogeologic conditions. Upward water flow closely related to evapo-transpiration (Ernstson and Scherer 1986) can directly affect SP readings. In some cases it may be necessary to place the electrodes beneath a dense root mat in order to obtain a good soil contact.

2.3.3. INTERPRETATION OF SELF-POTENTIAL DATA

In general, the interpretation of SP data is more difficult than data from other geophysical methods such as resistivity, temperature, magnetic, or seismic surveys. Self-potential anomalies generated by seepage flow in dams tend to be relatively small with a potentially high level of noise induced by either buried objects, the complex geometry of the embankment or by the varying seepage regime related to the pool level and seasonal effects. In addition, the nature, location and depth of the source for seepage investigations are not well defined. On the other hand SP anomalies generated by conductive minerals or high-temperature geothermal reservoirs are well-defined and they provide a clear indication of the location and depth of the source. Hence, it is important to take great care with data acquisition and reduction, and to use all available site data during the interpretation process.

The final result of an SP survey is usually a profile (Figure 2-6) or isocontour map (Figure 2-7) showing equipotentials. Anomalies greater than a few millivolts are often correlated with known features, and the selected interpretation procedures will depend on the goals of investigation, quality of field data and the availability of additional geophysical, geological and hydrogeological data. There are numerous methods cited in the literature for the interpretation of self-potential data. The most commonly used methods are qualitative interpretation, analytical models (dipolar sheet source, spherical source, cylindrical source, thin dipping sheet source, ...), SP modelling using point source and line source, and numerical modeling methods. A thorough description of most of these different methods is covered in detail in standard geophysical reference texts. A brief description is provided in the following paragraphs.

In most cases, qualitative interpretation involves visual inspection of SP data to look for patterns known to be the characteristic of the presumed source. For example, in the case of streaming potentials the driving force is the flow of liquid caused by a hydraulic gradient and the hydraulic and electric conductivities are two important material properties. The SP anomaly associated with seepage through or under an

embankment dam is well approximated by the electric potential distribution caused by a positive and a negative current source at the outflow and inflow areas, respectively.

This is well illustrated in the case of a concentrated seepage through a dike at the Churchill Falls Power Project in northern Canada, where three SP survey lines were made parallel to the dike axis at the waterline on the upstream slope, along the crest, and at the downstream toe (Godfrey 1984). The results of the survey are illustrated in Figure 2-6. Large amplitude negative SP values were centered around Station 22+50 on the crest and about 21+00 on the upstream slope along the water line, and a smaller positive SP value was located around Station 23+00 on the downstream toe. Proposed remedial work consisted of a grout curtain along the crest line, with grout holes spaced three meters apart. The grout take was not more than one sack at any boring outside the indicated SP anomaly, but within the anomaly zone, one boring required 600 sacks and a second 300 sacks. In this case it is clear that SP defined the area that needed repair.

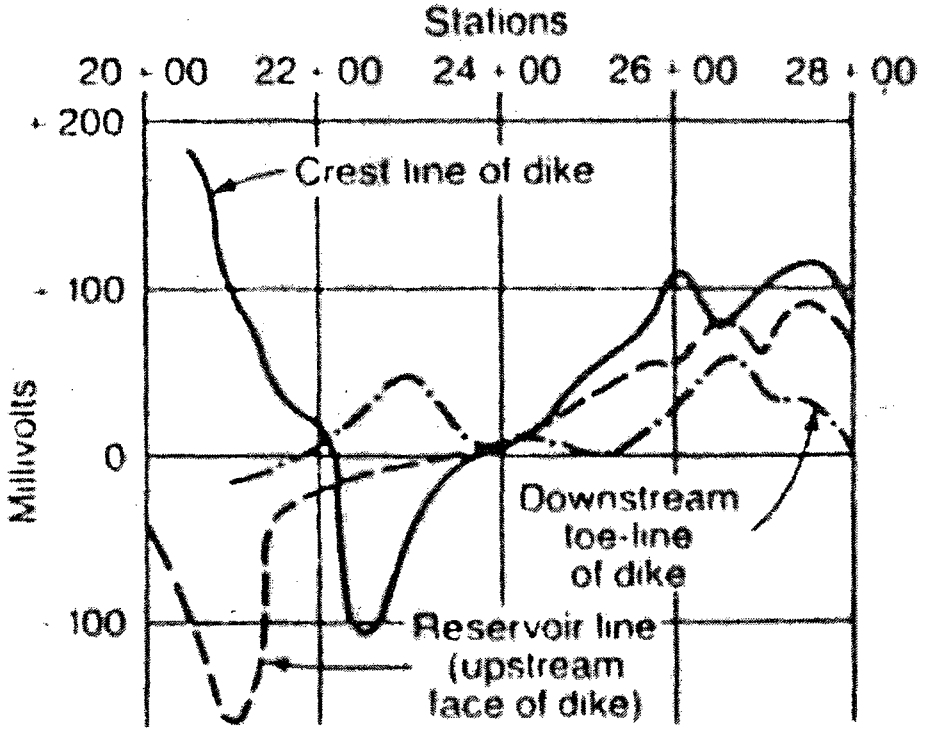

Figure 2-6: Self-potential profile on a leaking dike, Churchill Falls, Canada (After Gdofrey 1984)

Another example of qualitative interpretation is presented in Figure 2-7 (Corwin 1991). A large sinkhole, of several meters in diameter, appeared on the crest of the east embankment of Wells Dam (a large concrete hydroelectric dam). The aim of the SP survey was to help determine the existence and the extent of any seepage flow associated with the sinkhole. SP surveys were conducted along several survey lines (survey lines A to E) and electrical resistivity measurements (Corwin 1990b and c) were conducted along lines A and C; the downstream toe and upstream shoreline respectively.

It was reported that the SP measurements were strongly affected by time-varying (telluric) noise, and by the presence of rebars in the reinforced concrete structure of the East Endwall of the powerhouse. Both of these noise sources were removed from the field data prior to contouring and interpretation using the appropriate noise reduction techniques. The corrected isocontours show a well defined -90 mV contour centered close to the observed sinkhole and extending to the upstream shoreline. This relatively low value was interpreted as an indication of a strong seepage entering through the upstream slope. The east – west elongation of the contours along survey line B corresponds to a previously observed area of settlement. This elongation of the contours is an indication that seepage inflow is not confined to the sinkhole area but extends a considerable distance from the area.

The results of the qualitative interpretation were validated by a resistivity profile along the shoreline (line C) (Corwin 1990c). The results showed a large area of very low resistivity soil extending to a depth of around 30 m in the vicinity of the sinkhole. This anomaly was as attributed to high porosity soil associated with the water seepage indicated by the SP survey. Following an extensive geotechnical investigation and additional geophysical studies, remedial work was conducted by the installation of a slurry cutoff wall along the upstream crest line. Following the completion of the remediation, SP surveys were conducted along the same lines shown in Figure 2-7. The post-remediation results showed a background noise with no evidence of the previous anomaly.

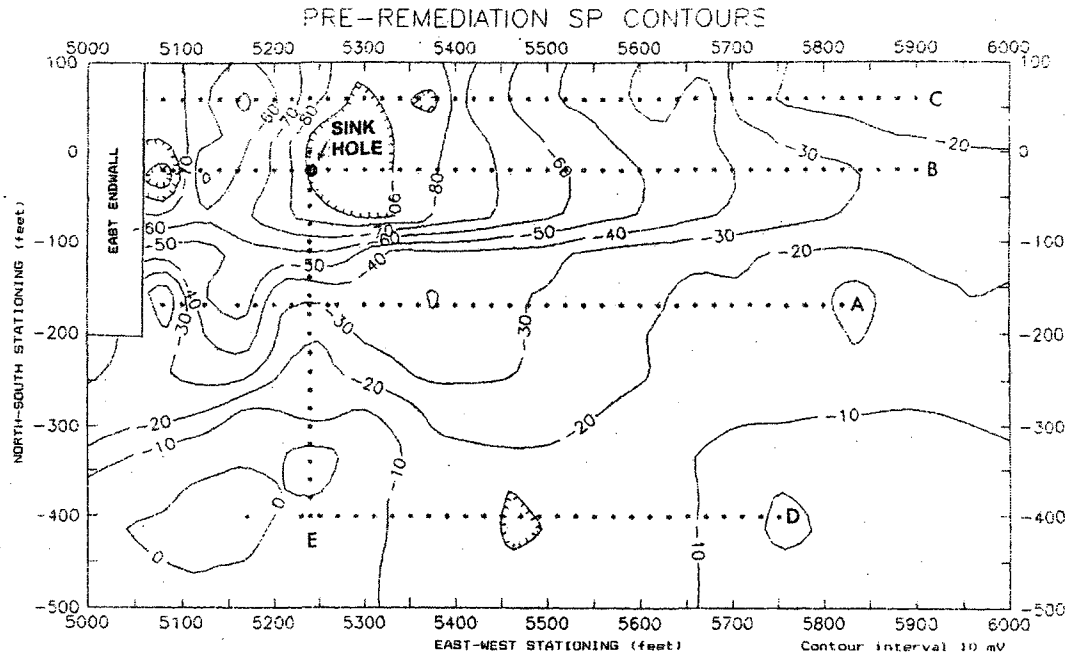

Figure 2-7: Isocontours on East Embankment, Wells Dam, U.S.A. (After Corwin 1991)

There have been several attempts at quantitative interpretation based on theoretical anomalies calculated for simple geometric bodies (sphere, thin plate, double layer) located in a homogeneous halfspace (Parasnis 1997, Sharma 1997). These analytical models were initially developed for the interpretation of SP data from mineral and geothermal surveys, which tend to have well defined anomalies and a higher signal to noise level than those usually observed at dam sites. The use of these geometric interpretation techniques can help provide information about the depth and configuration of the anomaly sources as well as their location. A thorough description of the different geometric interpretation techniques are presented in the following articles: Corwin and Butler 1989, Agarwal 1984, Stern 1945, Telford et al. 1976, DeMoully and Corwin 1980, Corwin et al. 1981, Rao et al. 1970, Bhattacharya and Roy 1981, Murty and Haricharan 1985, Fitterman 1979, 1982, 1983, Fitterman and Corwin 1982.

The advantages of the self-potential modeling techniques using analytical solutions such as points or lines of electric current are their relative simplicity and ease of use. In seepage flow related anomalies, the point sources technique provides a useful tool for the interpretation of SP data. It helps estimate the flow path configuration and seepage flow rate, and the maximum depth of the source of the observed anomaly. The use of multiple point sources can even be used to approximate relatively complex flow paths. The line source on the other hand can be used to model SP anomalies that have a significant length. For example a single line source can represent a seepage inflow and outflow, and multiple line sources can be used to approximate a 2D plane source such as seepage through a face or dam core. The major disadvantage of these methods is that it is difficult or impractical to incorporate the effects of topography and of complex site structure and seepage flow patterns.

Quantitative interpretation of streaming potential anomalies can also be achieved through numerical modeling. These techniques are based on the concepts of irreversible thermodynamics and coupled flow of fluid, heat, electrical current and chemical diffusion (Osanger 1931, Pourbaix 1949, Denbigh 1951, Prigogine 1955). The application of these concepts to flow was first discussed in Mitchell (1976). The study of application of these concepts to the interpretation of SP data was first reported by Nourbehecht (1963), followed by the work of Fitterman (1978, 1979, 1984), Ishido and Mizutani (1981), Sill (1983), Morgan et al. (1989), Jouniaux and Pozzi (1995 a and b, 1997), Ishido and Pritchett (1999), Lorne et al. (1999) and others.

Numerical models such as SPXCPL / SPPC (Sill and Killpack 1982), SPDIKE (Fitterman 1982), SPBC (USACE 2002) and SP3D (Sheffer and Howie 2003) require estimates of the cross-coupling coefficient, electrical resistivity and hydraulic conductivity for the materials at site. The consistency of the interpretation will depend on the accuracy of these parameters, so it is desirable to obtain as much information as possible from measurements rather than estimated values. A summary of the theory behind the numerical modeling of the streaming potential phenomena showing the required parameters is presented in the following chapter.

2.4. TEMPERATURE MEASUREMENTS

Several authors have proposed temperature measurements as a mean for the investigation of water seepage from embankment dams and groundwater flow (Kappelmeyer 1957, Cartwright 1968 and 1974, Melker et al. 1985 and 1989, and Johansson 1991). A comprehensive review of the theory and interpretation methods is presented in Johansson 1997.

Temperature measurements have been used successfully in several dams in Sweden, Canada, and the United States. Several monitoring system installed during the past decades include both manual measurements and automated acquisition systems using temperature sensors (such as thermistors, vibrating wire piezometers with temperature measurements, and platinum resistance thermometers PT100) with an absolute accuracy varying from 0.5°C to 0.01°C. Recent fibre-optic innovations allow for the use of such cables for temperature sensing in new and existing dams (buried in the embankment in the case of new dams and installed in standpipes or along the downstream toe) (Dornstadter 1997, Johansson and Farhadiroushan 1999). The accuracy of the fibre-optic cable when a standard system is used is of 0.3°C, while accuracy may be below 0.1°C when an advanced system is installed.

The temperature in an embankment dam depends mainly on the reservoir and ambient temperature. The influence of the ambient temperature on the embankment temperature is negligible when the embankment height exceeds 10 m (Johansson 1997). Temperature variations within the embankment are mainly controlled by the hydraulic and thermal properties of the embankment material. The thermal properties of saturated soils are strongly related to their mineral composition and porosity. The thermal conductivity of a saturated medium will decrease when the porosity increases, since the soil particles with high thermal conductivity are replaced by water with low thermal conductivity. For example the thermal conductivity of water and quartz at 20°C are respectively 0.58 and 3 W/mK (watt / meter kelvin).

2.5. RESISTIVITY MEASUREMENTS

The shape and magnitude of SP anomalies are strongly influenced by the subsurface resistivity. A fundamental knowledge of the subsurface electric conditions is greatly beneficial for the interpretation of SP measurements. The usual means of obtaining the subsurface resistivity is through the use of the earth resistivity method. It is also well documented that subsurface resistivity depends on material properties such as porosity, degree of saturation, clay content, pore water properties and temperature (Telford et al. 1976, Parasnis 1997, and Sharma 1997).

The resistivity method involves introducing a DC or low-frequency alternating current into the ground by means of two electrodes and measuring the resulting potential difference between a separate set of electrodes (Figure 2-8). Simple metal rods are usually sufficient for both current and potential electrodes, although the use of non-polarising electrodes is preferable for the potential electrode set.

Resistivity measurements provide information about the electric conductivity (σ) distribution in the subsurface. Resistivity (ρ) is simply the inverse of electric conductivity ($\rho = 1/\sigma$). It represents the material's inability to conduct an electric current. Resistivity varies between different geologic formations, depending mainly on variations in water contents and dissolved ions in pore water.

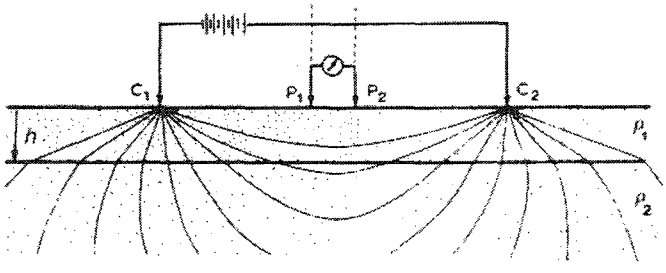

Figure 2-8: Sketch of the arrangement of a four electrode resistivity measurement. The current is transmitted between the current (C_1 and C_2) electrodes and the potential is measured between the two potential (P_1 and P_2) electrodes (After Sharma 1997).

2.5.1. ELECTRICAL RESISTIVITY OF ROCKS AND MINERALS

The electric resistivity of rocks and minerals can vary greatly and depends on several factors. The amount and interconnectivity of various minerals will play an important role in determining the bulk resistivity. Unconsolidated sediments usually have lower resistivity values than sedimentary rocks, with values ranging from 10 to less than 1000 Ωm (Loke 2000). The resistivity values depend mainly on the porosity (with the assumption that all pores are saturated) as well as the clay content.

Figure 2-9 shows the approximate resistivity ranges of different materials. For example the resistivity of silicate minerals is typically very high (106 Ωm and higher) whereas sulfides and most oxide minerals can be considered semiconductors with resistivity values in the range of 10^{-6} to 10^{-2} Ωm. Graphite minerals also exhibit semiconductor properties with resistivity values of the same order as sulfides. The resistivity of water for example strongly depends on the amount of dissolved ions which act as charge carriers; the resistivity of fresh water is in the order of 10 to 100 Ωm while saltwater is 100 to 1000 times more conductive with a resistivity of 0.2 Ωm or less.

Most rocks in the dry state act as insulators; however in nature they always contain some pore water, which will ultimately change their bulk resistivity. The relationship between the resistivity of a porous rock and the fluid saturation is given by Archie's Law, which is applicable to certain types of rocks and sediments, especially those with low clay content. The electrical conduction is assumed to be through the pore water. Archie's law is given by

$$\rho = a\ \rho_f\ \phi^{-m} \qquad \textbf{(Loke 2004)} \qquad \textbf{(Eq. 2-2)}$$

where ρ is the rock resistivity, ρ_f is the fluid resistivity, ϕ is the fraction of rock filled with the fluid, while a and m are two empirical parameters (Keller and Frischknecht 1966). For most rocks, a is equal to 1 and m is about 2 (Loke 2004).

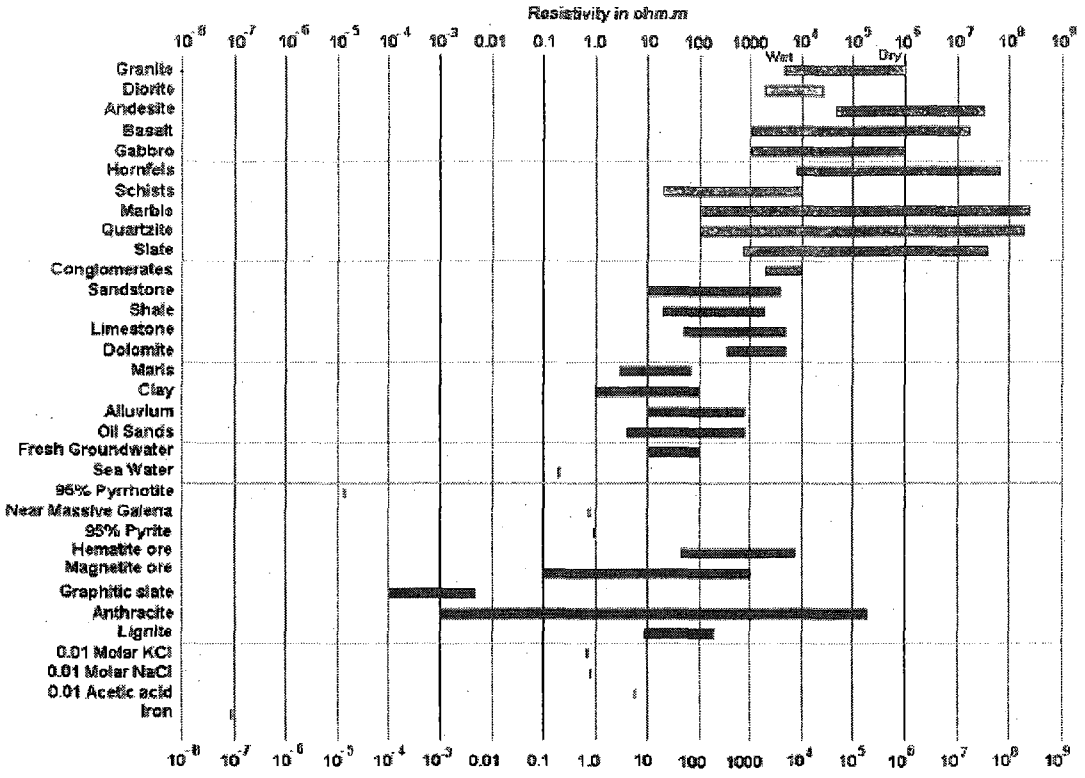

Figure 2-9: Typical ranges of electrical resistivity values of different materials (After Loke 2004)

2.5.2. APPARENT RESISTIVITY

Ohm's law defines the behaviour of an electric current (I) in a linear conductor having a uniform cross-section as

$$I = -\frac{dV}{R} \qquad \textbf{(Parasnis 1997)} \qquad \textbf{(Eq. 2-3)}$$

where dV is the potential difference (volts, V) between the conductor ends and R (ohm, Ω) is the resistance of the conductor. The resistance (R) is directly proportional to the conductor's length (dL) and inversely proportional to its cross-section area (s)

$$R = \rho\frac{dL}{s} \qquad \textbf{(Parasnis 1997)} \qquad \textbf{(Eq. 2-4)}$$

where the resistivity (ρ) is a proportional constant that depends on the conductor material.

It is important to note the difference between resistance (R) and resistivity (ρ). The resistance is a property of the path that the current takes through the conductor, whereas the resistivity is a physical property of the material. Combining equations (2-3) and (2-4) we get

$$\frac{I}{s} = -\frac{1}{\rho}.\frac{dV}{dL} \quad \text{or} \quad J = \frac{1}{\rho} E \qquad \textbf{(Parasnis 1997)} \qquad \textbf{(Eq. 2-5)}$$

where $J = I/s$ is known as the current density (A/m^2) and $E = -dV/dL$ is called the electric field (V/m).

When a single point source is placed on the surface of a homogeneous isotropic half-space, the current will spread through the half-space symmetrically and it is equal at all points that are at the same distance (r) from the electrode, which will allow us to replace in equation 2-5 dL with dr and s with the surface area of the hemisphere ($2\pi r^2$). Integrating the equation would provide the potential (V) at a distance (r) from the point current electrode

$$V(r) = \frac{I\rho}{2\pi}.\frac{1}{r} + C \qquad \textbf{(Sharma 1997)} \qquad \textbf{(Eq. 2-6)}$$

where C is an arbitrary constant that is equal to zero if V is assumed to be zero. In practice there are two current electrodes, a positive sending electrode (A) and a negative receiving electrode (B). The electric potential at any point in the half-space would be then

$$V = \frac{I\rho}{2\pi}.\left(\frac{1}{r_A} - \frac{1}{r_B}\right) \qquad \textbf{(Sharma 1997)} \qquad \textbf{(Eq. 2-7)}$$

where r_A and r_B are the distance from the point to the positive and negative electrodes respectively.

If M and N are respectively the positive and negative potential electrodes, then the potential difference (ΔV) between them can be calculated from equation 2-8

$$\Delta V = \frac{I\rho}{2\pi}\cdot\left(\frac{1}{AM}-\frac{1}{BM}-\frac{1}{AN}+\frac{1}{BN}\right)$$ **(Sharma 1997)** **(Eq. 2-8)**

where *AM*, *BM*, *AN* and *BN* represent the distance between the respective electrodes. The electrical resistivity is then calculated using the following equation

$$\rho = \frac{2\pi}{\left(\frac{1}{AM}-\frac{1}{BM}-\frac{1}{AN}+\frac{1}{BN}\right)}\cdot\left(\frac{\Delta V}{I}\right) = \frac{\Delta V}{I}\cdot\frac{2\pi}{G}$$

(Sharma 1997) **(Eq. 2-9)**

where $(2\pi/G)$ is the geometric coefficient of an electrode configuration.

2.5.3. FIELD PROCEDURES

There are several methods for measuring electric resistivity in the ground. The most common methods involve placing two electrodes in the ground and connecting them to a current source. The current is momentarily switched on, and the potential difference is measured across two potential probes also placed in the ground. Exactly how the current and potential probes are placed in the ground determines which area of the subsurface most influences the measurement.

2.5.3.1 Electrode Configurations

A variety of electrode configurations exist for performing resistivity surveys. The type of information required and existing geological conditions will influence the type of electrode configuration used. The following is a brief description of the most commonly used configurations.

a. Wenner Array

The Wenner array configuration is a special case in the Schlumberger array. It is achieved by placing the four electrodes along a straight line with the potential probes between the current electrodes (Figure 2-10) and with an equal spacing between them. For the Wenner array configuration, equation 2-9 can be reduced to

$$\rho_a = 2.\pi.a.\frac{\Delta V}{I}$$ **(Parsnis 1997).** **(Eq. 2-10)**

b. Schlumberger Array

The Schlumberger electrode configuration is achieved by placing the four electrodes along a straight line with the potential probes between the current electrodes. The distance between the two potential electrodes is kept much smaller than the distance between the two current electrodes (Figure 2-10). For the Schlumberger array, equation 2-9 can be reduced to

$$\rho_a = \frac{\pi L^2}{2l}.\frac{\Delta V}{I}$$ **(Parsnis 1997).** **(Eq. 2-11)**

c. Dipole – Dipole Array

A dipole-dipole array is created by separating the set of current electrodes from the potential electrodes (Figure 2-10). Typically both sets of electrodes will have a common spacing but they can be placed anywhere with respect to each other, then equation 2-9 can be reduced to

$$\rho_a = 2.\pi.n.a.(n+1).(n+2).\frac{\Delta V}{I}$$ **(Sharma 1997).** **(Eq. 2-12)**

For example the set of electrodes could be placed inline, parallel, perpendicular or at any angle to each other.

d. Pole – Dipole Array

A pole-dipole array is produced by connecting one of the current electrodes to a long cable and placing it far from the array. If a is the potential electrode spacing and the current pole is placed inline and at n distance from the set of potential electrode, then equation 2-9 can be reduced to

$$\rho_a = 2.\pi.n.a.(n+1).\frac{\Delta V}{I} \qquad \textbf{(Sharma 1997).} \qquad \textbf{(Eq. 2-13)}$$

One of the advantages of using a dipole – dipole or pole – dipole array is that the current and potential cables are separated from one another, which reduces noise induced by electromagnetic coupling (Sharma 1997).

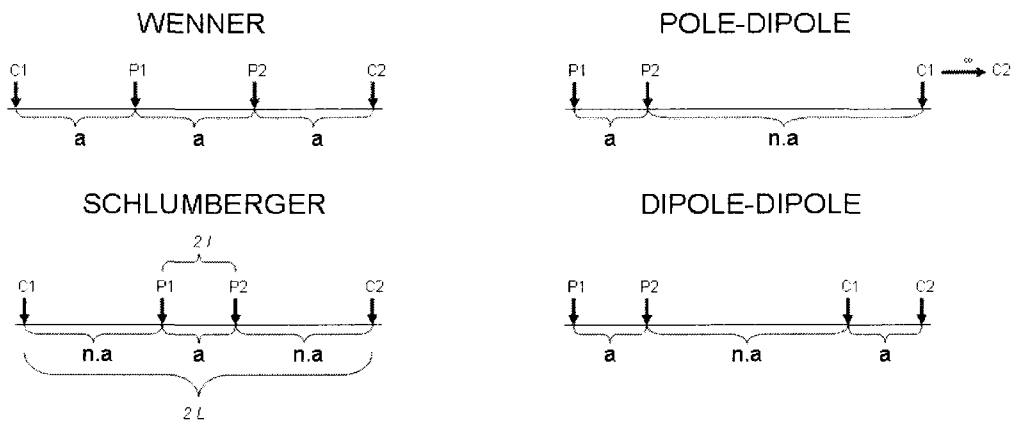

Figure 2-10: Commonly used electrode arrays in resistivity surveys (After Sharma 1997).

2.5.3.2 Apparent Resistivity Mapping

Resistivity mapping or profiling involves moving an electrode array along profile lines crossing the area of interest to investigate 2D or 3D subsurface structures. Usually a Wenner or dipole-dipole configuration is used and the electrode spacing is selected based on the desired depth of investigation. The spacing is typically kept constant, providing a lateral resistivity distribution at a constant depth along the profiles. Interpretation of data from profiling surveys is mainly qualitative (Loke 2000).

This method can be labour intensive when a large spacing is required as each measurement requires the displacement of all four electrodes. Recent technological advances render this type of resistivity survey obsolete. Commercially available multi-electrode resistivity surveying instruments and fast computer inversion software have made 2D and 3D resistivity surveys viable. For detailed information on the different resistivity surveys (1, 2D and 3D) the reader is referred to the following references (Loke 2000 and 2004).

2.6. LONG TERM RESISTIVITY AND SELF-POTENTIAL MONITORING OF HÄLLBY AND SÄDVA EMBANKMENT DAMS – A CASE STUDY

Hällby and Sädva embankment dams were the first Swedish embankment dams to get permanent resistivity and self-potential monitoring systems. Daily measurements at Hällby started in 1996 while measurements at Sädva started in 2001 (Johansson et al. 2003). A brief summary of the monitoring procedures and results is presented below. Further details are available in the following publications: Johansson et al. (2003), Dahlin (2001, and 2005) and Sjödahl et al. (2003, and 2004).

2.6.1. HÄLLBY EMBANKMENT DAM

The Hällby embankment dam is a glacial till central core rockfill dam with a reservoir capacity of 625 hm^3 and a maximum reservoir fluctuation of 0.8 m. The embankment is split in two by the power plant and spillway structures. The left embankment is 120 m long, while the right embankment is 200 m long. Both have a maximum height of 30 m.

In 1986 a sinkhole was observed on the left embankment close to where the dam connects to the concrete structure. Remedial measures consisted of grouting the affected area with a cement-bentonite and silicate mix. A total of 250 m^3 of grout was used. Additional grouting was performed in the bedrock and at the contact between the right embankment and the spillway structure.

The installation of the electrodes was not without its share of problems. The absence of information on the presence of a thermal insulation layer on the right dam crest resulted in the installation of the electrodes above that layer and the electrodes along the upstream slope were not positioned adequately. On the other hand, the measurements from the left crest and right downstream toe have been successful, but with a considerable amount of noise.

Detailed analysis of resistivity data was done by examining the variations over time in a certain area of the embankment. Figure 2-11 presents the variation of the resistivity along chainage -61.25 m and -43.75 m of Hällby's left embankment over a nine year period. The area around chainage -61.25 m was considered healthy as the resistivity results were stable over that period of time, whereas the area around chainage -43.75 m presents a deviation in the resistivity pattern at great depth over time. These high variations were interpreted as a sign of increased seepage, while the increase in resistivity was interpreted as a sign of internal erosion.

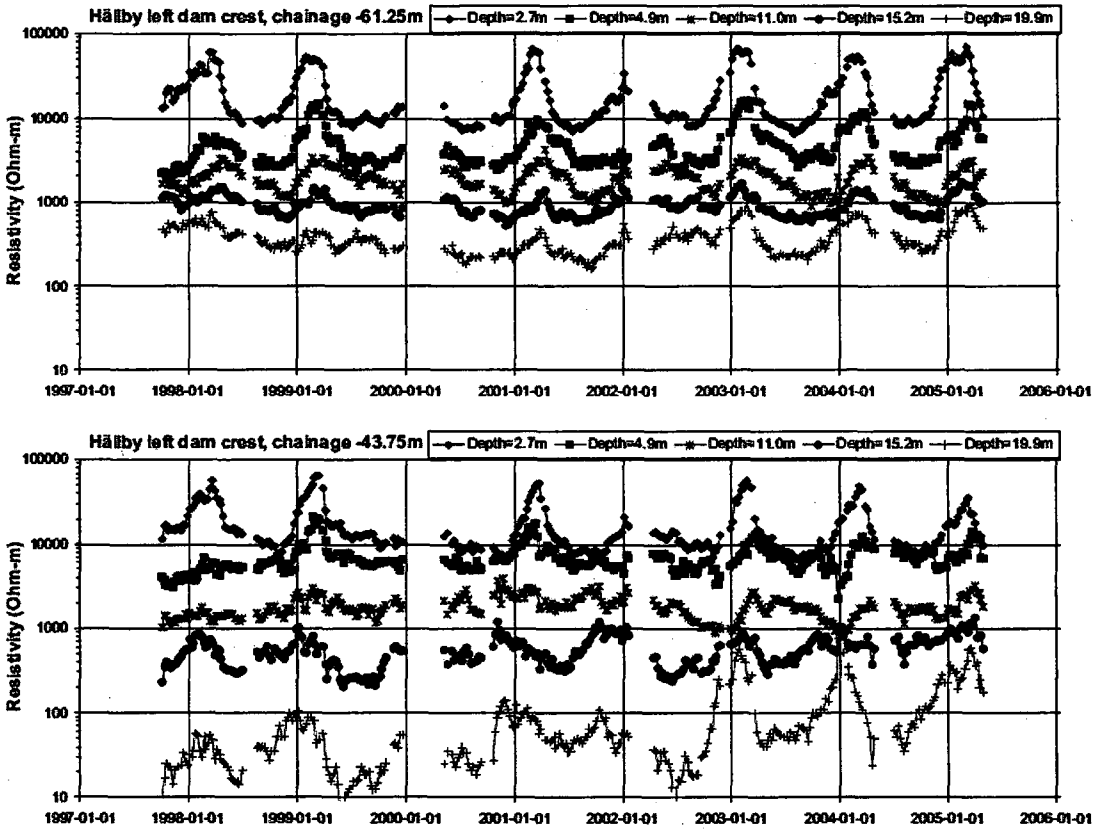

Figure 2-11: Time series of inverted resistivity data at five different depths from two different locations on Hällby left embankment over the period from 1997-01-01 to 2006-01-01. Top: healthy part of the embankment (chainage -61.25 m). Bottom: Presenting a tendency expected from internal erosion at depth (chainage -43.75) (Sjödahl 2006)

Due to the small variation in Hällby reservoir level, only one detailed self-potential survey was performed. For that survey the potential method was used. The reference electrode was placed downstream of the right embankment and the electrodes used were copper-copper sulphate for land based survey and silver-silver chloride for offshore data acquisition. The long-term self-potential survey was done using the same electrodes used for the long-term resistivity survey.

Figure 2-12 shows the isocontour map of the self-potential measurements at Hällby taken in 2000. The SP distribution was generally calm with only two well-defined positive anomalies extending from the upstream side to the downstream side. Seepage was ruled out as the cause of these anomalies since they lack the bipolar character generally associated with seepage induced anomalies (i.e.: negative SP values above areas of seepage inflow and positive SP values above areas of seepage outflow). Due to the similarity between the anomalies on both sides of dam, the cause was interpreted as being related to the presence of buried sheet piles within both embankments.

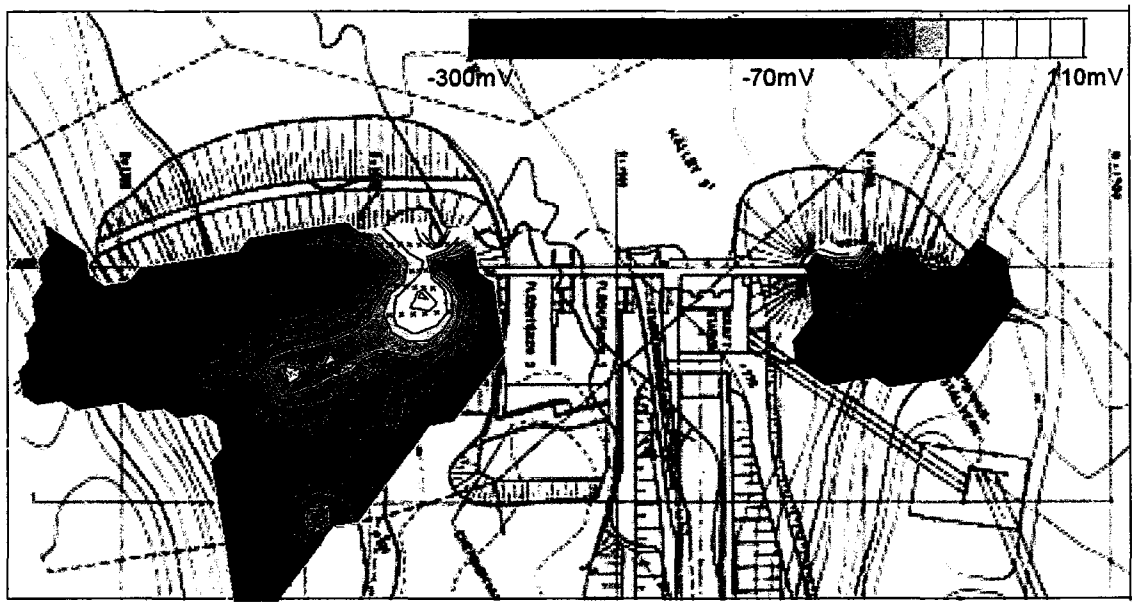

Figure 2-12: Isocontour map of SP data at Hällby dam collected in 2000 (the small black crosses represent the positions of the measuring stations) (Johansson el al. 2003).

Figure 2-13 shows time series plots of the long-term SP measurements (over a five years period) at the crest of the left embankment of Hällby. The different plots illustrate the various filtering steps used for the interpretation of the raw SP data. Although measured using stainless steel electrodes, the long-term SP data at Hällby dam turned out to be stable and of good repeatability.

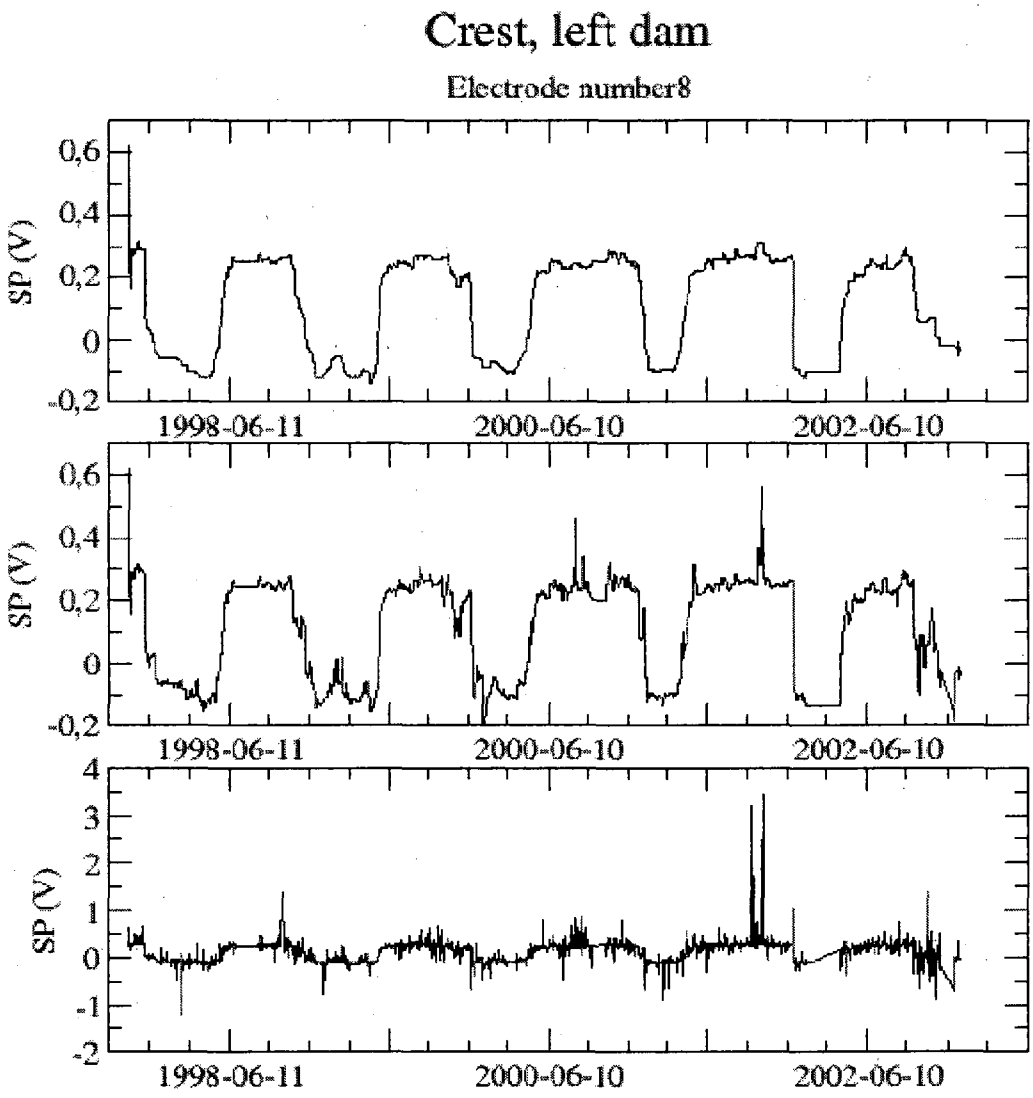

Figure 2-13: Time variation of SP data over a five years period at the crest of the left dam. Raw data (bottom), spike removal filtered data (middle), spike removal and 7 day median filtered (top) (Johansson et al. 2003).

2.6.2. SÄDVA EMBANKMENT DAM

The Sädva embankment dam is a glacial till upstream sloping core rockfill dam with a reservoir capacity of approximately 630 hm^3 and with an annual fluctuation of 16 m. The dam has a total length of 620 m, which is divided in a 210 m long, 32 m high dam across the river channel and a 410 m long, 10 m high dyke along an old river channel. The dam is founded on rock while the dyke is founded on glacial till except where it connects to the main dam.

The high water level fluctuation of the reservoir resulted in a complication in the resistivity and SP measurements. Numerical modeling showed that the effect of these fluctuations on resistivity numbered in several tenths of a percent (Sjödahl 2006).

The evaluation of monitoring data at Sädva dam was identical to that of Hällby dam. The comparison of the results revealed the obvious difference. First, due to the care taken during the installation of the electrodes the data quality has improved radically resulting in smoother data with less noise. Second, the resistivity variations along the length of the dam are smaller and more consistent, which is an indication of a well performing dam with lower seepage flow rates.

Figure 2-14 shows an example (at chainage 83 m) of the time series for the five depths at Sädva main dam, the results clearly show the homogeneous conditions that prevailed at the main dam till 2006. The appearance was found to be typical for most parts of the main dam, with all depths inside the embankment displaying similar conditions except for minor seasonal variations.

The resistivity measurements at the Sädva dyke were relatively higher than those taken in the main dam, and the conditions along the length of the dyke were not homogeneous (Figure 2-15 top). The most obvious anomaly is at chainage 450 m where a large variation in the foundation resistivity was detected. This anomaly was interpreted as being related to a change in rock type or rock quality. The relative variation of the

resistivity in the same area over the four years period indicated the possible presence of a seepage path in the foundation (Figure 2-15 bottom).

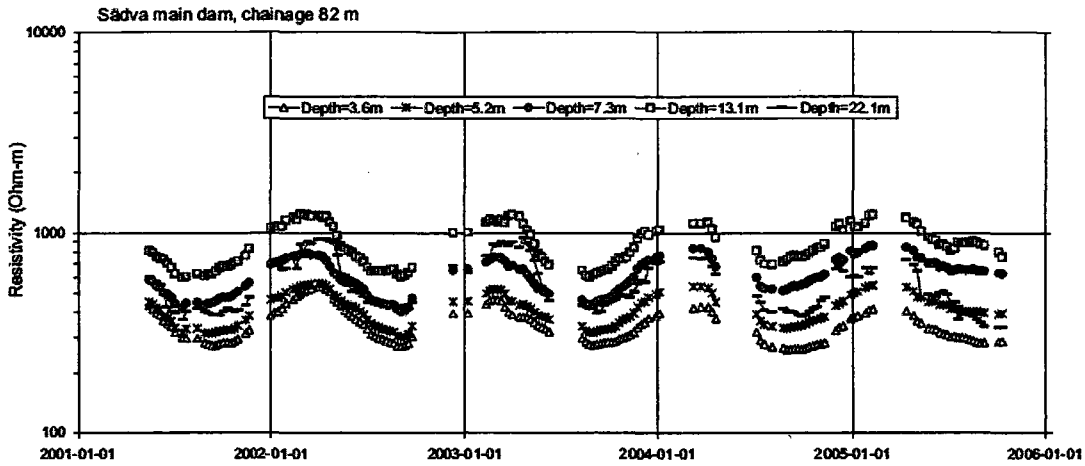

Figure 2-14: Time series of inverted resistivity data at five different depths from Sädva dam over the period from 2001-01-01 to 2006-01-01 at chainage 82 m (Sjödahl 2006).

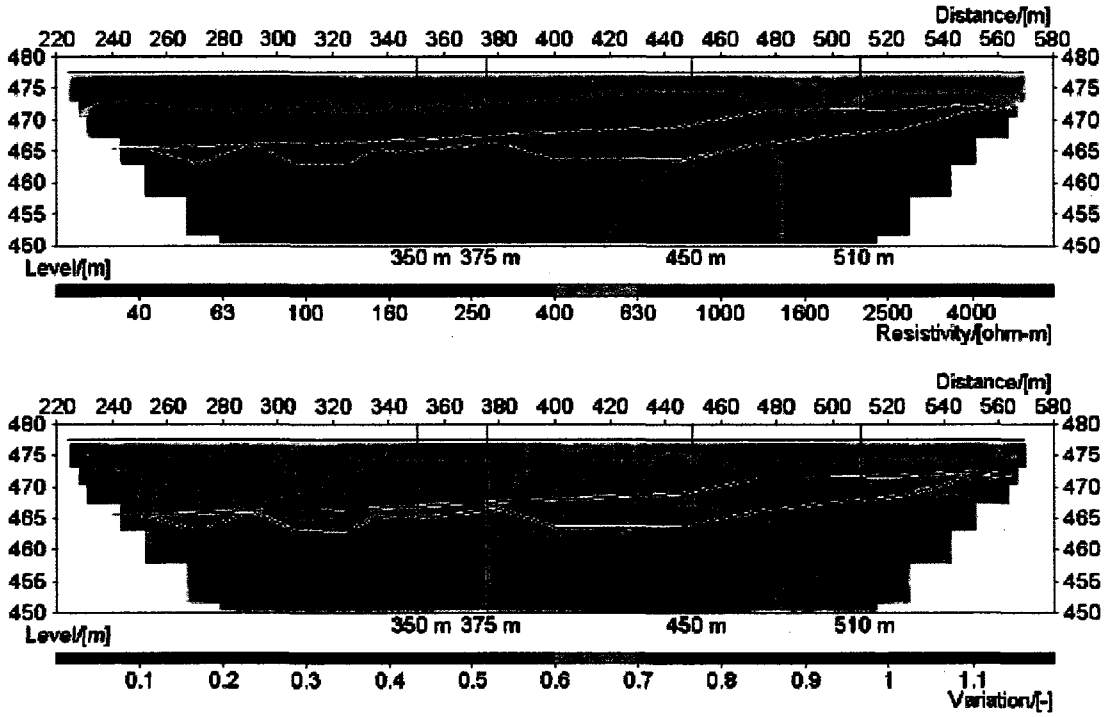

Figure 2-15: Longitudinal section of Sädva dyke showing the foundation and bedrock level (solid lines). Inverted resistivity distribution (top), relative variation of inverted resistivity models (bottom) over a four years period from 2001-09-20 to 2005-11-25 (Sjödahl 2006).

Two SP surveys (in October 2000 and June 2001) were carried out at Sädva dam. The primary goal was to provide a baseline for the interpretation of future SP data. The reservoir level for both surveys was respectively 476.5 m and 463.9 m. The potential method was used in both surveys and the reference electrode was one of the permanently installed copper-copper sulphate electrodes located on the main dams. For the offshore survey silver-silver chloride electrodes were used. The long-term land based self-potential survey was done using both copper-copper sulphate and stainless steel (used for the resistivity survey) electrodes permanently installed in the embankment.

Figure 2-16 shows the isocontour map of the self-potential data from the October 2000 survey. The data on land are absolute potentials referenced to the copper-copper sulphate electrode, while the offshore data are SP-gradients measured with a 10 m dipole. Figure 2-17 presents a comparison between the non polarizing (Cu-$CuSO_4$) and the stainless steels electrodes.

The results of the survey showed that variation of the SP in the area was very smooth and that all significant anomalies can be traced to different elements of the dam. For example, the distinctive positive anomaly induced by the concrete spillway near the southwest end of the survey area or the large negative anomaly in the northeast corner of the survey area most probably caused by topography (high points in the topography are often associated with negative SP anomalies).

Long-term SP data collected with the same measuring electrodes and instruments as the resistivity data turned out to be very noisy and practically impossible to interpret when compared with the copper-copper sulphate electrodes permanently installed at the crest of the main dam. Johansson et al. (2003) concluded that stainless steel electrodes generally do not give reliable SP results, contrary to what was observed at Hällby dam, while the Cu-$CuSO_4$ electrodes give reliable SP measurements, but with a considerable amount of noise that need to be filtered out.

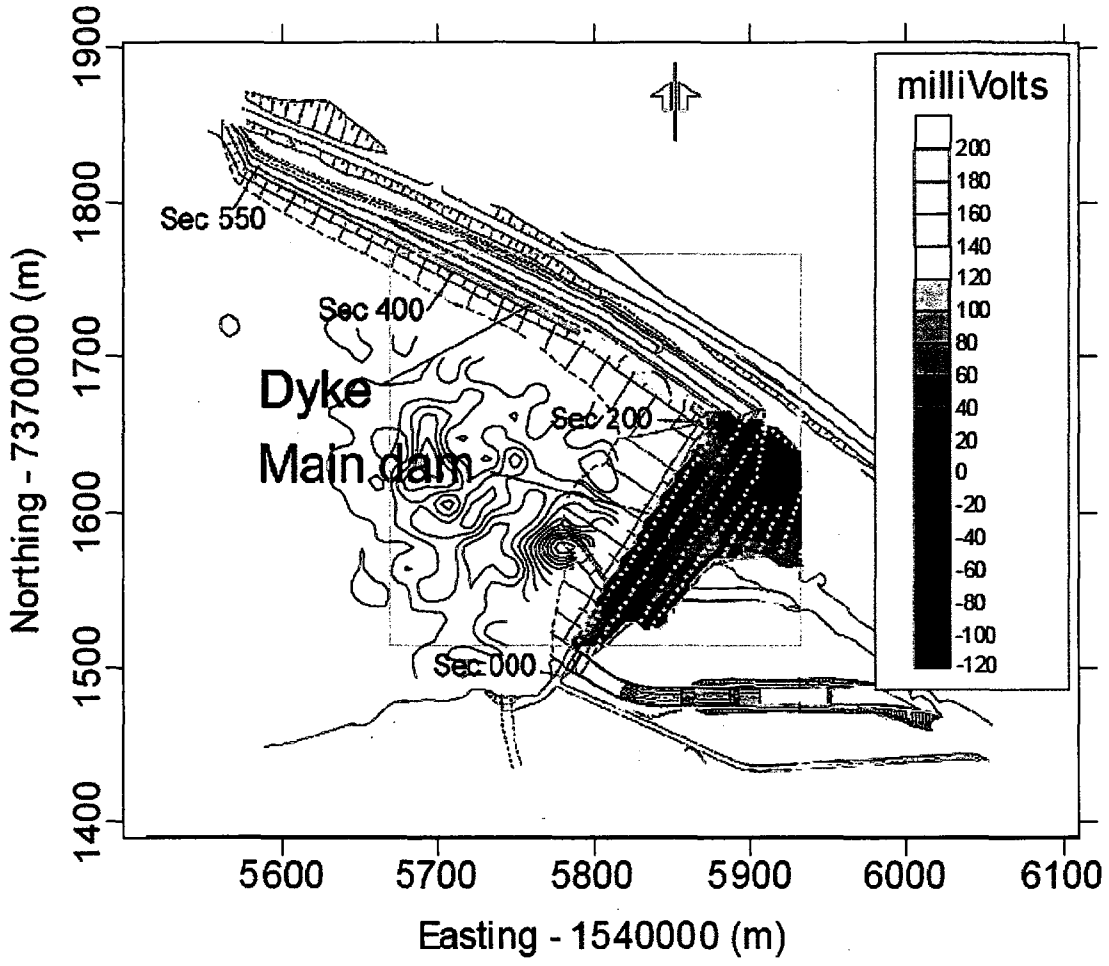

Figure 2-16: Isocontour map of SP data from the October 2000 survey. The data on the dam are absolute potentials referenced to electrode # 9 fixed on the dam. The data in the reservoir are absolute values of SP-gradient measured with a 10-m dipole (Johansson et al. 2003).

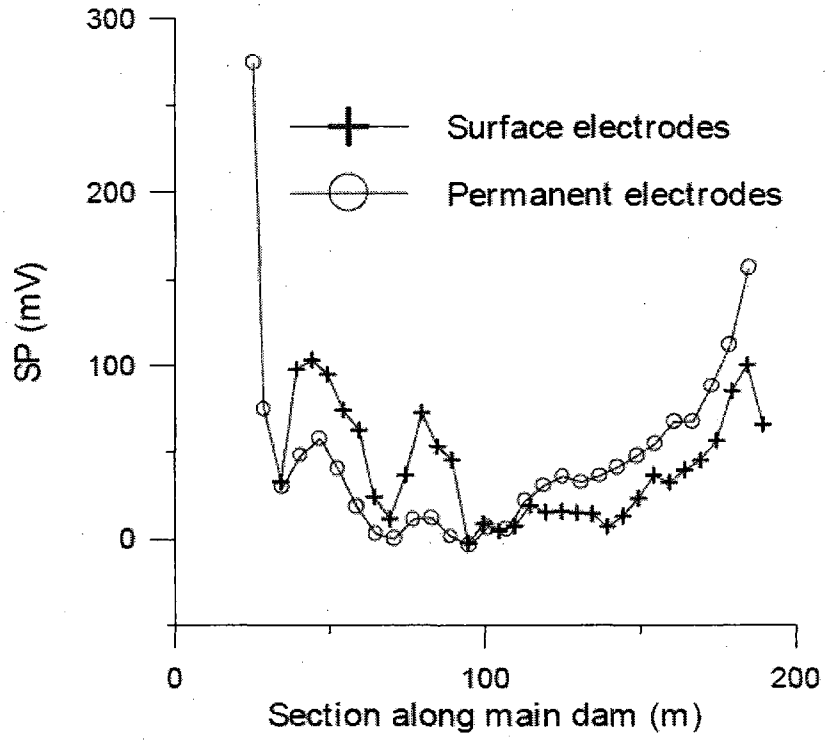

Figure 2-17: Comparison of SP data on the main dam acquired using the copper-copper sulphate (surface electrodes) and stainless steel electrodes (permanent electrodes). Both sets were acquired during the Oct. 2000 survey (Johansson et al 2003).

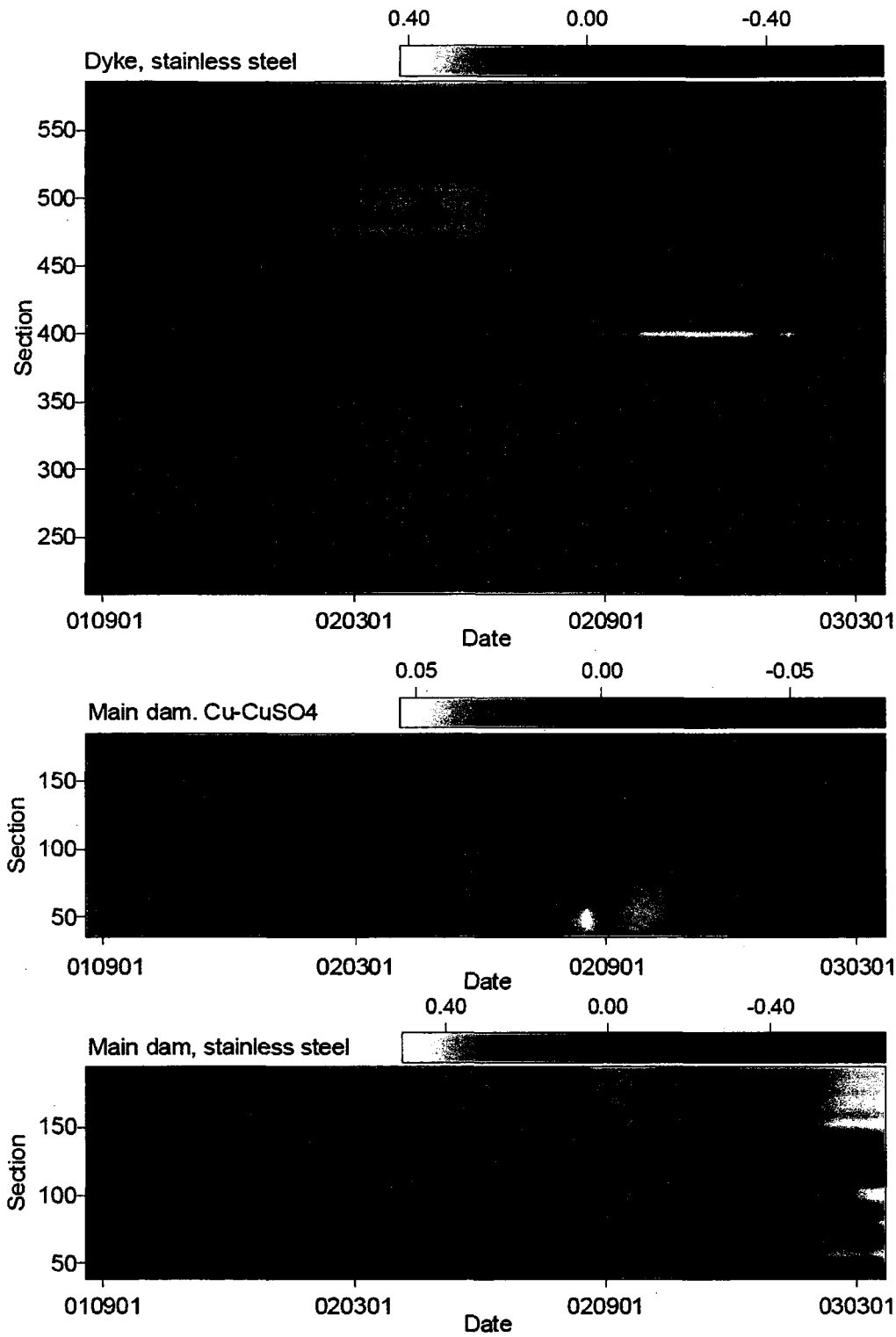

Figure 2-18: Time variation of SP data. The grey levels show residual SP values in Volts according to a colour chart on top of each plot (Johansson et al. 2003).

CHAPTER : 3 ELECTROKINETIC AND ZETA POTENTIAL - SOME THEORETICAL CONSIDERATIONS

3.1. INTRODUCTION

Electrokinetic potentials or streaming potentials (SP) have been used extensively in the well-logging industry, but in recent years, a renewed interest in SP has emerged, especially with respect to the detection of water leakage from embankment dams.

As previously stated, streaming potentials are caused by electro-filtration. There are four known electrokinetic phenomena. The first event is the transport of a liquid relative to a stationary solid as a response to an applied electrical field; this phenomenon is called electro-osmosis. The second event is the transport of a solid relative to a stationary liquid as a response to an applied electrical field; this phenomenon is called electrophoresis. The remaining two electrokinetic phenomena are the reverse effects of electro-osmosis and electrophoresis. The converse of electro-osmosis is electro-filtration (or streaming potential), which is the occurrence of an electric field in response to the relative movement of a liquid with respect to a stationary solid. As for the converse of electrophoresis, it is called sedimentation potential, which is the occurrence of an electric field in response to the relative movement of a solid with respect to a stationary liquid.

The electrokinetic phenomena can be simply explained as the interaction of pore fluid and mineral grains. The zeta-potential (ζ) and the streaming potential coefficient (C_s) are the most important parameters, however, these parameters are affected by other physical properties such as pH, electrolyte concentration, pressure, temperature, grain size, and type of mineral.

It has proven to be rather difficult to interpret streaming potential data quantitatively because of the many interdependent parameters. Numerical models using the coupled flow theory (relating water and current flow) have been developed to address this issue. The coupled flow theory has been successfully used in several numerical modeling programs (Sill and Killpack 1982, Sill 1983, Fitterman 1982 and 1983,

Wurmstich and Morgan 1994, Sheffer and Howie 2003, Darnet and Marquis 2004, Bérubé 2004). Cross-coupling conductivity plays an important role when using the coupled flow theory to model streaming potential problems. Even though several experimental studies have been performed to obtain streaming potential coefficient values, very few of them represent realistic geologic conditions and none of them measure the zeta-potential for mine tailings. Most of these studies were made using pure minerals in order to investigate the zeta-potential.

3.2. ELECTRIC DOUBLE LAYER

The streaming potentials or in other words the electrokinetic potentials are induced by the motion of ions with the flow of a liquid. In a two phase system such as a liquid and a solid medium, there has to be a balance of charge, which means, the system has to be electroneutral. This implies that the net charge on the surface of the solid medium has to be equal in magnitude and of opposite sign to the net charge within the liquid. At the interface of the two phases there is an aggregation of excess charge (ions and/or electrons) on each side, which constitutes an electric double layer.

The development of a surface charge on the solid phase in contact with a liquid phase is the driving mechanism behind all electrokinetic phenomena. The surface charge is usually induced by chemical interactions between the two phases. In general, most minerals develop a surface charge only when in contact with an electrolyte solution; however, clay minerals have a permanent imbalanced surface charge due to unbalanced crystalline structures.

The surface charge of the solid phase will attract, at the interface, charges of the opposite sign in the liquid, creating a diffused layer of counter-ions next to the solid surface. This redistribution of charge along the solid-liquid interface is known as the electric double layer.

When the liquid and solid phase move one with respect to the other, a small layer of the liquid remains attached to the solid. Hence, a shearing plane located at a small distance from the solid surface is created within the liquid. The shear plane will be situated somewhere within the diffused layer of counter-ions. The relative movement between the two phases will initiate the transport of some of the charges, generating an electric current. The opposite phenomenon is also true; the transport of some charges by an applied electric current will induce a relative movement between the two phases.

The application of an electric field to the solid-liquid interface will cause the electrostatic forces to act on the charges in the electric double layer, inducing a movement in the direction of the applied field. If the solid phase is stationary, the counter-ions in the liquid phase will move with respect to the solid inducing a movement of the liquid that will follow the motion of the charged particles, creating electro-osmosis. On the other hand, if the liquid is stationary, then the electrostatic forces will cause the solid particles to move with respect to the liquid, creating electrophoresis.

In the case of streaming potentials and sedimentation potentials, the relative movement between the solid and liquid phases is caused by mechanical forces such as pressure gradients or gravity. For example, the movement of an electrolyte solution parallel to a solid-liquid interface will shear off and transport with the flow some of the counter-ions present in the diffused part of the double layer. This will result in a surplus of the counter-ions at the downstream end and a lack of them at the upstream end. This charge separation creates an electric potential difference that in turn will drive a return current through the electrolyte solution but in the opposite direction. On the other hand, when solid particles move in a stationary liquid, the same mechanism operates to produce sedimentation potentials.

Several models of varying complexity have been proposed for the distribution of ions in the vicinity of the solid surface. In the Gouy-Chapman model the electric double layer is portrayed as a uniform surface charge on the solid phase. This is balanced by a surplus of ions of opposite sign in the liquid phase, creating a diffused layer where the charge density is greatest near the solid phase surface and then decreases, in accordance

with a Boltzmann distribution of the ions, to approach zero at some distance (Overbeek 1952, Morgan et al. 1989, Elimelech et al. 1998).

In the Stern model, which is a further improvement on the Gouy-Chapman model, there is a layer of strongly adsorbed ions next to the surface of the solid phase, called the Stern or Helmholtz layer, followed by a diffused layer (Figure 3-1). Usually, for the mineral – water systems, the surface charge is negative, therefore the electric potential (V) is lowest near the surface of the solid phase. The potential increases linearly in the Helmholtz layer and then nears zero as the remaining charge offset is balanced out by ions in the diffused layer (Figure 3-1, A). It is important to note that if the adsorption of ions in the stern layer is very strong the potential may rise above zero and will decrease as it approaches zero in the diffused layer (Figure 3-1, B).

The hydrodynamic slipping plane (S) represents the closest plane to the solid surface in which movement can take place. This plane constitutes the boundary between the mobile liquid phase and the stationary phases (solid phase plus immobile fluid). It is usually located close to the Helmholtz (H) plane separating the Stern and the diffused layer (Figure 3-1).

When the fluid moves with respect to the solid phase, the mobile part of the electric double layer is pulled along with the flow. Consequently, there is a transport of charge with the flow, which constitutes a convective electric current. The amount of charge transported is intimately related to the potential on the slipping plane, this potential is defined as the zeta-potential (ζ), the magnitude of which equals the potential charge in the mobile phase.

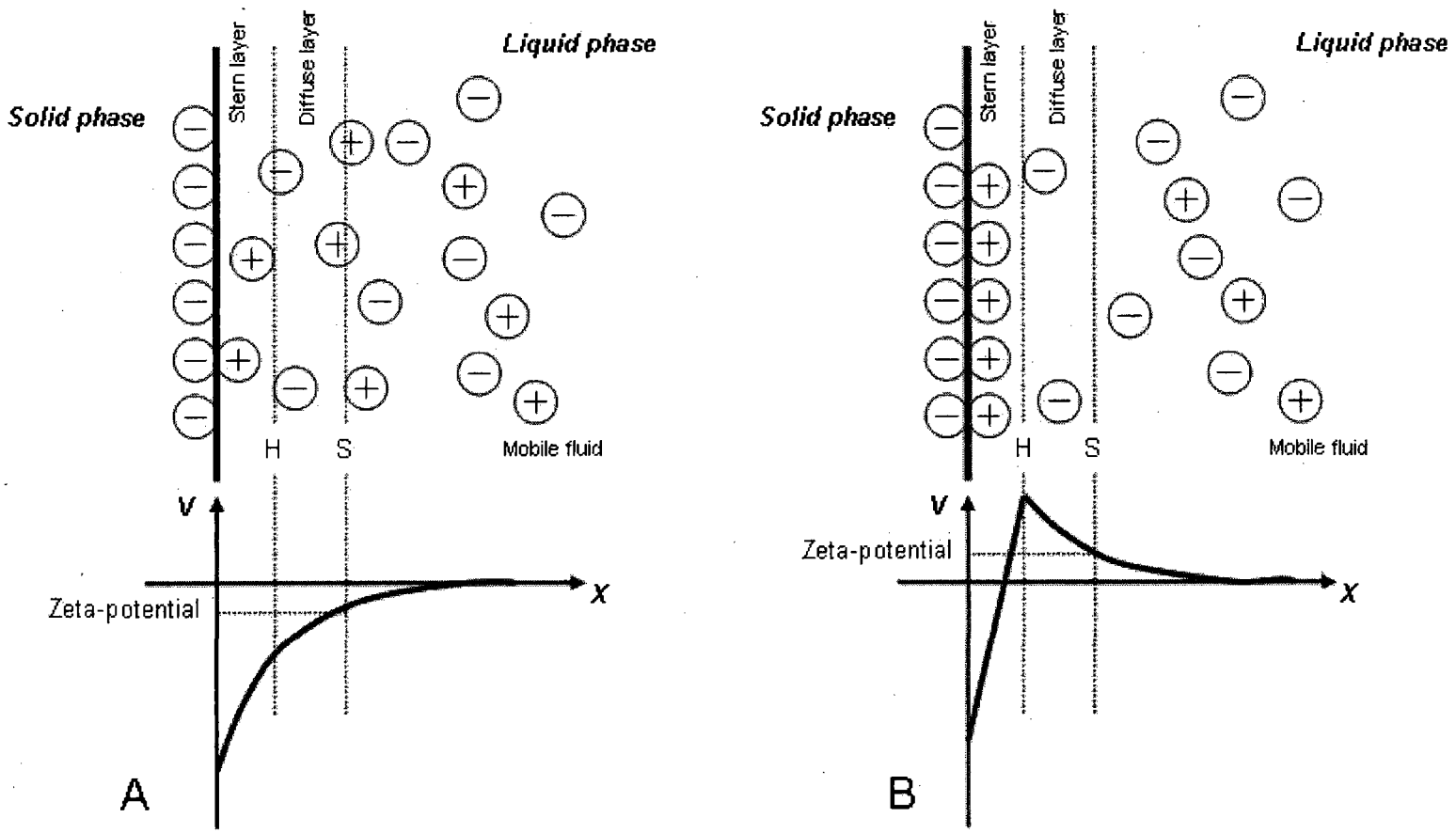

Figure 3-1: The electrical double layer at the solid – liquid phase interface according to the stern model, and the electric potential (V) distribution as a function of the distance (X) from the solid phase wall. The hydrodynamic slipping plane (S) separates the mobile and stationary liquid phase. The potential at this plane is called the zeta-potential (ζ). Depending on the amount of specific adsorption in the stern layer between the pore wall and the Helmholtz plane (H), ζ can be negative (A) or positive (B). For a negative ζ, more positive than negative ions are transported with the fluid.

3.3. ZETA-POTENTIAL MEASUREMENT

The zeta-potential (ζ) is a fundamental property of the double-layer; it is defined as the electric potential at the shear plane in the liquid phase. The zeta-potential is not directly measurable; it can be calculated from surface charge measurements or estimated from electrokinetic measurements. If the first method of finding the zeta-potential is used, the results will be dependent on the assumption utilised for the potential distribution in the electrolyte solution.

The zeta-potential is directly proportional to the surface charge that forms on the solid phase when it is in contact with an electrolyte solution. Adsorption of ions is the main chemical process that acts to develop a surface charge, unless the solid phase already possesses a surface charge induced by an unbalanced crystalline structure (clay minerals for example). The adsorption of ions is dependent on the chemical composition of both the solid and the electrolyte.

The pH value of the electrolyte solution is the main chemical property that has the most effect on the surface charge and hence the zeta-potential. Stumm (1992) showed that the surface charge density decreases with increasing pH, consequently the zeta-potential will also decrease with increasing pH.

The ionic strength of the electrolyte solution is another chemical property that affects the zeta-potential by influencing the thickness of the double layer. The ionic strength is a measure of the amount of charged particles in the electrolyte solution, it is defined as

$$I = \frac{1}{2}\sum c_i \, z_i^2 \qquad \textbf{(Eq. 3-1)}$$

where c_i is the number of charged particles of type i and charge z_i. A higher ionic strength will compress the diffused layer against the solid phase, reducing its thickness, hence reducing the zeta-potential.

The pH of the electrolyte solution has a further influence on the zeta-potential by affecting the ionic strength. At extreme pH values, high concentrations of negative or positive charges are available. These are negative in the case of high pH values and positive in the case of low pH value. These high concentrations will contribute to increasing the ionic strength of the solution, hence reducing the zeta-potential.

The temperature is another factor that has an indirect influence on the zeta-potential. The temperature influences all the chemical processes that contribute to the formation of the surface charge. The equilibrium constants of various minerals and electrolyte solutions are temperature-dependent and the thickness of the double layer is also affected by the temperature. The temperature influence on the zeta-potential is difficult to predict due to the simultaneous contribution of several temperature-dependent mechanisms.

3.3.1. ELECTROACOUSTIC MEASUREMENT OF THE ZETA-POTENTIAL

Recently, significant advances have been made in the theory and application of electroacoustic spectroscopy to characterise the zeta-potential (O'Brien et al. 1995, Hunter 1998, Ohshima 1998, Ohshima and Dukhin 1999, Dukhin and Gortez 2002).

Electroacoustic spectroscopy measures either the colloid vibration current / potential (*CVI / CVP*) or the electrokinetic sonic amplitude (*ESA*), which are directly related to the ζ potential. The ESA occurs when an alternating electrical field is applied to particles in suspension which generates a sound wave of the same frequency. On the other hand, when a sound wave passes through particles in suspension, tiny dipoles created on the charged particles add up to yield a macroscopic electric field alternating at the same frequency. The generated electric disturbance can be measured by two electrodes as a colloid vibration potential (*CVP*) or as a colloid vibration current (*CVI*) (O'Brien et al. 1995, Dukhin and Gortez 1996b, Hunter 1998, Dukhin et al. 1999 a & b).

Before the introduction of electroacoustic spectroscopy and related theoretical models, the zeta-potential was usually measured in either dilute systems (electrophoresis method and sedimentation method) or in high solid concentrations of large particles (electro-osmosis or streaming potential). Conversely, the electroacoustic method is applicable in either relatively dilute or quite concentrated suspensions.

A summary of the theory behind electroacoustic spectroscopy is presented below. For practical reasons, this paragraph is based on the theory and application of the DT-1200 (Dispersion Technology) instrument used in this thesis. Other different theoretical approaches and acoustically based instruments are available, for example the Matec Applied Sciences ESA-9800 based on the O'Brien 1995 theory.

3.3.1.1 Theory of electroacoustic spectroscopy

Electroacoustic spectroscopy deals with the electrokinetic losses resulting from the interaction of electric and acoustic fields in colloidal dispersions, the theoretical treatments require assumptions about the electrical properties of the solid surface.

The EDL on the solid surface is simplified, it is assumed to have two components, a hydrodynamically immobile layer (Stern layer) and a hydrodynamically mobile layer (diffuse layer). As discussed earlier, the thickness of the diffuse layer is dictated by the ionic strength of the solution. The two layers are considered to be separated by a slip plane and the electrical potential difference between the slip plane and the bulk solution is associated with the zeta-potential, which appears to be regulating the colloid interactions. A more thorough description can be found in Hunter (2001) and Lykelema (1995).

The density contrast between the particle and the medium causes a polarization in the EDL in response to an acoustic wave, creating a dipole moment (Figure 3-2) with a magnitude that varies with the amplitude of the acoustic wave (Hunter 1998).

The sum of the individual dipoles gives rise to an alternating electric field measured as a colloid vibration potential (CVP) or a colloid vibration current (CVI). On the other hand, an alternating electric field induces an oscillating electrophoretic motion, thus producing a sound wave or the electrokinetic sonic amplitude (ESA) effect.

There are several factors that determine the magnitude of the electroacoustic signal. Large differences in density between the particles and the medium and high suspension concentration yield a large signal, while a low zeta-potential will yield a small signal. The electrolyte solution contributes a small signal, which could be significant in very dilute systems or low zeta-potential (O'Brien et al. 1995). The surface current could be significant when particle size and/or the electrolyte concentration are small (Hunter 1998). Most theories assume that particles are spherical and the EDL is thin with respect to the particle size.

The colloid vibration current (CVI) is similar to the sedimentation current. The sedimentation current takes place when the potential generated by charged particles settled under gravity is short-circuited between vertically placed electrodes (Dukhin et al., 1999b). In electroacoustics, an alternating acoustic field provides the acceleration, instead of gravity. A tangential electric field is generated by the surface current (I_s), and the compensating current (I_n) is measured in the electroacoustics colloid vibration current (CVI) (Figure 3-2) (Dukhin and Goetz, 1996a).

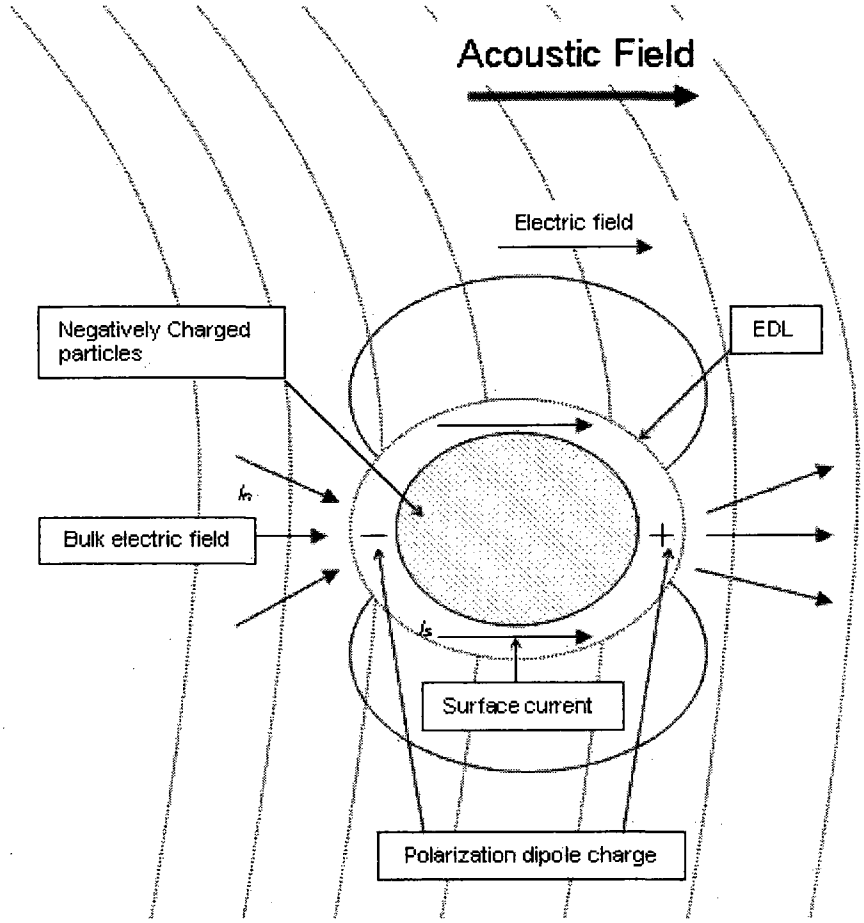

Figure 3-2: Schematic figure of dipole movements generated on a charged particle due to an applied acoustic field and the mechanism of polarization of the EDL (Adapted after Dukhin and Goetz, 1996a)

3.3.2. STREAMING POTENTIAL MEASUREMENT OF THE ZETA-POTENTIAL

Streaming potential occurs when a liquid phase in contact with solid phase is in motion due to mechanical forces. The electric double layer that forms at the interface (solid – liquid) causes the transport of excess charges along with the flow. This transport of charges results in a surplus of charges downstream and a deficiency upstream, this potential difference is the streaming potential.

The streaming potential will induce an electric conduction current that will flow in the opposite direction of liquid flow through both the solid matrix and liquid body, provided the solid matrix is conductive. If the solid material is electrically conductive, the magnitude of the streaming potential will be decreased.

Lamb (1945) demonstrated the direct relationship between the electric potential difference and the fluid pressure difference with a simple example of flow through a capillary tube. The surface charge develops on the side of the tube wall and the convection current is carried with the fluid through the tube. This example can be expanded to include flow through porous media.

A porous medium defines anything from a granular material filled space to a solid porous rock mass. Any liquid driven by a pressure gradient to flow through a porous medium will produce a streaming potential in the same manner as in a capillary tube. However, the geometry of the flow becomes considerably more complex in the porous medium; Overbeek (1952) demonstrated that the equation defining the streaming potential coefficient (C_S) in capillary tube applies equally to the case of a porous medium provided the surface conductance is negligible.

3.3.2.1 Formulation of the streaming potential in porous media

Assuming that the flow is laminar and the pore's radius is much larger than the thickness of the double layer, the convective current per unit area, i_{conv}, over a pore is given by (Overbeek 1952)

$$i_{conv} = \frac{\zeta \, \varepsilon_r \, \varepsilon_0}{\eta} \Delta P \qquad \textbf{(Eq. 3-2)}$$

i_{conv}	:	*convective current per unit area*
ζ	:	*zeta potential*
ε_r	:	*relative dielectric constant of the liquid*
ε_0	:	*dielectric constant of vacuum*
η	:	*viscosity of the fluid*
ΔP	:	*mean pressure gradient normal to the cross-section area*

It is important to note that since the fluid flows in the direction of the negative pressure gradient ($-\Delta P$), and as ε_r, ε_0 and η are positive constants, if ζ is negative, i_{conv} is positive in the direction of flow, and there is a transport of ions with the flow.

As a result of the convection current, an electric potential gradient is generated along the flow path. The potential gradient causes the current to flow back through the liquid by conduction. The conduction current per unit area is given by Ohm's law

$$i_{cond} = -\sigma_f \, \Delta V \qquad \textbf{(Eq. 3-3)}$$

i_{cond}	:	*conduction current per unit area*
σ_f	:	*bulk conductivity of the liquid*
ΔV	:	*potential gradient normal to the cross-section area*

In the absence of any external source of current the total current is the sum of the convective and conductive currents, $i_{total} = i_{conv} + i_{cond}$. In the case of steady-state conditions the two currents are balanced, $i_{cond} + i_{conv} = 0$ ($i_{cond} = - i_{conv}$), hence the total current is equal to zero.

Equating equations 3-2 and 3-3 yields a directly proportional relationship between the potential gradient (ΔV) and the mean pressure gradient (ΔP) known as the Helmholtz-Smoluchowski equation

$$C_S = \frac{\Delta V}{\Delta P} = \frac{\varepsilon_r \varepsilon_0 \zeta}{\eta \sigma_f} \qquad \textbf{(Eq. 3-4)}$$

C_S : *streaming potential coefficient*

The conductive part of the current flow can be described by equation 3-4 provided that the conduction takes place only in the bulk of the fluid. If the conduction on the solid surface is important, which is often the case for low-concentration electrolyte solutions or in the presence of conductive minerals (usually present in sulphide rich tailings), the return current will flow in both the fluid and on the surface of the solid medium, then the bulk conductivity of the porous media can be used in place of the fluid conductivity and the entire area will replace that of the capillaries. To account for the surface conductance, equation 3-4 transforms to

$$C_S = \frac{\Delta V}{\Delta P} = \frac{\varepsilon_r \varepsilon_0 \zeta}{\eta \sigma_b} \qquad \textbf{(Eq. 3-5)}$$

where σ_b is the bulk conductivity of porous media ($\sigma_b = \sigma_f + 2\sigma_s/r$), in the case of a cylindrical pore r_p is the radius and σ_s is the specific surface conductance (Overbeek 1952).

Water leakage from dams is driven by hydraulic head (ΔH) rather than pressure gradient (ΔP). Since $P = \rho_w\ g\ H_h$ where ρ_w is the density of the fluid (expressed in kg/m^3), g is the specific gravity (9.81 m/s^2) and H the hydraulic head, equation 3-4 can be written as

$$C_S = \frac{\Delta V}{\Delta H} = \frac{\varepsilon_r \varepsilon_0 \zeta \rho_w g}{\eta \sigma_f} \qquad \textbf{(Eq. 3-6)}$$

It can be concluded that the streaming potential gradient is proportional to the pressure gradient. In controlled laboratory experiments equations 3-5 and 3-6 can be used for determining the streaming potential coefficient (C_S) and the zeta-potential (ζ).

Numerous studies have been carried out to determine the zeta-potential for different types of rocks and minerals, using coarse crushed sample, and to investigate the dependency of C_S and ζ on different parameters such as pH, temperature, and electrolyte concentration (Ahmad 1964, Ishido and Mizutani 1981, Morgan et al. 1989, Jouniaux and Pozzi 1995a & b, Truesdail et al. 1998, Lorne et al. 1999, Revil et al. 1999a & b).

In models relating streaming potential to water (or any other fluid) leakage from embankment dams, the seepage is regarded as the main flow producing the electric current flow, and the induced current flow effect on leaking water (electo-osmosis) can safely be neglected (Sill 1983, Fitterman 1978, Ishido and Pritchett 1999). The water and current flow are interdependent and are referred to as coupled. Because water leakage is usually described by Darcy's law

$$\frac{Q}{A_a} = -\frac{k}{\eta}\Delta P = -\frac{k\,g\,\rho}{\eta}\Delta H = -K\,\Delta H \qquad \textbf{(Eq. 3-7)}$$

Q	:	*fluid flux (volume / time)*
A_a	:	*cross-sectional area (m^2)*
k	:	*intrinsic permeability (m^2)*
K	:	*hydraulic conductivity (m/s)*
Q/A_a	:	*Darcy's velocity ($Q / A_a = v$)(m/s)*

and the voltage gradient ΔV can be expressed in term of fluid flux Q

$$\Delta V = \frac{C_s\,\eta}{k}\frac{Q}{A_a} \qquad \textbf{(Eq. 3-8)}$$

3.3.2.2 Numerical modelling of the streaming potential phenomenon and the coupled flow theory

The numerical modelling of the streaming potential is a powerful tool for understanding and interpreting the measured anomalies. As previously stated, several simple models have been devised involving charged bodies of various shape, however this approach does not consider the nature of the source generating the anomaly. Hence an approach that takes into account the source generating the anomaly as a function of the physical properties of the medium and the driving forces will provide a more realistic interpretation.

The streaming potential anomalies are due to an electric current generated by the flow of a liquid with respect to a solid. The liquid flow is defined by Darcy's law while the current flow is defined by Ohm's law. Both are related to one another by the theory of coupled flow. This approach was used by several researchers who developed different numerical modeling tools SPXCPL (Sill and Killpack 1982), SPDIKE (Fitterman 1982), SP3D (Sheffer and Howie 2003), SPiso3D (Bérubé 2004). The following is an example of the formulation of the coupled flow theory (Bérubé 2004) used in modeling streaming potential phenomenon.

Formulation of the coupled flow theory used in SPiso3D (Bérubé 2004)

The coupled flow theory is a thermodynamic theory that is used to relate different flow phenomena such as hydraulic flow, heat transfer, electric current and chemical flow. These flows are usually driven by gradients of the same type. However, it is necessary to consider coupled flows under some circumstances. A coupled flow is a flow driven by another type of gradient, such as an electric current driven by a liquid flow. The generalized coupled flow equation is as follows (Yeung, 1990)

$$J_i = \sum_{j=1}^{n} L_{ij} \; X_j \qquad \textbf{(Eq. 3-9)}$$

J_i : *flow density of type i*
L_{ij} : *coupling coefficient (relating the flow of type i to a force of type j)*
X_j : *gradient (driving force) of type j*

Using this equation to account for all possible coupled flows would be extremely difficult; hence the outcomes of some of the driving forces are assumed to be negligible.

In the case of streaming potentials only the hydraulic and electric gradients are considered. The chemical and thermal gradients are assumed to be equal to zero. These assumptions will result in the following equations

$$Q_a = -L_{11}\Delta\xi - L_{12}\Delta\phi \qquad \textbf{(Eq. 3-10)}$$

and

$$J = -L_{21}\Delta\xi - L_{22}\Delta\phi \qquad \textbf{(Eq. 3-11)}$$

Q_a : *liquid flow density (volume / unit area)*
J : *electric current density*
$\Delta\xi$: *pressure potential gradient*
$\Delta\phi$: *electric potential gradient*
L_{11} : *relates the fluid flow to a pressure gradient and becomes the hydraulic conductivity (K)*
L_{22} : *relates the current flow to a potential gradient and becomes the bulk conductivity (σ_b)*
L_{12} : *cross-coupling conductivity that relate the liquid flow to a potential gradient (electro-osmosis phenomenon)*
L_{21} : *cross-coupling conductivity that relate the current flow to pressure gradient (stream-potential phenomenon)*

According to Onsager reciprocal relations, the cross-coupling conductivities L_{12} and L_{21} are equal ($L_{12} = L_{21} = L$) (Yeung and Mitchell 1993). If the cross-coupling conductivities in equations 3-10 and 3-11 are neglected, then the only direct flow terms remaining will reduce equation 3-10 to Darcy's law and equation 3-11 to Ohm's law.

The main limitation of the coupled flow theory is that it assumes a linear relationship between the flows and each driving force, which has been proven to be the case within wide limits by various researchers; however this limitation should be kept in

mind when dealing with large flows and gradients. Another simplification in the use of the coupled theory is that the medium is locally homogeneous, which implies that average values of the coupling coefficients are used rather than separate values for pore and matrix, resulting in average flow values.

With the total current density J within a homogeneous area of a porous medium equal to zero at all points, equation 3-11 becomes

$$\frac{\Delta\phi}{\Delta\xi} = -\frac{L}{\sigma_b} \qquad \textbf{(Eq. 3-12)}$$

For a volume of one unit area by length l, the potential and pressure gradient can be approximated respectively by $\Delta\phi = \Delta V / L$ and $\Delta\xi = \Delta P / L$. This allows a comparison with equation 3-4, giving a streaming potential coefficient C_S

$$C_S = -\frac{L}{\sigma_b} = \frac{\Delta V}{\Delta P} = \frac{\varepsilon_r \varepsilon_0 \zeta}{\eta \sigma_f} \qquad \textbf{(Eq. 3-13)}$$

CHAPTER : 4 CHARACTERISATION OF PYRITE RICH TAILINGS

4.1. INTRODUCTION

Three pyrite rich tailings from three different base metal mines from the Abitibi region in Quebec were selected for this research because of their diverse characteristics. They are representative of existing pyrite rich tailings in Abitibi and they are considered representative of typical sulfide tailings from hard rock Canadian mines. A brief description of these mines is given in Table 4-1. In the following, the tailings obtained from the three different mines are identified as LA, LV and BH.

Table 4-1: Mine description.

	Type of deposit	Valuable metals	Sulphide minerals	Silicate minerals
Mine LA	VMS*	Au, Ag, Cu, Zn	Pyrite	Quartz
Mine LV	VMS*	Cu, Zn (Au, Ag)	Pyrite	Quartz
Mine BH	VMS*	Cu, Zn (Au, Ag)	Pyrite	Quartz

* Volcanogenic Massive Sulphide

It is well known that tailings evolve with time due to numerous chemical reactions taking place in the pond. The main chemical reaction taking place is the oxidation of the sulfides which is a complex biogeochemical process involving hydration, oxidation, and hydrolysis (Nordstorm 1982). This process can be summarized in a simplified form in the reaction proposed by Stumm and Morgan (1981)

$$FeS_2 + 3.75\,O_2 + 3.5\,H_2O \rightarrow Fe(OH)_3 + 2\,H_2SO_4$$

In order to establish a basis for comparison between the three sampled tailings, to eliminate any adverse effect of the oxidation of the pyrite rich tailings on the measured zeta-potential and resistivity, and to establish base line measurements for these

parameters, the samples had to be "fresh". The three samples were collected from the tailings discharge pipe as slurry with approximately 40 to 50 % wt. solids and were stored with minimal air contact to preserve their physicochemical properties as much as possible and to prevent the oxidation of the sulfides.

This chapter provides a physical and mineralogical characterisation of the selected mine tailings. Standard soil mechanics and mineralogical techniques were used in the tailings characterisation.

4.2. PHYSICAL CHARACTERISTICS OF THE TAILINGS

The permeability of the tailings is primarily governed by particle grain size distribution and particle shape and texture, as they affect the way the tailings pack together upon deposition. An increase in the fines portion decreases the permeability by filling up the voids between the coarse particles. The shape and texture of the particles reduces the flow rate. Elongated or irregular particles create a more complex flow path and the surface roughness offers more frictional resistance to the flow. Hence, the gradation and particle shape and texture are regarded as one of the most important factors affecting the permeability of mine tailings.

The hydraulic conductivity (K) of the mine tailings from the Abitibi region has been extensively studied by several researchers (L'Ecuyer et al. 1992; Aubertin et al. 1993, 1996; Bussiere 1993; Monzon 1998; Chapuis and Aubertin 2003). The hydraulic conductivity value for these tailings usually varies between 10^{-6} and 10^{-7} m/s (Aubertin et al. 1996). It is important to note that the hydraulic conductivity measured in either a rigid-wall permeameter or in a triaxial cell and the K value estimated using the Kozeny-Carman equation is that of homogenized tailings under saturated conditions (Aubertin et al. 1996; Mbonimpa et al. 2002; Chapuis and Aubertin 2003). These measurements or estimations cannot be used to predict the exact value of the hydraulic conductivity of intact saturated samples because of the existence of a high horizontal anisotropy in the hydraulic conductivity induced by the stratification of the tailings (Chapuis and Aubertin 2003).

4.2.1. PARTICLE SIZE ANALYSIS

There are numerous techniques used to determine the grain size distribution of the tailings. These include among others sieving, hydrometer, cyclosizer, microscopy, light / laser scattering particle size analyser and acoustic particle size analyser.

In this thesis, the particle size distribution of particles larger than 0.075 mm (retained on the No. 200 sieve) was determined by sieving, while the distribution for the particle sizes smaller than 0.075 mm was determined by sedimentation process using a Cyclosizer (Warman International) and validated by using a light scattering particle size analyser (Horiba LA-920).

The Cyclosizer is a laboratory precision apparatus for accurate determination of particle size distribution for particles smaller than 0.075 mm. Particles are separated according to their Stokesian setting characteristics by a principle based on the hydraulic cyclone principle. The Horiba LA-920 is also a laboratory precision apparatus for accurate determination of grain size distribution for particles ranging from 0.02 μm up to 2 mm.

The resulting grain size distributions of the three tailings are shown in Figure 4-1. Also shown in Figure 4-1 are the ASTM and British standard and M.I.T. classifications (Holtz and Kovax 1981), which were used to classify the tailings. The particle size distributions of the LA and LV samples are fairly similar, with 80 % passing sieve # 200 while the BH tailings sample is considerably finer with 93 % passing sieve # 200. Table 4-1 shows the distribution of the basic particle sizes based on the B.S. classification. This table shows that the bulk of the material analysed can be categorised as silt, with a considerable amount of fine sand.

In classical soil mechanics, the classification of any granular material is mainly determined by the uniformity coefficient and the coefficient of gradation (Holtz and Kovax 1981). The uniformity coefficient C_u, is defined as the ratio of 60 % particle size to the 10 % particle size: (Head 1992)

$$C_U = \frac{D_{60}}{D_{10}} \qquad \textbf{(Eq. 4-1)}$$

The uniformity coefficient is a measure of the general slope of the grain size distribution. Hence, a single-sized soil has a C_u equal to one, a uniform soil has a C_u less than three, and a well graded soil has a C_u greater than 5.

The coefficient of gradation (C_k) measures the shape of the particle size distribution curve between D_{10} and D_{60}. It is defined as:

$$C_k = \frac{D_{30}^2}{D_{10}\ D_{60}} \qquad \textbf{(Eq. 4-2)}$$

A C_k value between 0.5 and 2 indicates a well-graded soil, while a C_k less than 0.1 indicates a possible gap-graded soil (Head 1992).

Table 4-2: Physical characteristics of the sulphide rich tailings.

Tailings	B.S. & M.I.T. classification			C_u	C_k
	Sand (%)	Silt (%)	Clay (%)		
LA	20	78	2	5	0.92
LV	20	78	2	5.8	1.07
BH	10	86	4	5.6	1.74

4.2.2. SPECIFIC GRAVITY

The specific gravity is defined as the ratio between the weight of a mineral and the weight of an equal volume of water. The specific gravity of the different tailings was determined using the ASTM D854-06 (ASTM 2006) method. The average specific gravity (G_S) results for the LA, LV and BH tailings are respectively 3.53, 3.44 and 3.85. These relatively high values are mainly due the presence of pyrite in the tailings in considerable quantities. The specific gravity of pyrite ranges from 4.95 to 5.10.

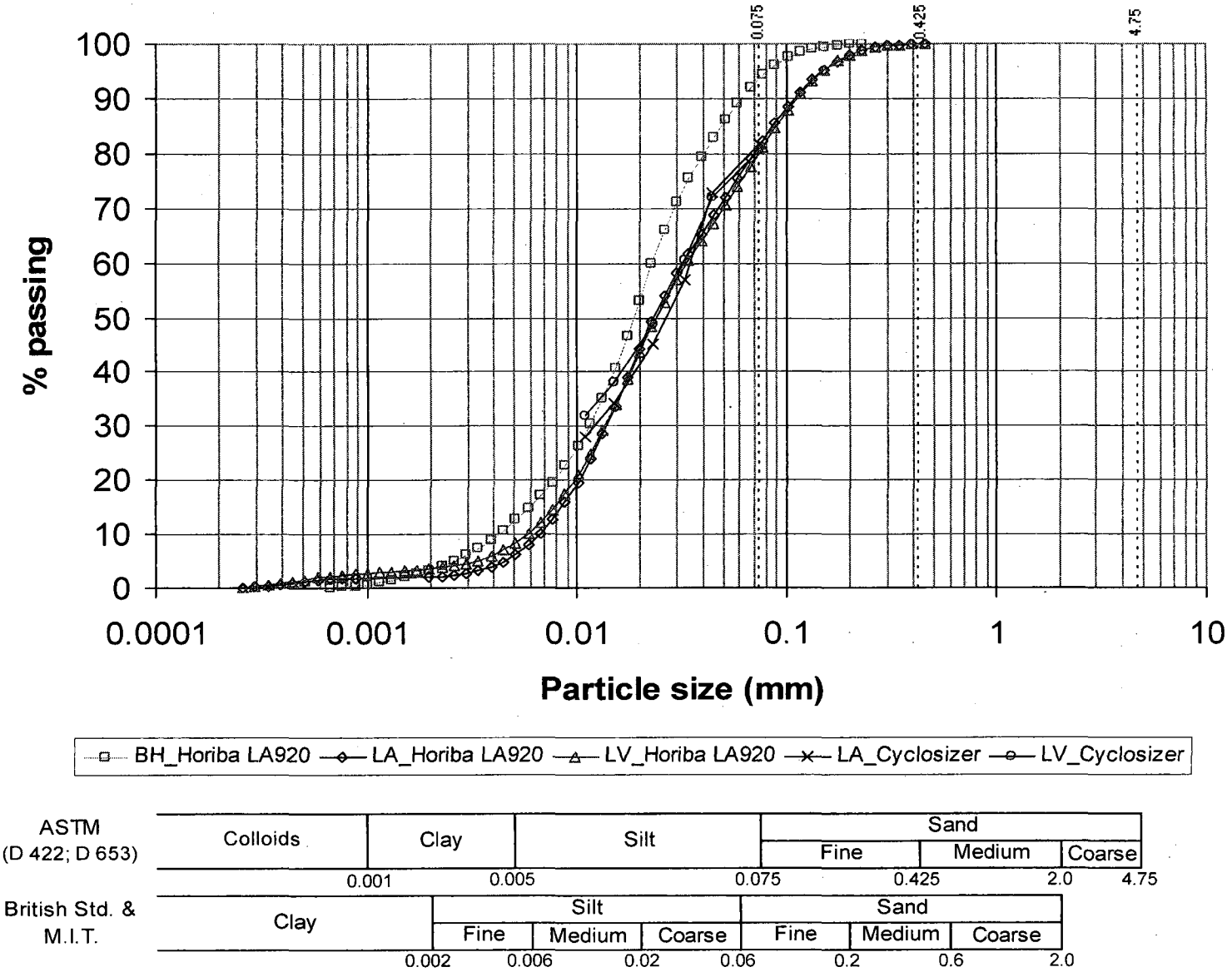

Figure 4-1: Particle size distribution of the three studied tailings (cumulative curves).

4.2.3. PARTICLE SHAPE AND SURFACE TEXTURE

As discussed earlier, particle shape and texture have a significant impact on the water flow through the tailings. The particle shape is commonly described by visual observations as it is categorized by the relative sharpness of the edges and corners. The surface texture is also described by visual observations; this observation is based on the degree of roughness of the particle surface.

The particle shape and surface texture of the studied tailings were determined using the Scanning Electron Microscopy (SEM) photographs. The samples for the SEM were prepared by sprinkling the tailings on a double sided adhesive tape fixed on an aluminum sample holder. The particles were then coated with gold before being tested in the SEM (JOEL 840-A). The microphotographs of the studied tailings are shown in Figures 4-2, 4-3 and 4-4. The Powers's (Powers 1953) grain images for estimating the roundness of sedimentary particles was used in conjunction with the petrographic analysis and the microphotographs to determine the tailings particle shape and texture. The results are shown in Table 4-3.

Table 4-3: Particle shape and texture based on the Powers's grain image.

Tailings	Particle Shape	Surface Texture
LA	Angular & Acicular	Smooth
LV	Angular & Acicular	Smooth
BH	Angular	Smooth

In table 4-3, Angular is defined as possessing well defined edges formed at the intersection of several planar faces, while acicular shape is define as needle-shaped grains. The smooth surface could be due to breakage of laminar or fine grained rock, for the pyrite grains it could be the breakage along the cleavage plane. The studied tailings are as expected, fine grained and angular which is typical of most hard rock mine tailings.

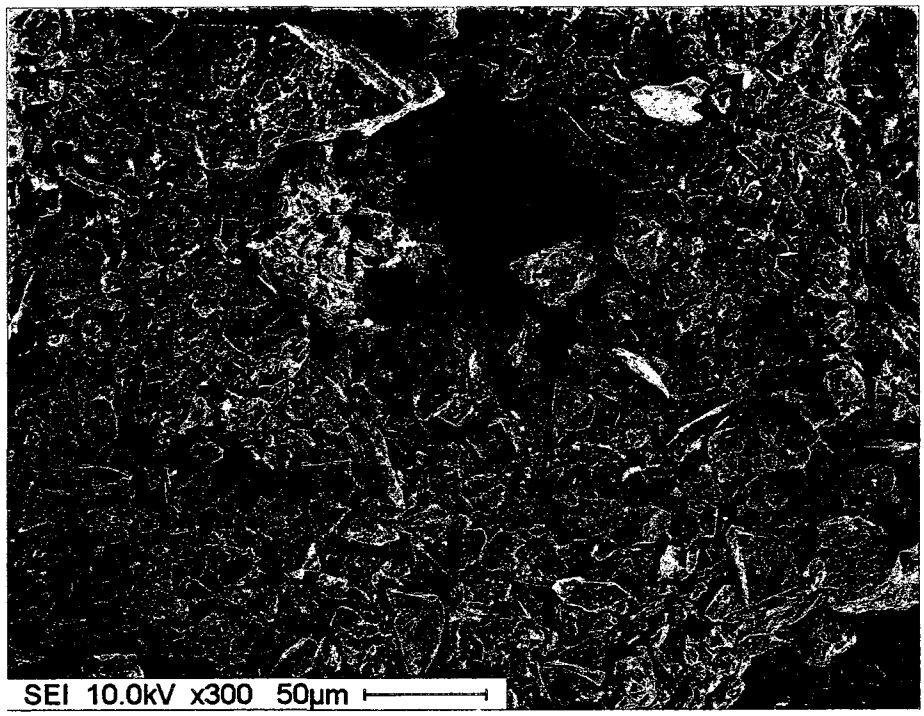

Figure 4-2: Microphotograph of the LA tailings. (Magnification 300)

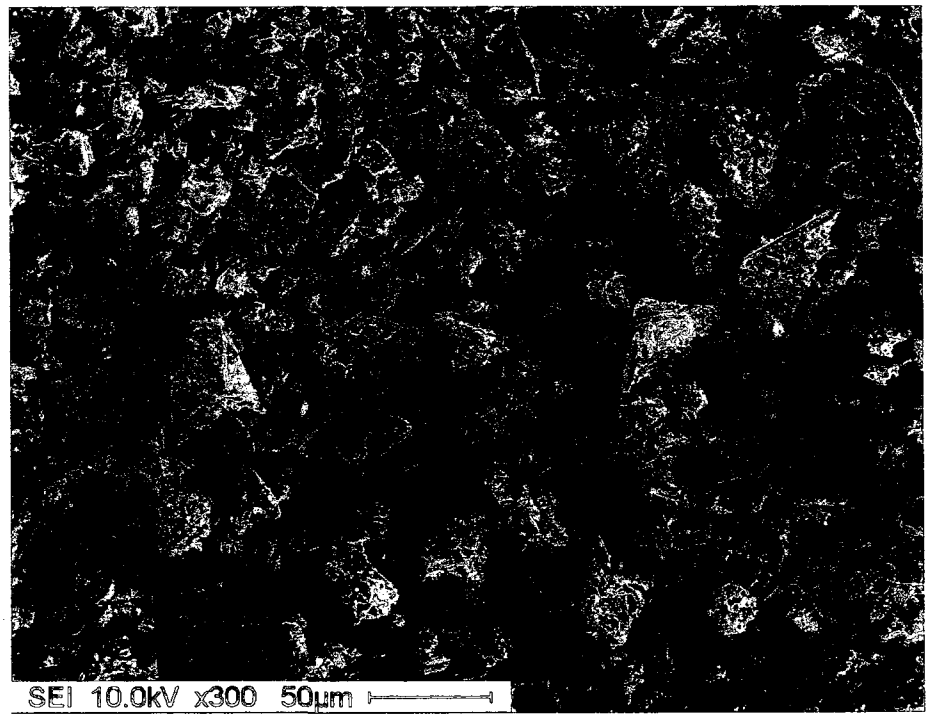

Figure 4-3: Microphotograph of the LV tailings. (Magnification 300)

Figure 4-24: Microphotograph of the BH tailings. (Magnification 300)

4.2.3. EVALUATION OF THE HYDRAULIC CONDUCTIVITY

Chapuis and Aubertin (2003) demonstrated, using various experimental results on a wide variety of soils and tailings, that the hydraulic conductivity (K) estimated using the Koseny-Carman equation, expressed in the appropriate form (Eq. 4-3), provided satisfactory estimates of the K value.

The K value of the three tailings LA, LV and BH was predicted using the modified Kozeny-Carmen equation (Eq. 4-3) proposed by Chapuis and Aubertin (2003) for a void ratio varying between 0.2 and 0.9. The required specific surface area was determined using the Chapuis and Légaré (1992) equation (Eq. 4-4). This equation requires the knowledge of the entire particle size curve, including the smallest sizes, which can significantly influence the value. The calculated specific surface for the LA, LV and BH tailings was respectively 182.67, 224.45, and 172.48 m^2/kg. The variations of the predicted hydraulic conductivity with the void ratio are presented in Figure 4-2, it is

important to note that the presented K values represent the hydraulic conductivity for homogenized tailings samples.

$$\log\left[K_{predicted}\right] = A_c + \log\left[\frac{e^3}{D_R^2\, S_s^{\,2}\,(1+e)}\right] \qquad \textbf{(Eq. 4-29)}$$

K : *hydraulic conductivity (m/s)*
A_c : *constant equal to 0.29 – 0.51*
e : *void ratio*
D_R : *specific weight of the solids ($D_R = \rho_s / \rho_w$)*
S_s : *specific surface (m^2/kg) determined using equation 4-4*
ρ_w : *density of water*
ρ_s : *density of solids*

$$S = \frac{6}{\rho_s}\left[\sum \frac{\left(P_{No\,D} - P_{No\,d}\right)}{d}\right] \qquad \textbf{(Eq. 4-30)}$$

where ($P_{No\,D} - P_{No\,d}$) is the percentage by weight smaller than size D ($P_{No\,D}$) and larger than the next size d ($P_{No\,d}$).

Several researchers (Aubertin et al. 1996; Mbonimpa et al. 2002; Chapuis and Aubertin 2003) compared laboratory measured and predicted K values using the KC equation. They concluded that the results for tailings do not match due to the angular and acicular shape of the tailings grains, which introduces an increased effect of tortuosity (Aubertin 1996). In addition, tailings are prone to particle breakage when compacted during the sample preparation and to chemical reactions during the permeability test (Bussière 1993). All of these phenomena have a tendency to decrease the measured value of the hydraulic conductivity. In order to take all these phenomena into account Chapuis and Aubertin (2003) introduced a best fit linear equation which when combined with Eq. 4-3 yields Eq. 4-5 which represents modified values of the predicted hydraulic conductivity.

$$\log\left[\frac{K}{1\,m/s}\right] = 1.5\left\{0.5 + \log\left[\frac{e^3}{D_R^2\, S_s^{\,2}\,(1+e)}\right]\right\} + 2 \qquad \textbf{Eq. 4-31}$$

It is well known that grain size and clay content are important factors controlling the in-situ void ratio. The in-situ void ratio for most hard-rock mine tailings of sand size generally ranges from 0.6 to 0.9, while the in-place void ratio for slimes of low to moderate plasticity generally ranges from 0.7 to 1.3 (Vick 1983).

The variation of the modified predicted K values are also presented in Figure 4-2, with the K value as a function of the void ratio for the three samples. For a void ratio varying between 0.6 and 0.9, the K values fall between 10^{-7} and 10^{-6} m/s, which is the usual range for homogenized hard rock mine tailings (Pettibone and Kealy 1971; Mittal and Morgenstern 1976; Mabes et al. 1977; Volpe 1979; Matyas et al. 1984; Nowatzki and Robertson 1988; Schiffman et al. 1988; Haile and Kerr 1989; Kamon and Katsumi 1994; Aubertin et al. 1996; Chapuis and Aubertin 2003). From a geotechnical perspective, these tailings are considered to have a low hydraulic conductivity (Head 1992; Cedergren 1997).

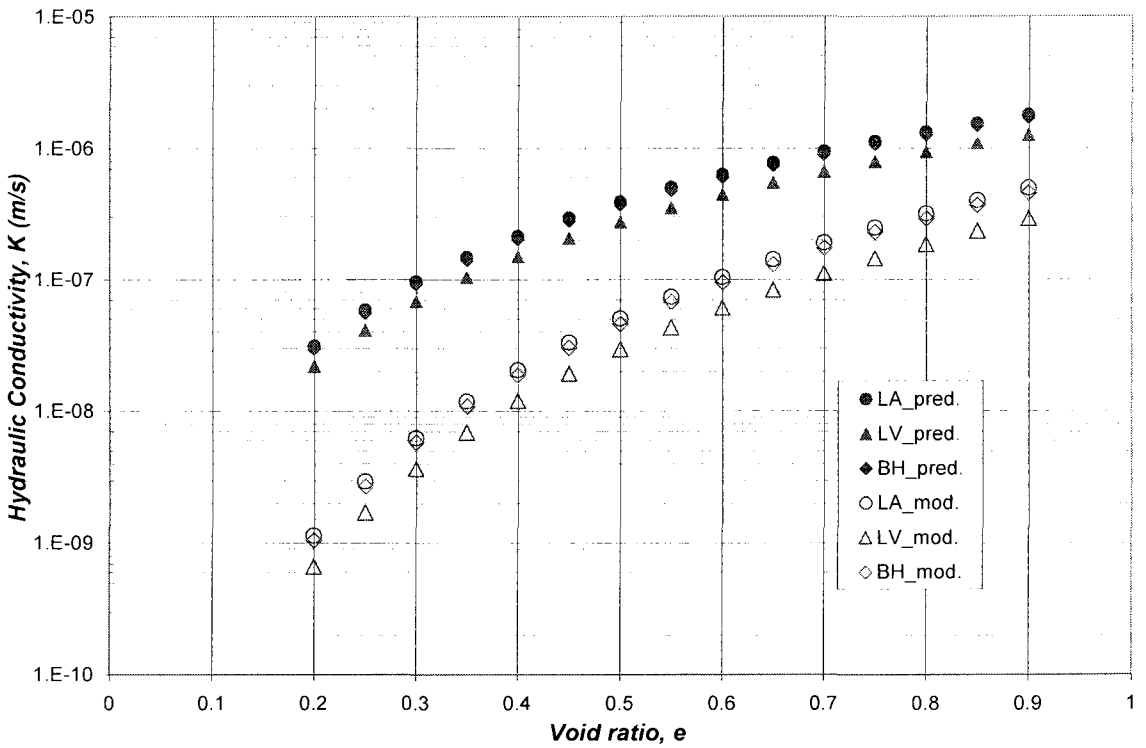

Figure 4-25: Calculated hydraulic conductivity for the LA, LV, and BH tailings from the modified Kozeny-Carman equation.

4.3. MINERALOGICAL ANALYSIS OF THE TAILINGS

Detailed mineralogical analysis was conducted using petrographic study and X-ray fluorescence analysis (XRF) of the three tailings. In order to reinforce the results of the previous study an X-ray diffraction (XRD) analysis was also conducted.

4.3.1. PETROGRAPHIC ANALYSIS

Petrographic microscopy is an extremely useful technique for the identification of minerals, observation of texture, structure, genesis and digenesis. Petrographic microscopy differs from ordinary microscopy in the use of a polarized light source acting from below the specimen. Plane polarized light vibrates in only one plane; it is created by passing ordinary light through a polarizer. For further details concerning this technique the reader is referred to optical mineralogy textbooks which provide a complete description of the physics of polarized light and mineral identification procedure (Nesse 2004 and Gribble 1992).

The samples were prepared for polished thin sections by impregnating the loose tailings with resin. The resin used was Bueheler epoxy, the birefringence of the epoxy used is nil. The cutting was done with water, and polishing with silica diamond. At first, the polishing was performed with 17 micron size and finally, with 1 micron size silica diamond.

The detailed mineralogical analysis of the different samples is presented below. The purpose of this analysis was to determine the amount of sulfides, more precisely pyrite, present in these samples. The sulfides in the studied tailings are almost exclusively pyrite, the other sulfides are rare and only a few grains are present among the pyrite (FeS_2), these include chalcopyrite ($CuFeS_2$), arsenopyrite ($AsFS$) and sphalerite ($(Zn,F)S$). The pyrite grains present are angular, broken fragments with sharp termination. Their grain sizes range from a few microns to 0.3 mm. A summary of the visually estimated percentages of the minerals present in the tailings samples is presented in Table 4-4.

Table 4-4: Summary of the visually estimated percentage of minerals.

Mineral		LA	LV	BH
Quartz	SiO2	35	35	25
Muscovite/Sericite	KAl2 (AlSi3O10)(F, OH)2	7	10	1.5
Carbonate	-	X	5	3
Fragments	-	-	10	15
Pyrite	FeS_2	60	40	55

x = trace amount

– *Petrographic Description of the LA Tailings Sample*

The minerals and lithic fragments present in the LA tailings sample are more coarse-grained than the ones present in the other two samples; LV and BH. The texture however is comparable, as the pyrite-rich areas are sand size particles surrounded by a silicate rich matrix. The pyrite grains, which make up approximately 60 % of the thin section area, are angular, fractured and fragmented grains with sharp terminations. The pyrite grain size ranges from 15 μm to 0.3 mm.

The type of sulfides and silicates present in the LA sample have a wider range than the ones in the LV or BH samples. The sulfides contain few grains of chalcopyrite ($CuFeS_2$), as well as a few poorly crystalline sphalerite ($(Zn,F)S$), magnetite , rutile (TiO_2) and oxyhydroxide.

The quartz grains occur as broken, angular to sub-rounded clasts. The quartz grain size ranges from 10 μm to 0.3 mm. The silicates present in the LA include quartz and muscovite aggregates, single grains of albite laths and a few grains of carbonate and rutile. A summary of the mineralogical analysis is presented in Table 4-5.

Figure 4-6 shows the texture of the sample. Note the numerous anhedral quartz grains, and the plagioclase lath in the center. Figure 4-7 shows the texture and shape of the angular pyrite grains.

Table 4-5: Mineralogical description of the LA tailings sample.

Mineral	%	Grain size (mm)	Comments
Pyrite	60	0.015 - 0.3	Fractured and fragmented pyrite grains of sand-size particles. The angular shape, and the sharp terminations of grains are comparable to the other two tailings samples (LV and BH).
Quartz	35	0.010 - 0.3	The Quartz grains occurs as broken, angular to sub-rounded clasts within the pyrite-rich matrix, and as part of the matrix interstitial to the sand-size pyrite-rich particles.
Muscovite	5	0.020 - 0.3	Muscovite occurs in aggregates, as well as single grains.
Sericite	2		Fine-grained sericite aggregates are common as an alteration in the lithic fragments. They also occur as slightly fibrous aggregates disseminated through the silicate-rich matrix.

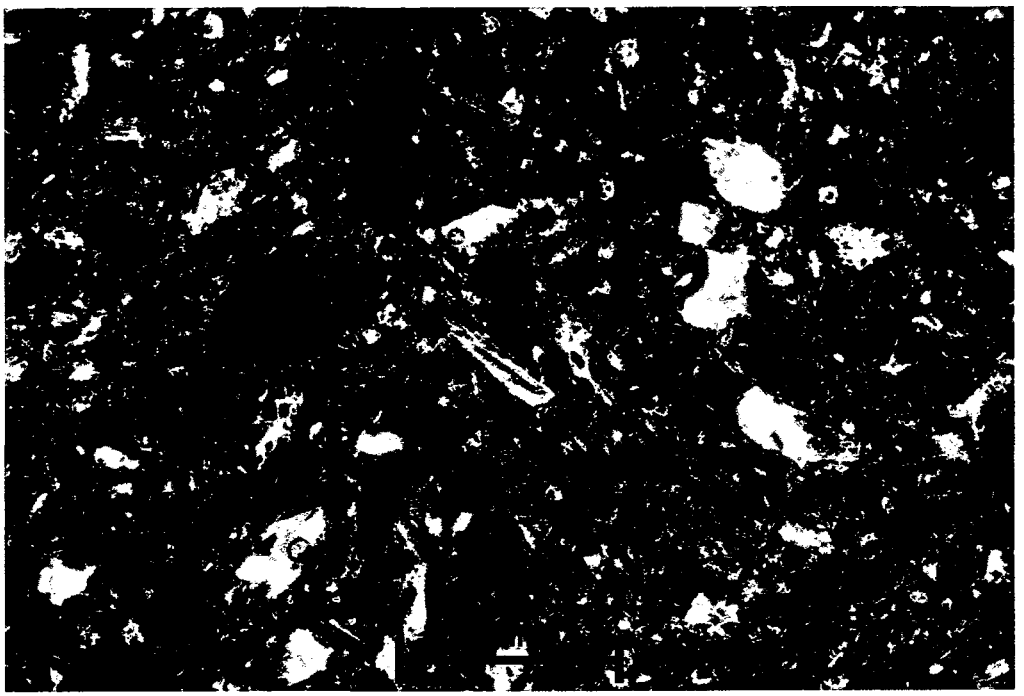

Figure 4-6: Quartz (light colored grains) in dark pyrite and epoxy matrix.

(Width of photo: 2.3mm. XN)

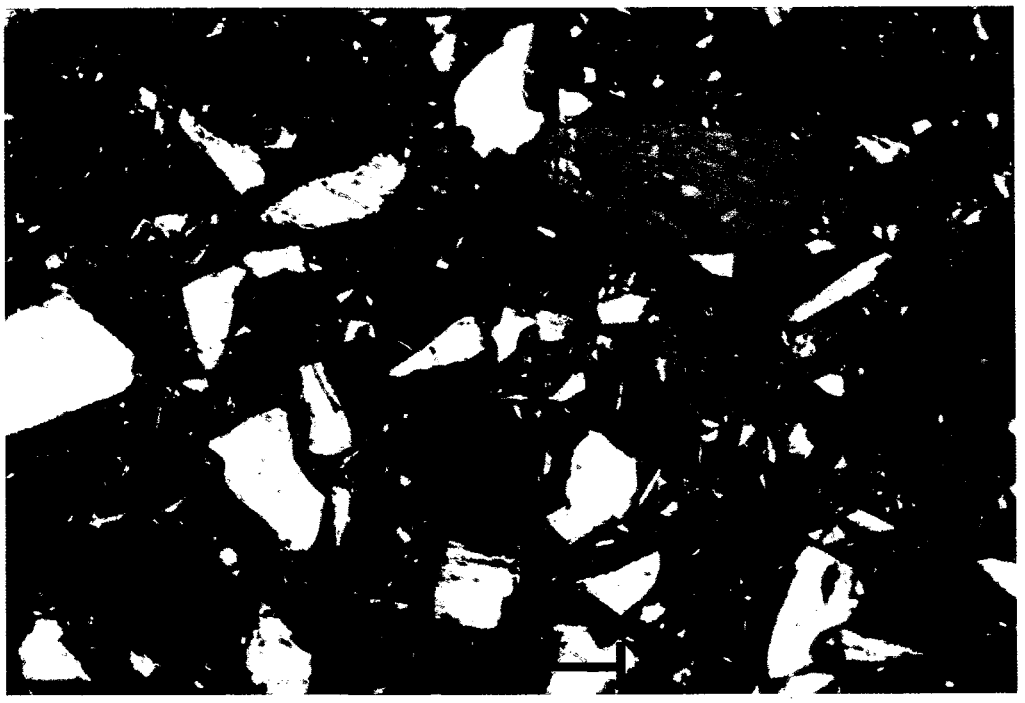

Figure 4-7: Angular pyrite fragments and one large grain that is possibly sphalerite.

(Width of photo: 0.45mm. Refl. Light)

– *Petrographic Description of the LV Tailings Sample*

The mineralogy of the LV tailings sample is similar to that of LA and BH, but pyrite is somewhat less abundant. The petrographic analysis revealed that pyrite occurs in clusters with quartz, sericite aggregates and some lithic fragments. These clusters are of sand size particles. Fine-grained silicates are interstitial to these pyrite-rich particles.

The pyrite grains, which make up approximately 40 % of the thin section area, are all fine-grained, angular grains with sharp terminations. The pyrite grain size ranges from 5 μm to 0.1 mm. The other minerals present in the sample includes small fragments of muscovite, anhedral aggregates of carbonate, apatite inclusions in some the quartz grains, rutile and magnetite. A summary of the mineralogical analysis is presented in Table 4-6.

Figure 4-8 shows the texture of the sample (under transmitted, plane polarized light). The dark areas are the sand-size particles that contain most of the fine-grained pyrite; note also the light colored silicate grains and fragments within the particles. The interstitial silicate and the carbonate rich matrix are light colored. Figure 4-9 shows the same area with reflected light. The fine-grained pyrite is light yellow/tan colored and the gray areas contain the silicates and the epoxy. Figure 4-10 shows the texture of pyrite (at higher magnification).

Table 4-6: Mineralogical description of the LV tailings sample.

Mineral	%	Grain size (mm)	Comments
Pyrite	40	0.005 - 0.1	The pyrite grains are angular with sharp terminations, some are rimmed with Rutile.
Quartz	35	0.001 - 0.2	The broken quartz clasts are relatively abundant.
Carbonate	5	0.010 - 0.05	The anhedral carbonates occur as single grains interstitial to the quartz-rich matrix, but also as fine-grained aggregates.
Sericite / Muscovite	10		Sericite aggregates (with or without quartz) are relatively common in the matrix. Lath-shaped and partly deformed muscovite clasts generally occur as inclusions within the pyrite-rich particles.
Fragments	10	0.001 - 0.2	Fragments are predominantly made of quartz, sericite and carbonate aggregates, The fragments are generally larger than the fragments present in the other two samples. Because of their size, the minerals within fragments are more easily identified.

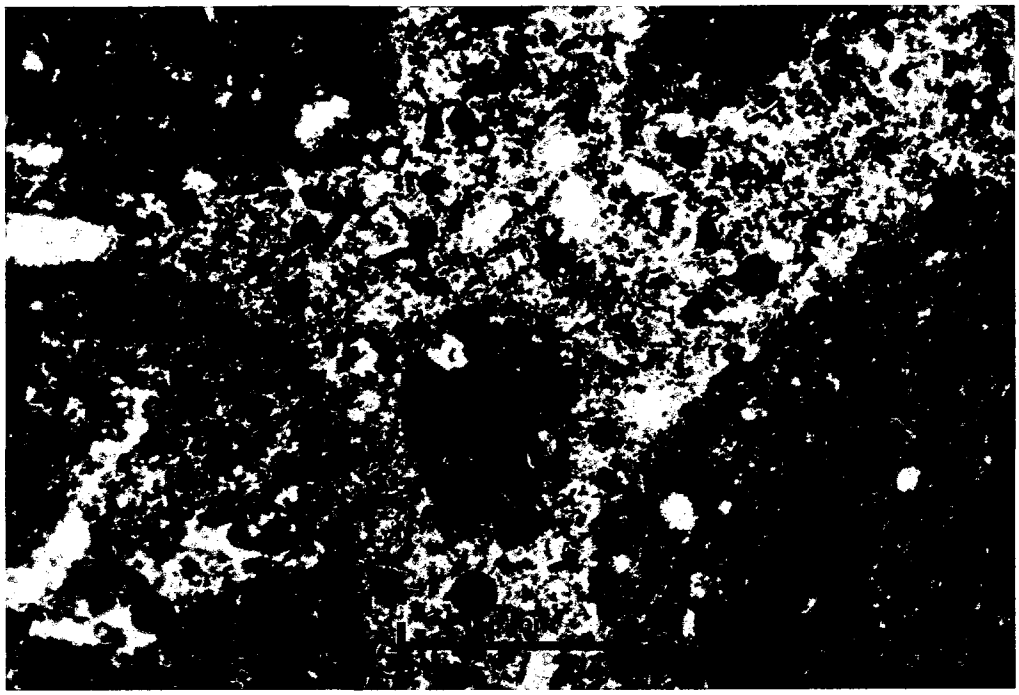

Figure 4-8: Pyrite-rich sand size particles (large black areas) with interstitial quartz-rich matrix. (Width of photo: 2.3 mm. Ppl.)

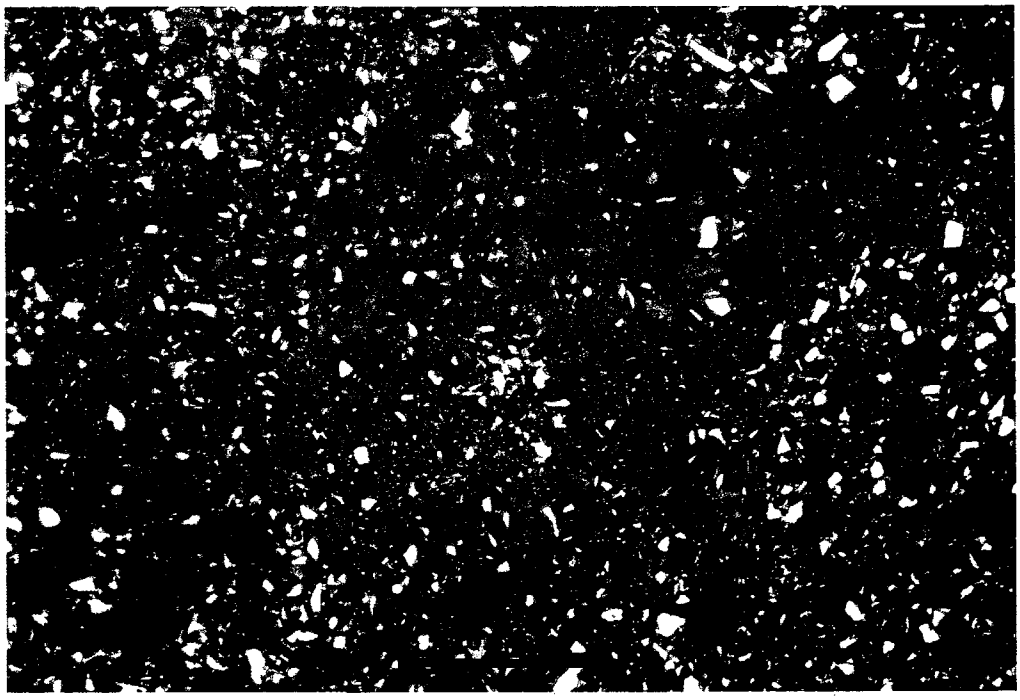

Figure 4-9: As above, with reflected light. Note corresponding letters for same areas in Figure 4-7.

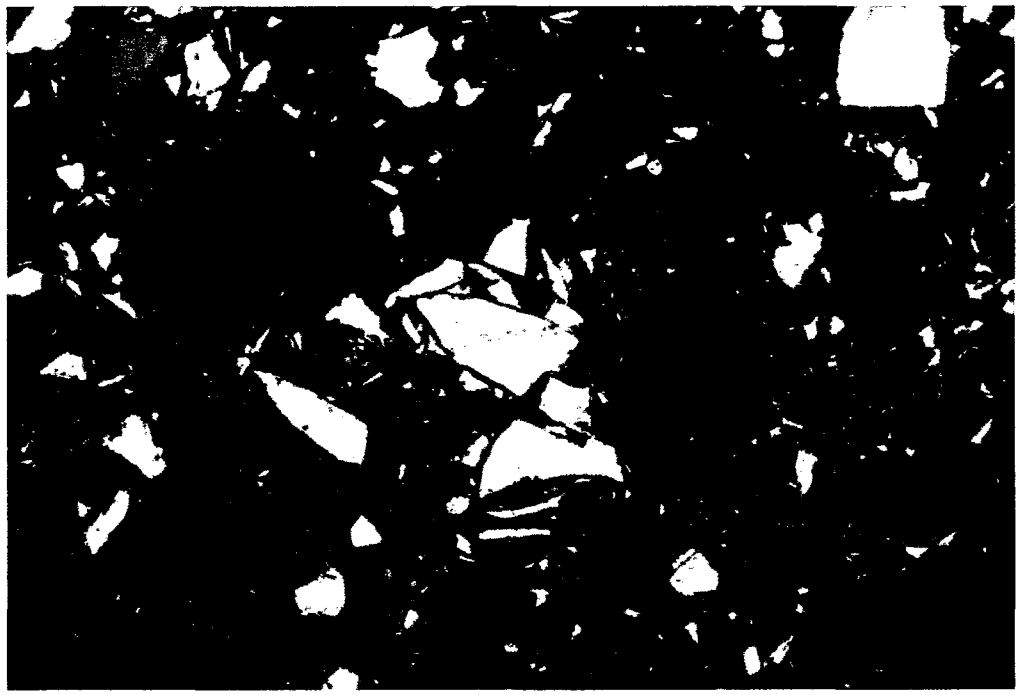

Figure 4-10: Angular pyrite forms aggregate (light colored).
(Width of photo: 0.45mm. Refl. Light.)

– *Petrographic Description of the BH Tailings Sample*

The mineralogy of the BH tailings sample is similar to that of LA and LV. The thin section is composed of sub-rounded, oval and angular sand-size particles with a fine-grained interstitial matrix. The sand-size particles are made up of aggregates of very fine-grained pyrite and to a lesser extent silicates. The silicates are mainly quartz, sericitized quartz fragments and carbonates.

The matrix consists of very fine-grained, anhedral, often cherty quartz, sericite, angular pyrite, minute anhedral grains of carbonate, and rutile. Some of the pyrite-rich sand-size particles contain several inclusions of quartz, whereas others contain mostly sericitized fragments. A summary of the mineralogical analysis is presented in Table 4-7.

Figure 4-11 shows the texture of the sample in reflected light. The sand-size particles consist of angular, fine-grained pyrite (light-colored) separated by the silicate-rich zones. Figure 4-12 shows the same area with transmitted light (and crossed nicols).

The fine-grained light particles are predominantly quartz, with minor sericite, and the dark areas are mainly fine-grained pyrite. Figure 4-13 shows the texture and shape of the fine-grained pyrite at higher magnification under reflected light.

Table 4-7: Detailed mineralogical description of the BH tailings sample.

Mineral	%	Grain size (mm)	Comments
Pyrite	55	0.001 - 0.1	Pyrite are generally angular grains, some are cuspate-shaped and most have sharp terminations. Pyrite makes up much of the sand-size particles which also contain fine-grained quartz and sericitized quartz fragments.
Quartz	25	0.002 - 0.05	Quartz occurs as anhedral, angular to subrounded clasts interstitial to the pyrite-rich sand particles, and make up part of the matrix. Some are chert with slightly fibrous texture, and some occur as aggregates with interstitial sericite.
Carbonate	3	0.005 - 0.03	Minute, anhedral carbonates are interstitial to pyrite aggregates and to the matrix.
Sericite	1.5		Minute sericite aggregates occur as replacement in some lithic fragments and as fibrous, interstitial to the matrix.
Lithic fragments	14	0.03 – 0.3	The lithic fragments consist of anhedral quartz aggregates and interstitial sericite, or carbonate + quartz. The "sericite" may be hydro muscovite or illite. Optical distinction between the species is not possible.

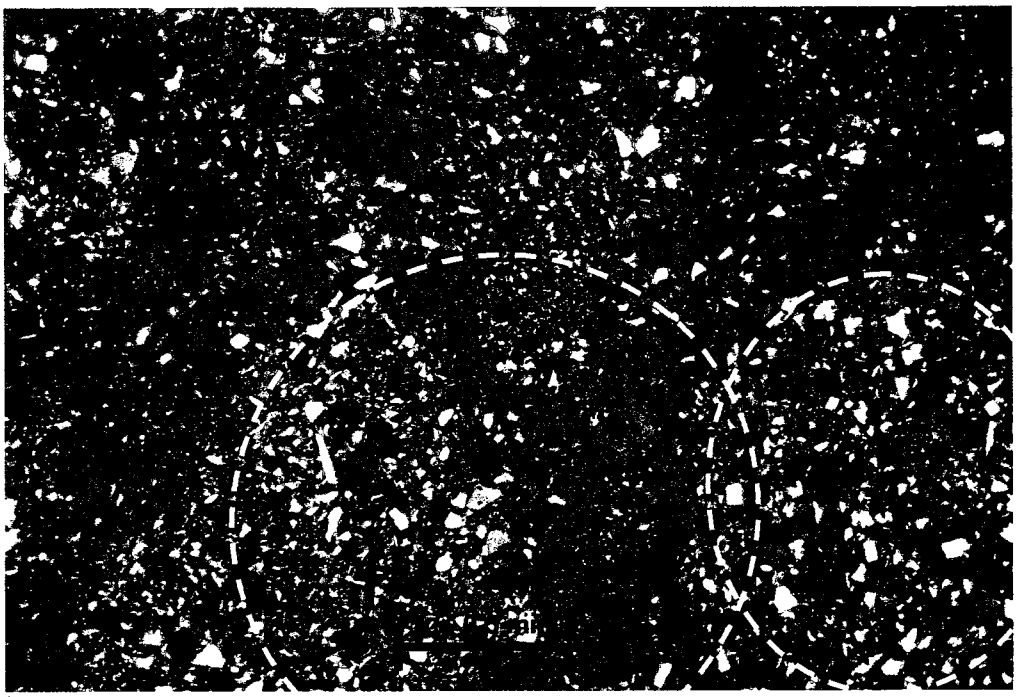

Figure 4-11: Fine-grained pyrite (light colored) in sand-size particles.
(Width of photo: 2.3mm. Refl. Light)

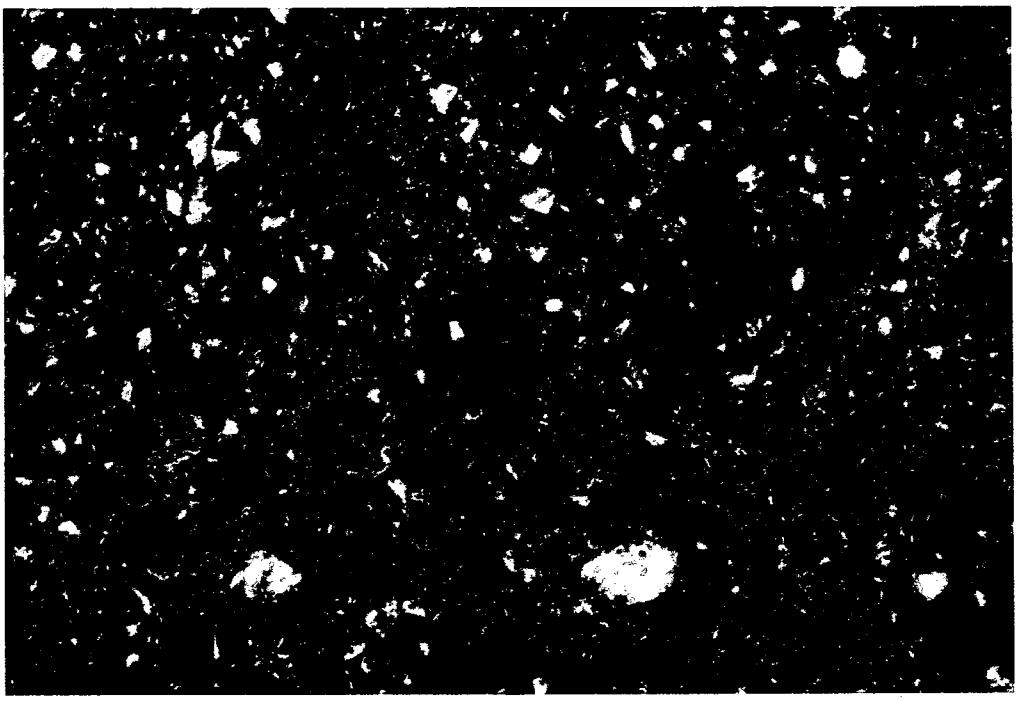

Figure 4-12: As above, with crossed nicols. White grains are mostly quartz.

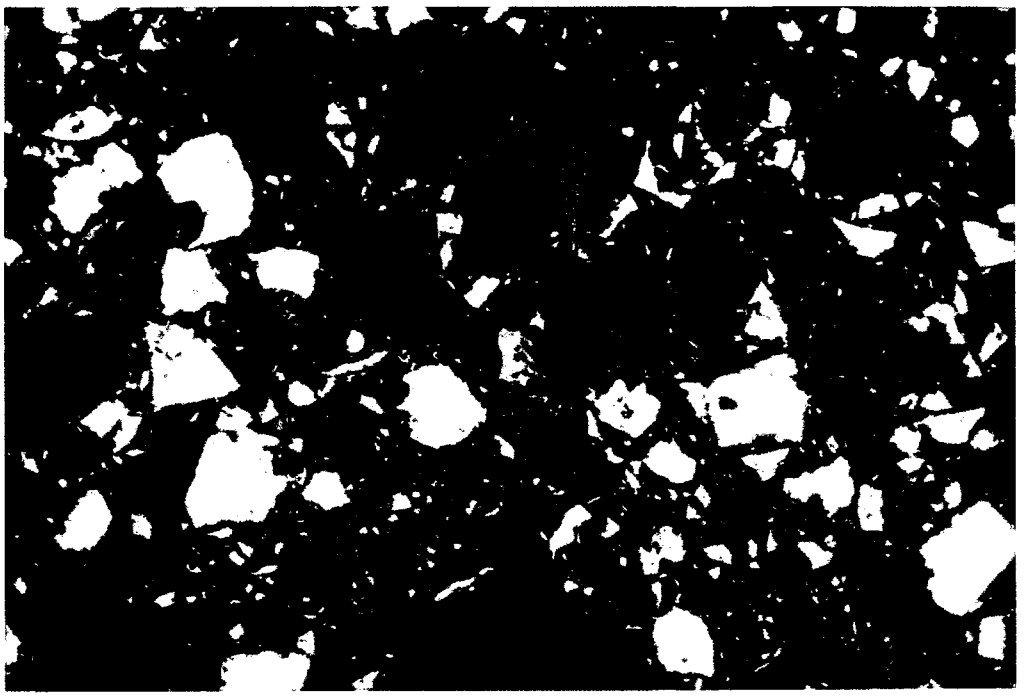

Figure 4-13: Anhedral pyrite fragments (light colored) and interstitial rutile (arrows).
(Width of photo: 0.45mm. Refl. Light)

4.3.2. X-RAY FLUORESENCE

X-ray fluorescence (XRF) is a powerful analytical instrumental method used in a wide variety of industries to determine the elemental composition of various materials. The quantitative X-ray fluorescence method was used for the detailed chemical analysis of the LA, LV and BH tailings. The XRF method is based on the fact that any element when bombarded with high energy electrons will emit a characteristic line spectrum, which is then analyzed in a spectrometer.

Quantitative XRF analysis requires proper calibration standards. International Standard Reference Materials were used in the calibration process. First, standards are analysed and intensities are obtained. Then, an X-ray intensity versus concentration curve (calibration curve) is determined for each analyte. The XRF instrument then compares the spectral intensities of tested samples to those of the standards. The results of the XRF analysis are tabulated in Table 4-8.

Table 4-8: Chemical composition of the LA, LV and BH mine tailings.

Compound	Content %		
	LA	LV	BH
SiO_2	37.710	35.120	17.880
TiO_2	0.464	0.418	0.231
Al_2O_3	8.660	8.200	4.360
Fe_2O_3	33.350	30.930	51.370
MnO	0.030	0.279	0.137
MgO	0.190	3.490	1.670
CaO	0.670	2.230	0.600
Na_2O	1.260	0.620	0.250
K_2O	0.750	0.770	0.480
P_2O_5	0.054	0.161	0.038
SO_3	59.501	50.945	60.183
S	23.830	20.40	24.105
	Content ppm		
Cr_2	122	127	246
Cu	1108	944	1173
Ni	44	31	26
Zn	3403	2426	4725
Pb	942.9	600	185.7
Note: Determined using a PHILIPS PW2440 4kW automated XRF spectrometer system. The test was conducted on pressed tailings pellets			

4.3.3. X-RAY DIFFRACTION

X-ray diffraction (XRD) is one of the main methods used in the determination of soil mineralogy. The basic principle of XRD is each mineral in crystalline form has a unique spacing between crystal planes determined by it atomic structure. This particular spacing causes the X-ray directed at the sample to diffract and produce an identifiable pattern. The X-ray diffraction technique is suitable for the analysis of mineral mixtures. However, it is not suitable for amorphous or poorly crystallised substances.

The XRD technique was used to complement and validate the results of the petrographic study and the XRF analysis of the different tailings. The X-ray diffraction patterns for LA, LV and BH are shown in figures 4-14, 4-15 and 4-16 respectively. The obtained X-ray diffraction patterns are compared with patterns of known minerals. The

results of the diffractograms and the semi-quantitative analysis are tabulated in Table 4-9. The X-ray diffractograms and the semi-quantitative analysis show that the most common phases found in the three tailings samples are quartz and pyrite which is in good agreement with performed quantitative and elemental analysis.

Table 4-9: Results of the diffractograms and the semi-quantitative analysis

Sample	Compound Name	Chemical Formula	Semi-Quantitative %
LA	Pyrite	FeS_2	47
	Quartz	SiO_2	51
	Wustite	$Fe_{11}O_{12}$	2
LV	Quartz	SiO_2	27
	Dolomite	$CaMg(CO_3)_2$	18
	Clinochlore	$Mg_{2.5}\ Fe_{1.65}\ Al_{1.5}\ Si_{2.2}\ Al_{1.8}\ O_{10}\ (\ O\ H\ )_8$	26
	Pyrite	FeS_2	30
BH	Quartz	SiO_2	19
	Siderite	$Fe(CO_3)$	24
	Pyrite	FeS_2	53
	Clinochlore	$Mg_{2.5}\ Fe_{1.65}\ Al_{1.5}\ Si_{2.2}\ Al_{1.8}\ O_{10}\ (\ O\ H\ )_8$	2
	Dolomite	$CaMg(CO_3)_2$	3

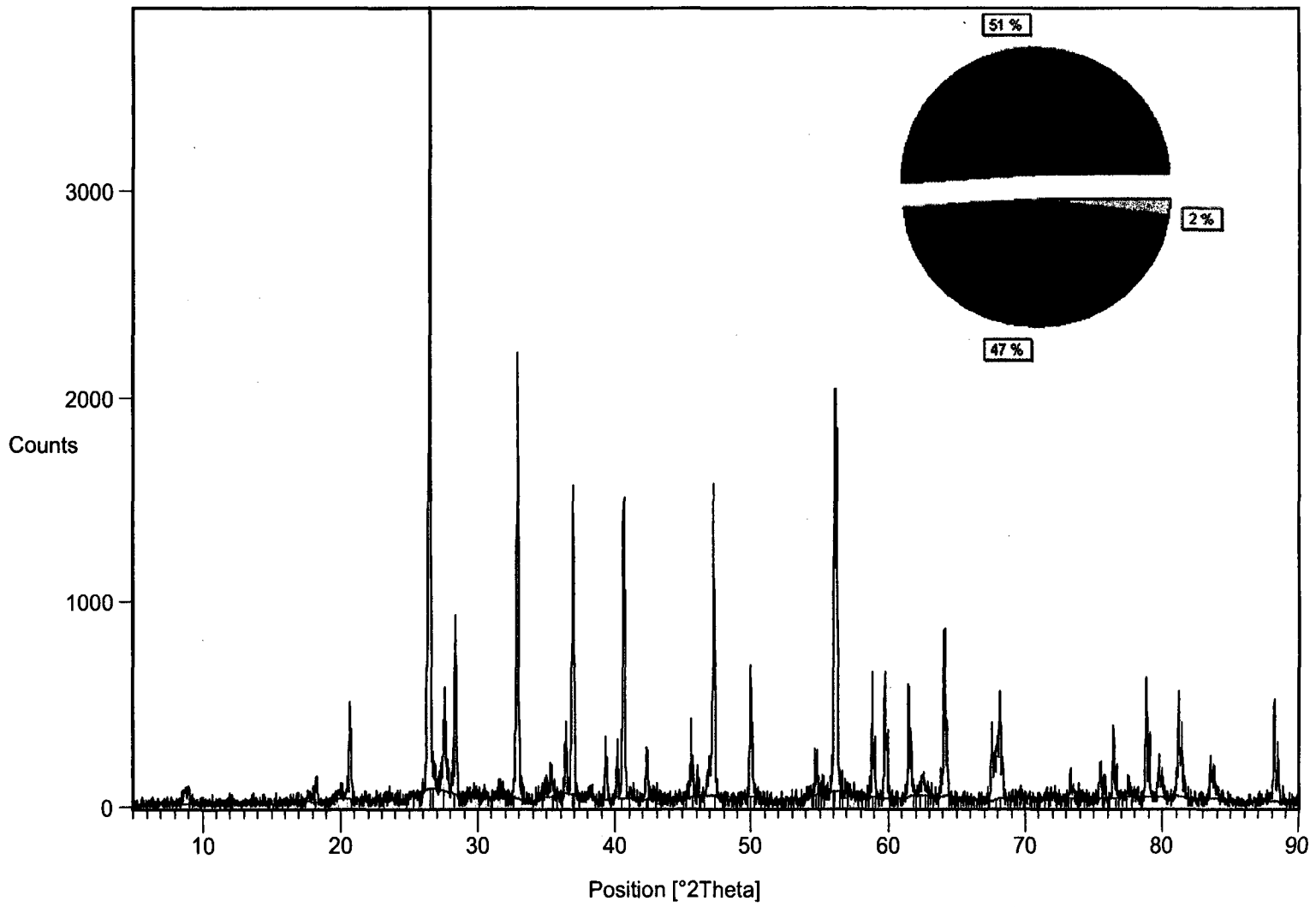

Figure 4-14: X-ray diffraction pattern and semi-quantitative analysis for LA mine tailings.

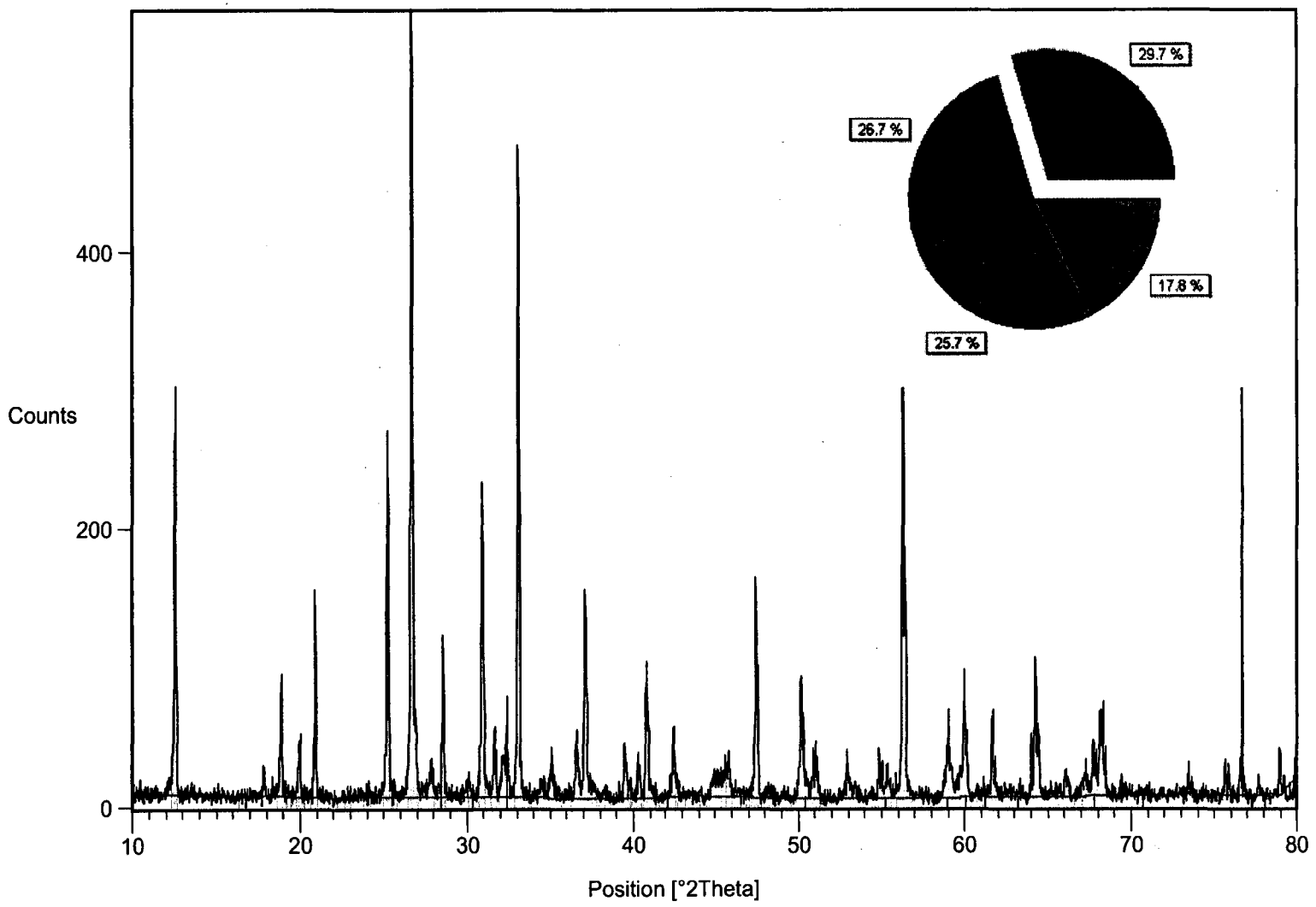

Figure 4-15: X-ray diffraction pattern and semi-quantitative analysis for LV mine tailings.

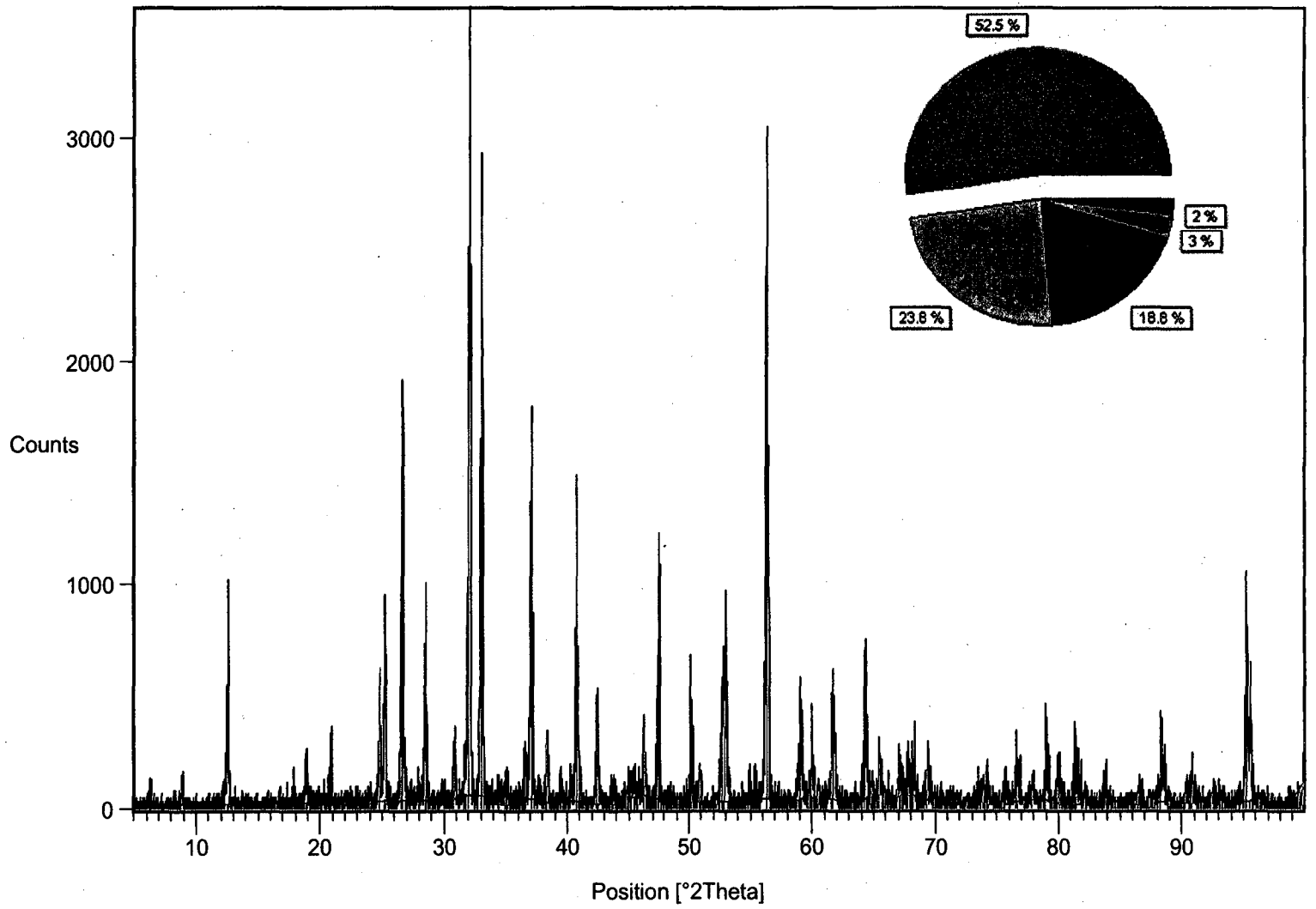

Figure 4-16: X-ray diffraction pattern and semi-quantitative analysis for BH mine tailings.

CHAPTER : 5 RESISTIVITY AND STREAMING POTENTIAL MEASUREMENTS IN SULFIDE-RICH TAILINGS

5.1. INTRODUCTION

As previously stated, self-potential and resistivity measurements are being used with relative success to assess the seepage conditions in water retention embankment core rockfill or earthfill dams. The application of these two geophysical techniques on sulfide rich tailings dams require further investigation to link the geophysical anomalies associated with seepage to changes in tailings and/or fluid properties, and to evaluate their capacity to detect zones of anomalous seepage, especially seepage induced by internal erosion. In the current state of practice, field data may be interpreted qualitatively to detect areas of anomalous seepage. However, qualitative interpretation and the current understanding of the measured anomaly do not permit a comprehensive interpretation that directly associates the anomaly to the physical property of interest (internal erosion). Numerous studies are underway and necessary to assess the potential of numerical modelling to further this understanding.

Forward numerical modeling enables a relatively accurate estimation of the geophysical response to anomalous seepage or structural defect. However, the lack of accurate information on the basic physical properties that dictates the geophysical response, limits the value and usefulness of any modelling procedure.

As stated earlier, self-potential numerical modeling requires knowledge of the hydraulic conductivity distribution, the resistivity of the subsurface and the cross-coupling coefficient, thus the zeta-potential. This chapter summarizes the procedures and results of a laboratory program aimed at developing an understanding of the influence of tailings and fluid parameters on the electrical properties of sulfide rich tailings. It is important to note that, the zeta-potential measurements presented in this chapter are the first reported measurements of sulfide rich tailings and tailings in general.

5.2. EXPERIMENTAL PROCEDURE

The laboratory testing was carried out on the three previously characterised tailings: LA, LV and BH. The electrical resistivity was measured as a function of the electrolyte solution concentration while the zeta-potential was measured as a function of the electrolyte solution concentration and the pH value.

5.2.1. RESISTIVITY MEASUREMENTS OF SULFIDE-RICH TAILINGS

Most common minerals like silicates can be regarded as electrical insulators, while iron sulfides, pyrite, chalcopyrite, sphalerite, and galena are semiconductors with a wide range of reported conductivity that is dependent on their chemical composition (Shuey 1975). The electrical conductivity of a sulfide mineral can be affected by its surface composition, which is dependent on the degree of oxidation and by the adsorption of various chemicals. The electric current is conducted through the sample by the liquid present in the pores. A high resistivity is thus expected for soils with low porosity, low saturation and / or low pore liquid salinity.

Electrical resistivity is a function of a number of soil properties, including the grain size distribution, mineralogy, porosity, pore size distribution, permeability, water content, electrical resistivity of the pore fluid, and temperature (Keller and Frischknecht 1966, Ward 1990). These parameters affect the electrical resistivity in different ways and to varying extents.

The formula relating the electrical resistivity of saturated soil (ρ_B) to the electrical resistivity of its pore fluid (ρ_f) is generally referred to as Archie's law (Huntley 1986)

$$\rho_B = a_c \ \rho_f \ n_p^{-m_c} \qquad \textbf{(Eq. 5-1)}$$

n_p : *porosity*
a_c & m_c : *constants that depend on the type of soil*

Archie's law shows that the electric resistivity of saturated soil is sensitive to the porosity, the electrical resistivity of the pore fluid, the characteristics of the solids and the structure of the pores (different soils with the same pore fluid and porosity may have a different a_c & m_c).

The resistivity of the solid matrix is the result of electron conductance through the grain to grain contacts. The electrical conduction in clean quartz grains occurs almost exclusively in the liquid contained in the pores. Due to the fact that quartz is a non conducting material, the solid's matrix resistivity is considered infinitely high. In sulfide rich tailings, the electrical conduction occurs in the pores and on the surface of the electrically charged minerals. The surface conductance can be a significant factor affecting the bulk electrical resistivity of the tailings.

The ionic strength of the pore fluid determines its electrical resistivity. An increase in the ionic strength will lead to a decrease in the electrical resistivity. The resistivity will decrease if insulating contaminants are present in the pore liquid (Campanella and Weemees 1990).

Because ions flow through the same paths as the liquid, electrical resistivity is affected by the same factors that influence hydraulic conductivity. Among these factors are fluid viscosity, pore-size distribution, grain size distribution, void ratio, roughness of mineral grains, and degree of saturation. It is important to note that the relationship between hydraulic conductivity and electrical resistivity varies with different soils.

5.2.1.1 Apparatus

For resistivity measurements of tailings samples, it is necessary to compact the tailings into a regular shape such as a cylinder or a box in order to be able to calculate its cross sectional area. A laboratory built apparatus was designed for measuring the vertical electrical resistivity of compacted tailings (Figure 5-1), the design is similar to that proposed by Abu-Hassanein (1996). The apparatus is made of a polyvinyl chloride (PVC) cylinder, which is an electrical insulator (electrical resistivity ~ 1016 ohm-cm). Abu-Hassanein (1996) studied the influence of the PVC cylinder and the shape of the sample

on the measured electrical resistivity. He concluded that the PVC cylinder and the shape of the sample had no effect on the measured electrical resistivity.

An electrical field is induced through the sample via two stainless steel discs pushed against the ends of the sample. The disks have the same diameter as the sample. A potential difference ΔV is measured between the two stainless steel rods (diameter = 3 mm) that are pressed through the sample near its center. The vertical spacing of the rods is 2.5 cm (Figure 5-1). A voltmeter with an accuracy of 1 mV is used to measure the potential difference between the electrodes.

The electrical resistance (R) is then calculated using Ohm's law

$$R = \Delta V / I \qquad \textbf{(Eq. 5-2)}$$

and the vertical electrical resistivity (ρ) is subsequently calculated from the electrical resistance using the following equation

$$\rho = \frac{R A_a}{L} = \frac{\Delta V A_a}{I L} \qquad \textbf{(Eq. 5-3)}$$

R	:	*electrical resistance*
A_a	:	*cross sectional area*
I	:	*current*
L	:	*length between the stainless steel rods*

5.2.1.2 Electrolyte Solution Chemistry

The electrical resistivity of the tailings was measured as a function of the electrolyte concentration. Different electrolyte solutions were prepared by mixing deionized water and the proper amount of laboratory grade KCl salt (from Fisher Scientific) to obtain the following concentrations 0.1 M, 0.01M and 0.001 M. Solution conductivity was measured using a calibrated WTW TetraCon 325 conductivity probe as well as a calibrated EP 10 Myron L Conductivity Meter.

5.2.1.3 Sample preparation

The tailings samples were sieved and separated into two grain size fractions in order to investigate the effect of grain size distribution on the electrical properties of the tailings, which could be helpful in determining the effect of internal erosion. The tailings were sieved using a 0.075 mm sieve (sieve # 200). The resistivity of the fractions coarser and finer than 0.075 mm and the resistivity of the complete gradation were measured.

The samples were compacted in the PVC mould. Prior to compaction the tailings samples were moistened with different electrolyte solutions as well as deionised water and put in a closed container for a 24 hour period. It is important to note the solutions used to prepare the samples will affect their electrical resistivity, thus the results apply only to the solutions that were used. In a field application, a laboratory test would need to be carried out using the pond and pore water (mine water) when measuring the electrical resistivity of the tailings in order to be able to relate these results to field acquired data.

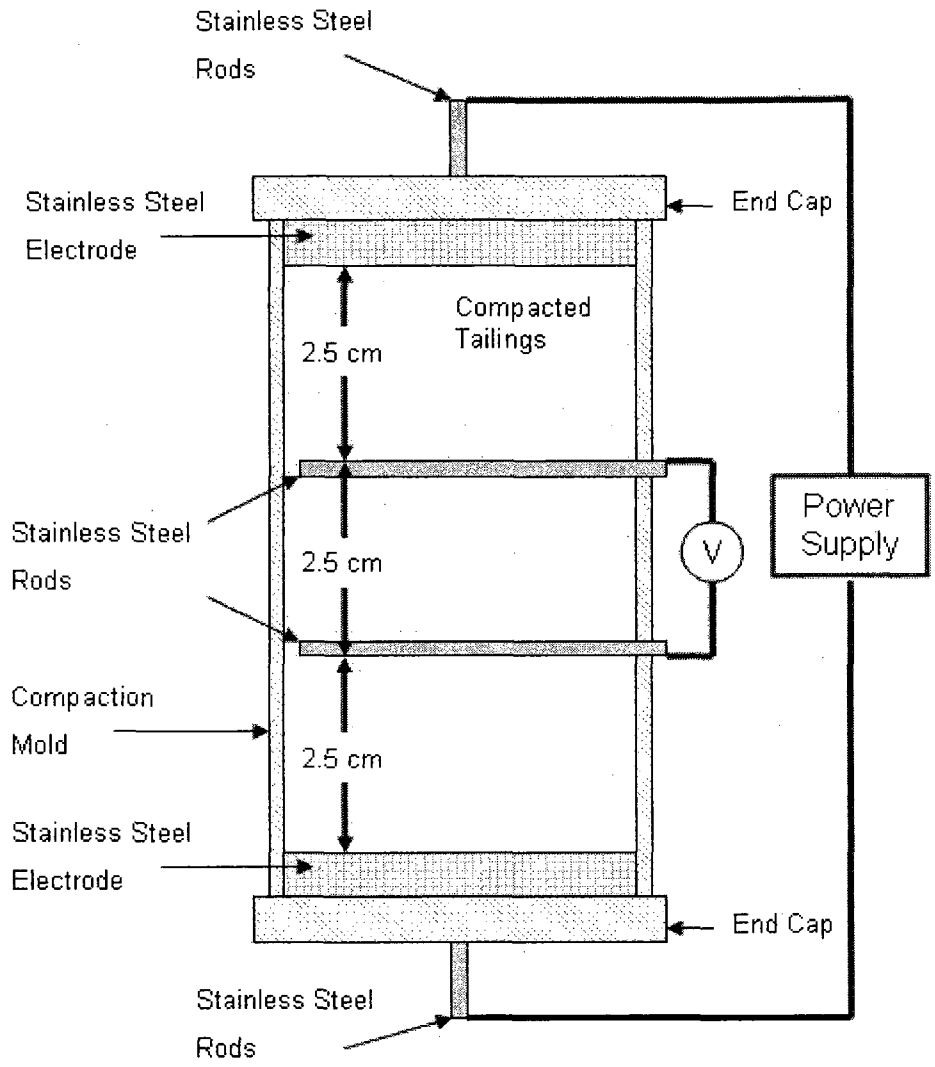

Figure 5-1: Laboratory apparatus for measuring the electrical resistivity of compacted tailings (After Abu-Hassanein 1996)

5.2.2. STREAMING POTENTIAL MEASUREMENTS OF THE ZETA POTENTIAL

As previously stated, streaming potential is the only geophysical method that relates directly to seepage flow. The initial concept was to use the same apparatus for simultaneously measuring the resistivity and the streaming potential. A prototype (Figure 5-2) was designed and tested using coarse and medium to fine sands. The idea was to combine the Tuesdail et. al (1998) apparatus for measuring the streaming potential with the Abu-Hassanein et. al (1996) apparatus for measuring electrical resistivity. After much testing this design was dropped in favour of two separate tests one for measuring the resistivity as previously stated, and another test using a commercially available apparatus to measure the streaming potential.

The designed cell was dropped out in favour of a commercially available apparatus mainly because the unidirectional flow of the electrolyte solution prevented the ionic equilibrium between the sample and the fluid to be attained, and induced polarization of the stainless steel electrodes. This rendered the calibration of the designed cell unattainable. Hence, the zeta-potential measurements of the sulfide rich tailings using the streaming potential method were carried out using a commercial streaming potential analyser (BI-EKA, Brookhaven Instruments Corp.).

The BI-EKA is based on the streaming potential methods. This method is used to measure the electrokinetic potential based on the relative movement of an electrolyte solution through a porous medium. The streaming potential method works very well with samples which could be held in capillary tubes through which an electrolyte solution is forced. The excess charges are carried along by the liquid. The accumulation of these charges induces a build-up of an electric field which is measured via two non-polarizing electrodes. Details on the instrument and testing procedures are given below.

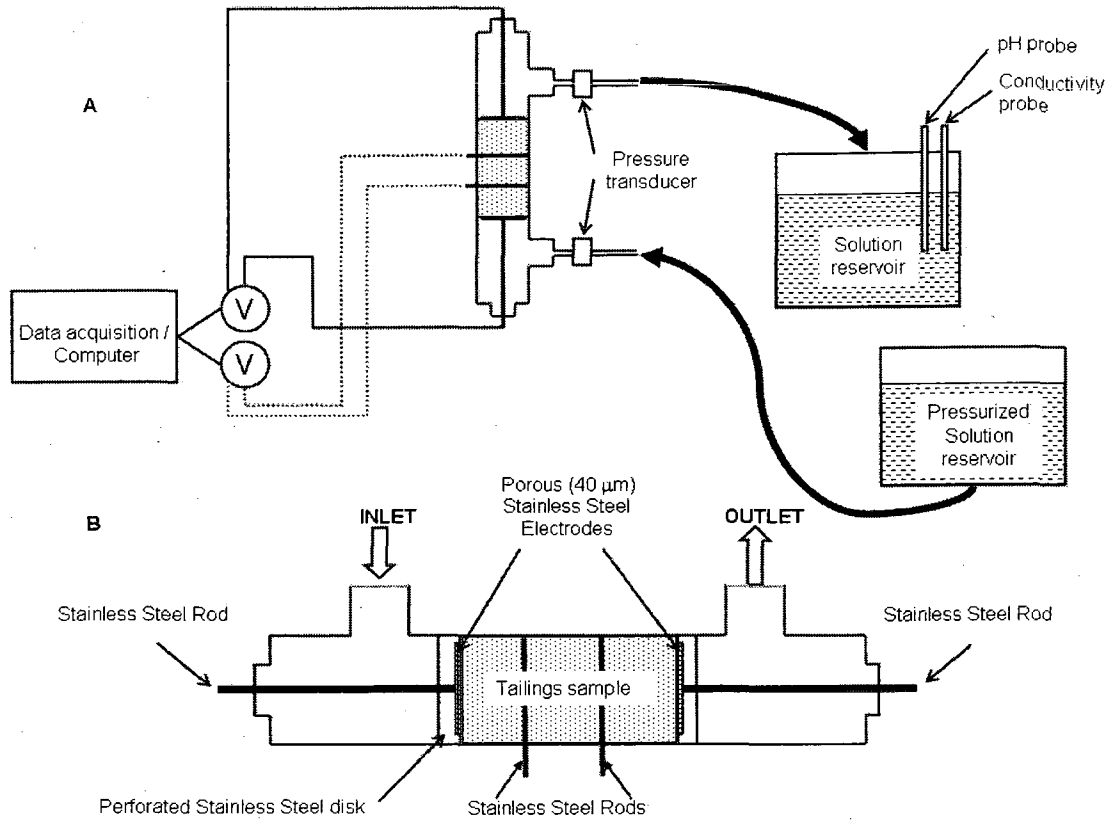

Figure 5-2: Schematic of the preliminary laboratory testing apparatus.

5.2.2.1 Apparatus

The instrument used for measuring the streaming potential is in principal similar to that used by previous researchers (Ahmad, 1964; Ishido, 1981; Morgan et al., 1989; Jouniaux et al., 1995b; Truesdail et al., 1998; Lorne, 1999). The BI-EKA instrument includes an analyzer, a data control system, a measuring cell and electrodes. A schematic illustration of the streaming potential analyser and associated measuring cell is presented in Figure 5-3A.

The analyzer consists of a bidirectional pump with a flow capacity of 1.3 l/min and pressure transducers to produce and measure the pressure that drives the electrolyte solution from the reservoir through the measuring cell. The analyzer can be controlled either manually or by computer. The streaming potential, as well as the streaming current

are measured simultaneously by the instrument. Sensors for conductivity and temperature measurements of the electrolyte solution are integrated in the analyzer, additional pH and conductivity probes were added externally.

The measuring cell consists of a glass cylinder with perforated Ag/AgCl (Silver / Silver Chloride) electrodes at each end through which the electrolyte solution passes in and out of the porous material under investigation (Figure 5-3B). In order to prevent polarization of the Ag/AgCl electrodes, the direction of the flow through the cell alternates for each run. Furthermore, the electrodes are stored overnight in a 0.01 M KCl solution to prevent the build-up of charge.

Finally, In order to prevent the tailings from migrating with the flow through the electrodes, filter membranes were used to retain the sample inside the measuring cell (Figure 5-3B). The pore size of these membranes was optimised to maintain a uniform sample plug and to avoid any pressure drop inside the membrane pores. The pore size used is 50 μm. With this precaution the filter membranes do not contribute to the zeta-potential of the tailings.

The streaming potential is calculated using the following equation

$$\varsigma = \frac{V_s}{\Delta P}\,\frac{\eta}{\varepsilon\,\varepsilon_0}\,\frac{L}{A}\,\frac{1}{R} \qquad \textbf{(Eq. 5-4)}$$

where V_s is the streaming potential, ΔP the hydrodynamic pressure difference across the sample, η the viscosity and ε the permittivity of the electrolyte solution; and ε_0 the permittivity vacuum. L and A are the length and cross sectional area of the sample. R is the electrical resistance across the sample.

The first term in Eq. 5-4, $Vs/\Delta P$, is determined by the measurement of the potential generated by a given pressure. In order to improve the repeatability and the precision of the ζ-potential measurements, the EKA determines $Vs/\Delta P$ from the slope of the streaming potential against increasing pressure difference curve. For a given temperature, the viscosity (η), the permittivity (ε) and the permittivity of vacuum (ε_0) are constant. The

electrical resistance (R) across the sample can be directly measured. However, in the EKA, both the streaming potential (V_s) and the streaming current (I_s) are measured, hence R can be determined by the ratio ($Vs/\Delta P$) / ($Is/\Delta P$).

5.2.2.2 Electrolyte Solution Chemistry

In general, it is recommended to use chlorinated solutions which constitute ideal conditions for the AgCl electrodes provided with the BI-EKA. The streaming potential was measured as a function of the electrolyte concentration and the pH. Different electrolyte solutions were prepared by mixing deionized water and the proper amount of laboratory grade KCl salt (from Fisher Scientific) to obtain the following concentrations; 0.1 M, 0.01M and 0.001 M. The pH was adjusted by adding the proper amount of 10% HCl to obtain the following pH values; 5, 4, 3 and 2.

To avoid variation in the concentration or the pH during the experiment, due to solution left in the EKA tubes or even in the sample itself, a new solution was used for each flow test. The solution conductivity was measured using a calibrated WTW TetraCon 325 conductivity probe as well as a calibrated EP 10 Myron L Conductivity Meter. The pH of the solution was measured using a calibrated WTW SenTix 41-3 pH probe as well as a Hanna Instruments HI98103 pH Meter. The conductivity and pH were measured before, during, and at the end of each flow test.

5.2.2.3 Sample Preparation

Due to the fine gradation of the sulfide rich tailings and the low hydraulic conductivity associated with that gradation, the streaming potential measurements of the zeta-potential of the full gradation turned out to be impractical. Hence, the zeta-potential was only measured for the coarse fraction (particles $\geq$ 0.075 mm) of the tailings. Several kilograms of the tailings had to be washed on sieve # 200 repeatedly to get the needed amounts required for the tests. In order to make sure that the results presented are accurate and repeatable, each measurement of the zeta-potential was repeated at least three times. A total of 96 tests were performed.

For each test a 15 g sample of tailings was washed three times with deionized water by agitation and settling, and then it was washed another three times with the working solution (the solution that will be used to do the experiment) using the same method. The sample is then introduced into the measuring cell in a vertical position with a spatula. It is important to note that the sample must be very moist in order to obtain a homogeneous mixture. The cell was gently taped on the side to eliminate any air bubbles.

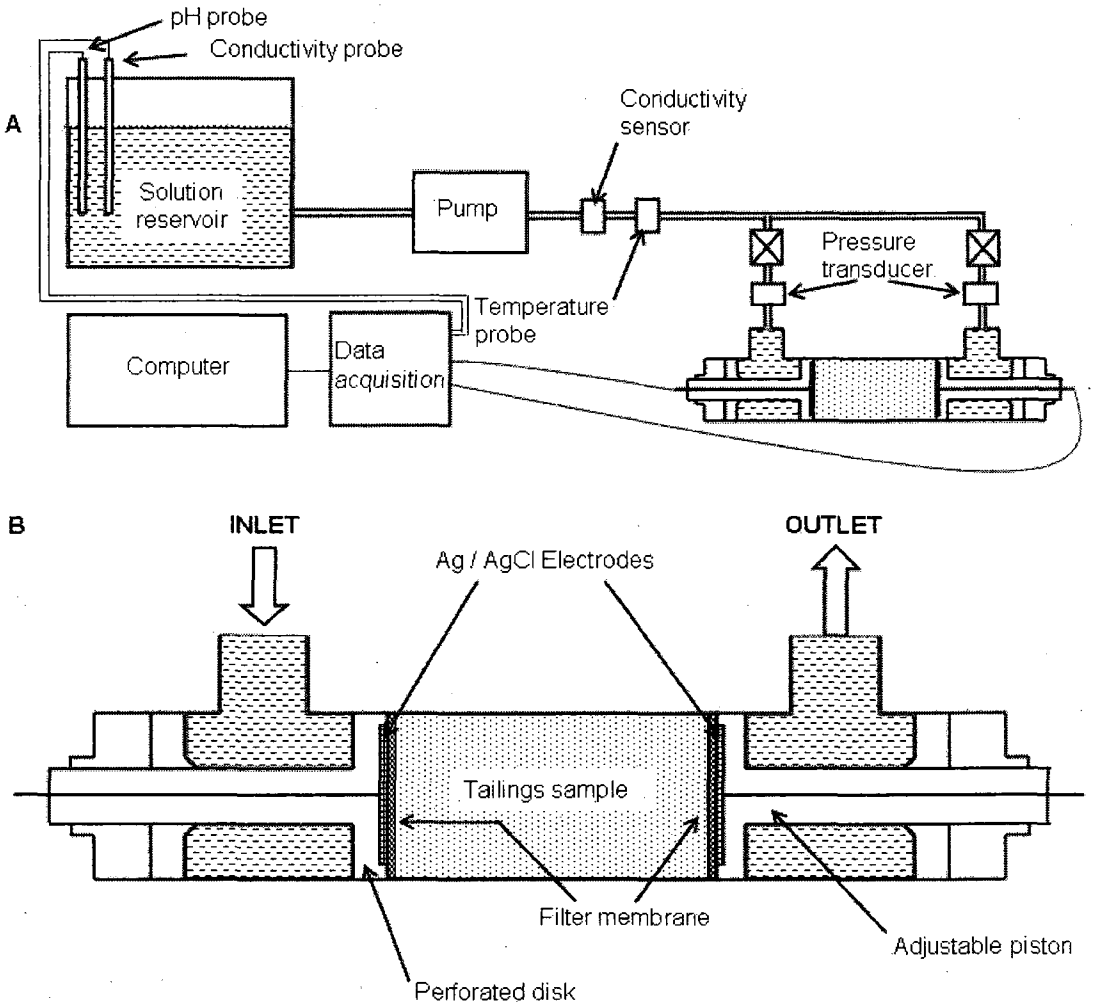

Figure 5-3: Schematic illustration of the BI-EKA streaming potential analyzer (A) and associated measuring cell (B).

5.2.3. ELECTROACOUSTIC MEASUREMENTS OF THE ZETA-POTENTIAL

Electroacoustic spectroscopy deals with the interaction between electric and acoustic fields resulting in two possible applications. One can apply an acoustic field and measure the induced electric field which is referred to as colloid vibration potential (CVP), or one can apply an electric field and measure the induced acoustic field which is referred to as electrosonic sonic amplitude (ESA).

The zeta-potential measurements of the sulfide rich tailings using the electroacoustic method were carried out using a commercial electroacoustic spectrometer (DT-1200, Dispersion Technologies). Details on the instrument and testing procedures are given below.

5.2.3.1 Apparatus

The Dispersion Technology DT-1200 is a modern instrument for determining the zeta-potential of particles in suspension by measuring their electroacoustic properties, the CVI to be more precise, and the subsequent analysis of the acquired data. The DT-1200 combines two sensors in one instrument, one for the measurement of particle size distribution and the other for the measurement of the CVI. Only the CVI option was used.

The CVI probe consists of two parts: a transmitting and a receiving transducer. The transmitter (Figure 5-4A) consists of a piezoelectric transducer with a resonant frequency in the range of 2 to 10 MHz that converts a radio frequency pulse into acoustic energy, and a quartz delay rod with an acoustic delay of about 2.5 u sec. that sends the generated pulse into the slurry. The acoustic excitation of the slurry causes the particles in suspension to gain induced dipole moments. These dipole moments will add up to create an electric field, which can be measured by the receiver.

The receiver consists of a two-element antenna immersed in the slurry. The current is measured between the gold electrode and stainless steel shell of the probe (Figure 5-4B). The electric field created by the acoustically induced dipole moments changes the

potential of one element with respect to the other. If the impedance of the measuring circuit is relatively high with respect to the slurry, the antenna will sense an open circuit voltage, which is known as the colloid vibration potential (CVP). On the other hand, if the impedance of the circuit is low compared to that of the slurry, the electric field will induce a current flow in the antenna. This short circuit current is known as the colloid vibration current (CVI).

5.2.3.2 Electrolyte Solution Chemistry

In order to compare the measured zeta-potentials using the electroacoustic technique with that of the streaming potential technique the same electrolyte solutions were used. The CVI was measured as a function of the electrolyte concentration and the pH. Different electrolyte solutions were prepared by mixing deionized water and the proper amount of laboratory grade KCl salt (from Fisher Scientific) to obtain the following concentrations: 0.1 M, 0.01M and 0.001 M. The pH was adjusted by adding the proper amount of 10% HCl to obtain the following pH values: 5, 4, 3 and 2.

To avoid variation in the concentration or the pH during the experiment, the slurry was allowed to equilibrate for approximately one hour after which the conductivity and pH were measured. In the case where a rise in the pH, induced by the neutralisation effect of the carbonates present in some of the tailings was noted, the pH was brought back to the desired value by adding the proper amount of 10% HCl.

The supernatant conductivity was measured using a calibrated WTW TetraCon 325 conductivity probe as well as a calibrated EP 10 Myron L Conductivity Meter. The pH of the slurry and the supernatant was measured using a calibrated WTW SenTix 41-3 pH probe as well as a Hanna Instruments HI-98103 pH Meter. The conductivity was measured before each test, while the pH was measured before and during the test.

5.2.3.3 Sample Preparation

Since the electroacoustic technique can measure the zeta-potential for a wide range of particle size, the full gradation of the tailings was used. The tailings samples were washed three times with deionized water by agitation and settling, after which they were oven dried for 24 hours.

The suspensions were prepared by dispersing the tailings samples in the previously prepared electrolyte solutions under vigorous agitation. The particles are maintained in suspension during the test by a special magnetic stirrer. The volume fraction of tailings used in the suspension was 10%.

In order to make sure that the results presented are accurate and repeatable each test was repeated at least three times. The result of each test is the average of ten zeta-potential measurements. A total of 108 tests were performed.

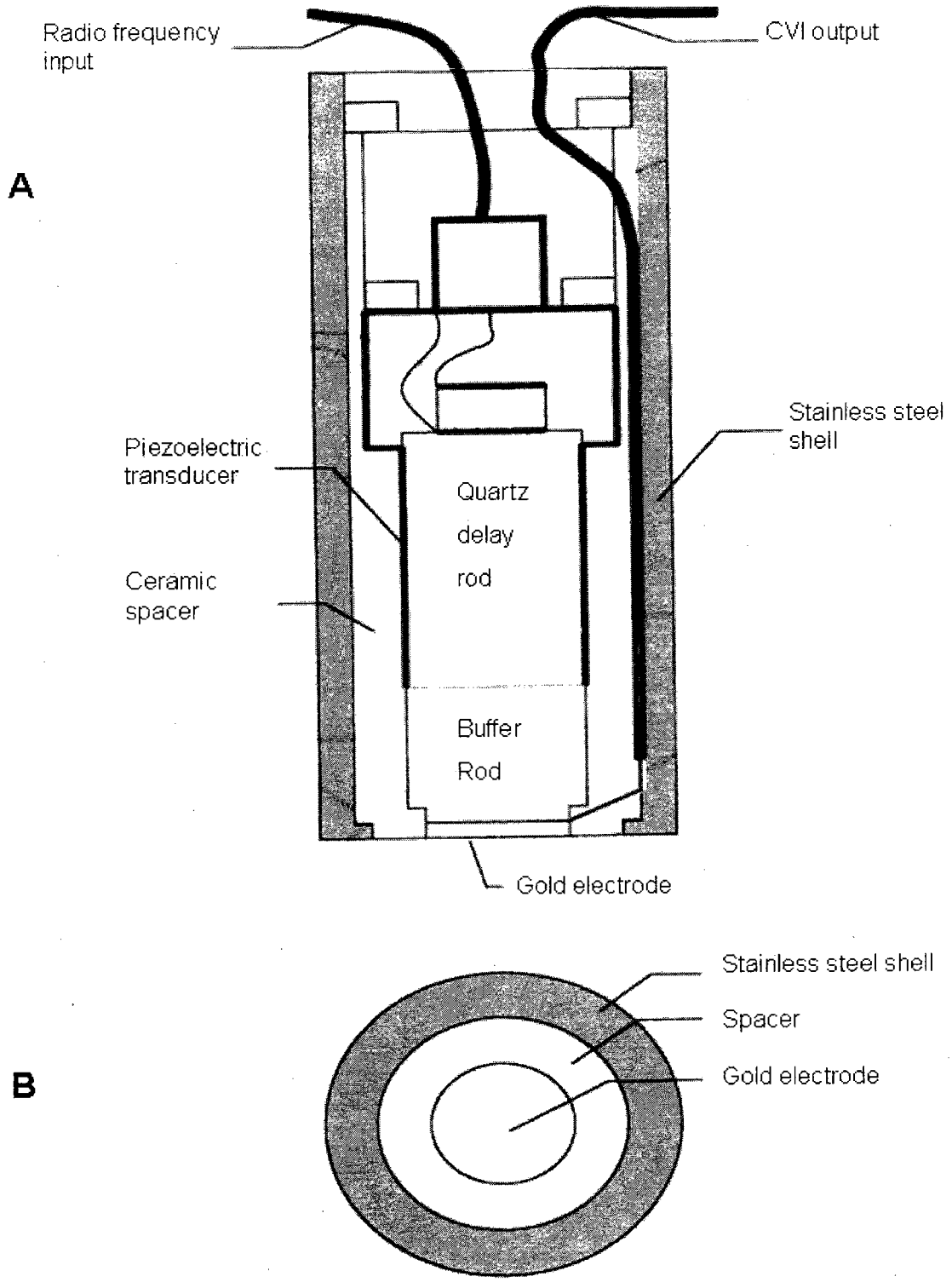

Figure 5-4: a- Cross section of the colloid vibration current measuring probe. b- End view of the measuring probe (After Dukhin and Goetz 2002)

5.3. EXPERIMENTAL RESULTS AND DISCUSSION

5.3.1. RESISTIVITY MEASUREMENTS

The resistivity values determined in the laboratory test are only an approximation of the true in situ values. They give us an idea of what to expect when taking in situ measurements. There are several factors that may induce an error when comparing measurements from the laboratory to in situ measurements. The most obvious ones are:

- the laboratory samples are fresh, while the tailings in the field are mainly a mixture of oxidised and fresh tailings;
- the laboratory samples are not compacted to exactly the same degree as in the field;
- the laboratory samples do not have the same moisture content as the tailings in the pond;
- the laboratory samples are not tested at the same temperature;
- the pore fluid conductivity in the field is different than the one used in the laboratory.

The results of the tailings resistivity measurements are presented in Figure 5-5, 5-6, and 5-7. As expected, the resistivity decreases significantly due to an increase in concentration of the electrolyte solution. It is important to note that the measured resistivity is the combined resistivity of both the liquid and the solid matrix.

The laboratory resistivity measurements of the tested sulfide rich tailings show a decrease in resistivity of the fine portion of the tailings with respect to the coarse fraction. This leads to a decrease in the resistivity of the full gradation with respect to the resistivity of the coarse fraction. This is mainly due to the presence of pyrite grains, which were identified in the petrographic analysis of the tailings presented in the previous chapter, as having particle sizes ranging from a few microns to a tenth of a millimetre.

Abnormal seepage from tailings dams might induce internal erosion, as previously discussed. During this process, the fine particles will be transported with the flow. The remaining material will have an increased permeability and porosity, hence a decrease in resistivity should be expected because fine particles have a tendency to decrease permeability and porosity, which evidently leads to an increase in the resistivity. However, the laboratory measurements revealed the resistivity of the full gradation of the tailings is lower than that of the coarse fraction for the three tailings tested. This can be explained by the presence of semi-conducting minerals, mainly pyrite which affected the bulk electric resistivity of the tailings. Hence, an increase in resistivity may reflect an internal erosion problem. But, in order for this information to be used in interpreting a field anomaly, an initial resistivity survey prior to the internal erosion problem has to be available for the basis of a comparison.

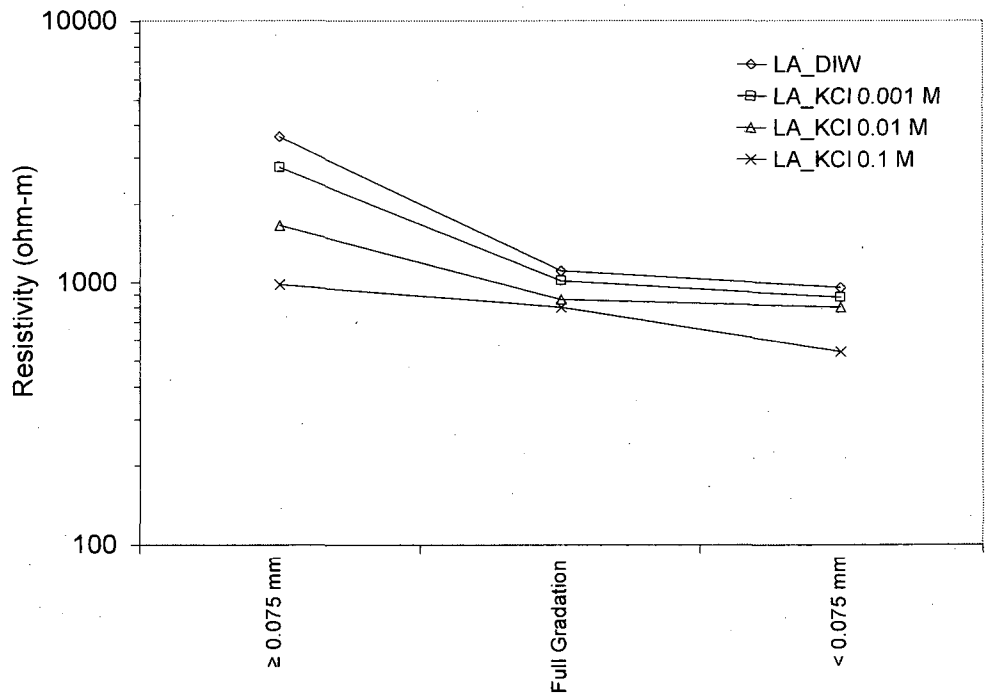

Figure 5-5: Relationship between electrical resistivity, grain size and electrolyte concentration for LA tailings.

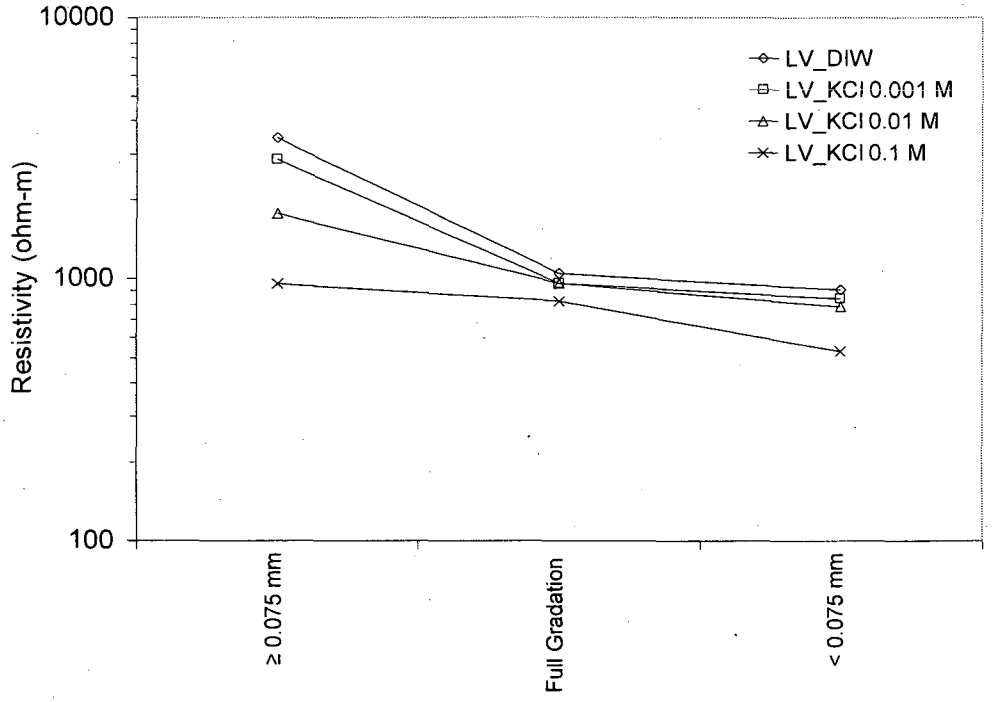

Figure 5-6: Relationship between electrical resistivity, grain size and electrolyte concentration for LV tailings.

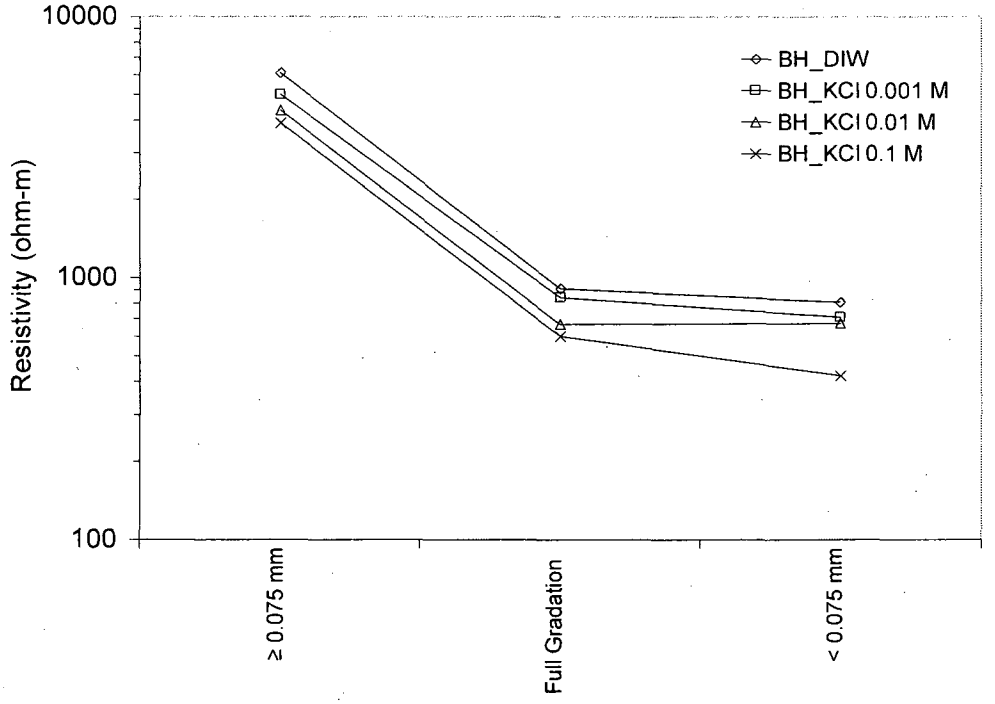

Figure 5-7: Relationship between electrical resistivity, grain size and electrolyte concentration for BH tailings.

5.3.2. ZETA-POTENTIAL MEASUREMENTS

The effect of solution pH and ionic strength on the ζ-potential of the sulfide rich tailings is shown in Figures 5-8 to 5-12. The ζ-potential of the three mine tailings was measured over the pH range 2 - 5 for three different solutions (10^{-3}, 10^{-2}, and 10^{-1} mol / l KCl). Based on these results, the following general observations have been made:

- the zeta potential is negative at all pH values investigated;
- the zeta potential decreases as the pH increases;
- the zeta potential measurements at 10^{-1} mol / l yielded values close to zero and within the error margin of the measuring equipment, hence, these values are discarded;
- the electroacoustic measurements of the zeta potential proved to be more reliable and repeatable than measurements using the streaming potential method;
- due to the grain size distribution of hard rock tailings, the electroacoustic measurements of the zeta potential is the most effective method.

The variation of the ζ-potential as a function of the pH for two concentrations of KCl (10^{-3} and 10^{-2} mol / l) is depicted in Figures 5-9 and 5-10. Extrapolation of the curves shows that the pH for which the ζ-potential is zero is the same in each case. Thus the KCl electrolyte behaves indifferently, and the point of zero charge (p.z.c.) is for pH 1.8 ± 0.1. The p.z.c. is the point at which the surface charge equals zero. Hence, at p.z.c. the zeta-potential equals zero. Unfortunately no other measurements of the ζ-potential of sulfide rich tailings exist in the literature to serve as a basis for comparison.

Controlled room temperature at 20 °C was maintained when measuring the pH dependence of the ζ-potential of the sulfide rich tailings. At each controlled pH value the ζ-potential was measured five times for the streaming potential test and ten times for the electroacoustic test on three separate samples. In all Figures only the average values are plotted with an error bar representing the variations encountered in the results.

The variations of the ζ-potential of sulfide rich tailings, from the three different mines; LA, LV and BH, as a function of the pH in aqueous solution (10^{-3} and 10^{-2} mol / l

KCl) are shown respectively in Figures 5-10, 5-11 and 5-12. The strong dependence of the ζ-potential which is also displayed in these Figures illustrates conclusively that the potential-determining ions for the mineral-electrolyte systems are H^+ and OH^-. The curves of the variation of the ζ-potential of the three tailings as a function of the pH are similar. The main difference in the variation of ζ-potential of the tailings is the difference in the variation of point of zero charge.

Attempts to compare the results of ζ-potential measurements made by electroacoustic spectroscopy and streaming potential methods have been limited by:

- the lack of truly comparable samples, it was initially assumed that the coarse and fine fraction of the tailings will have the same mineralogy, since the grains size for the major constituents of the tailings (quartz and pyrite) span over the full range;
- the streaming potential equipment and procedure were not devised to measure the ζ-potential of fine powder, because it is not easy to force a liquid through this finely grained material;
- to effectively characterise representative values of the zeta-potential using the streaming potential method, the tailings and the electrolyte solution must achieve a state of ionic equilibrium, which is extremely difficult due to the low permeability of the tailings.

The results of both methods for the three tailings are depicted in Figures 5-11, 5-12 and 5-13. The variations in the streaming potential results were considerable. They average + 20 mV and – 20 mV.

The ζ-potential is sensitive to the potential distribution near the surface. The higher the electrolyte concentration, the more sharply the potential falls off with distance. Therefore, the ζ-potential decreases in magnitude as the electrolyte concentration increases. If no supporting electrolyte is added to the solution, the measured ζ-potential will fluctuate due to unpredictable variation in the electrolyte concentration, which may be induced by contaminations, such ionic species dissolution from minerals. Therefore, in order to obtain reproducible values, a sufficient amount of supporting electrolyte must be added to the solution.

In measuring the pH dependence of the ζ-potential using the streaming potential method, the required concentration was maintained by adding KCl to the solution, and the sample was prewashed using deionized water and the electrolyte solution to avoid any contamination. As for the electroacoustic tests, it was extremely difficult to pre-wash adequately the sample due to the presence of a considerable amount of fines. Conductivity measurements of the supernatant of the electroacoustic spectroscopy test showed an increase in conductivity probably due to the dissolution of soluble salts still present in the sample. The effect of the change in conductivity of the electroacoustic spectroscopy solution could explain small variations in the ζ-potential between the 10^{-3} and 10^{-2} mol / l KCl solutions.

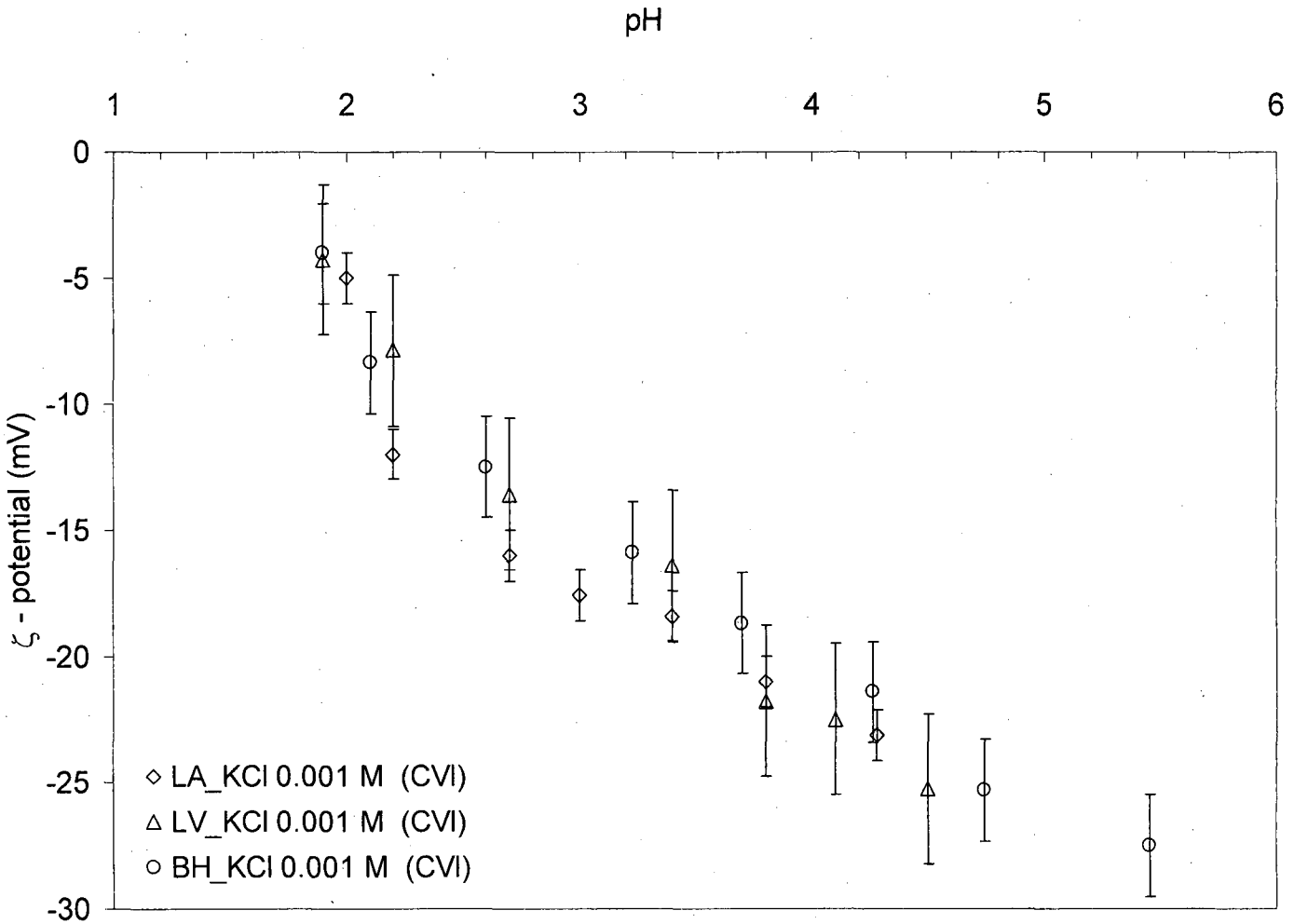

Figure 5-8: Variation of the zeta-potential of LA, LV and BH mine tailings as a function of pH in aqueous solution of 10^{-3} mol/l KCl.

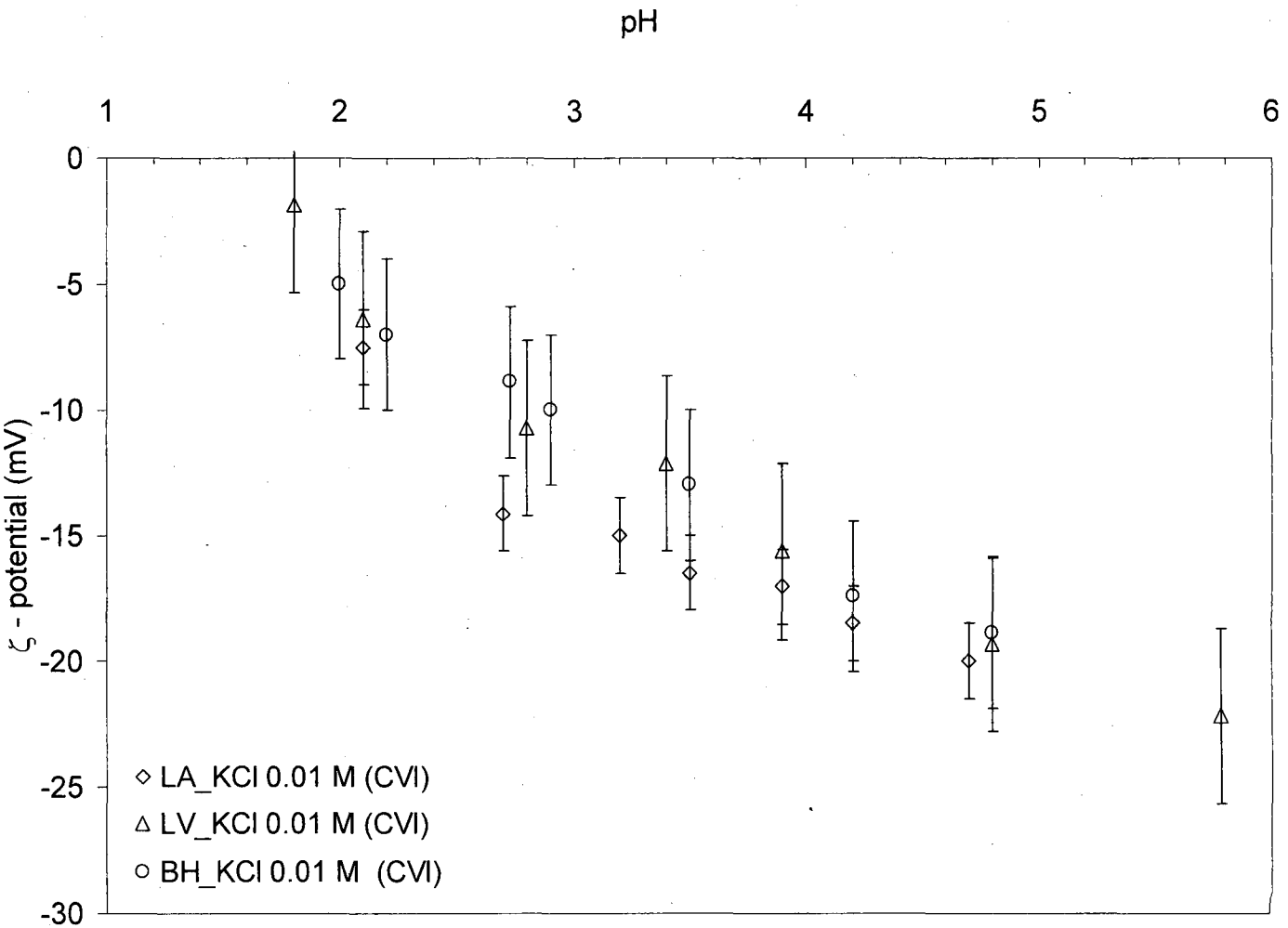

Figure 5-9: Variation of the zeta-potential of LA, LV and BH mine tailings as a function of pH in aqueous solution of 10^{-2} mol/l KCl.

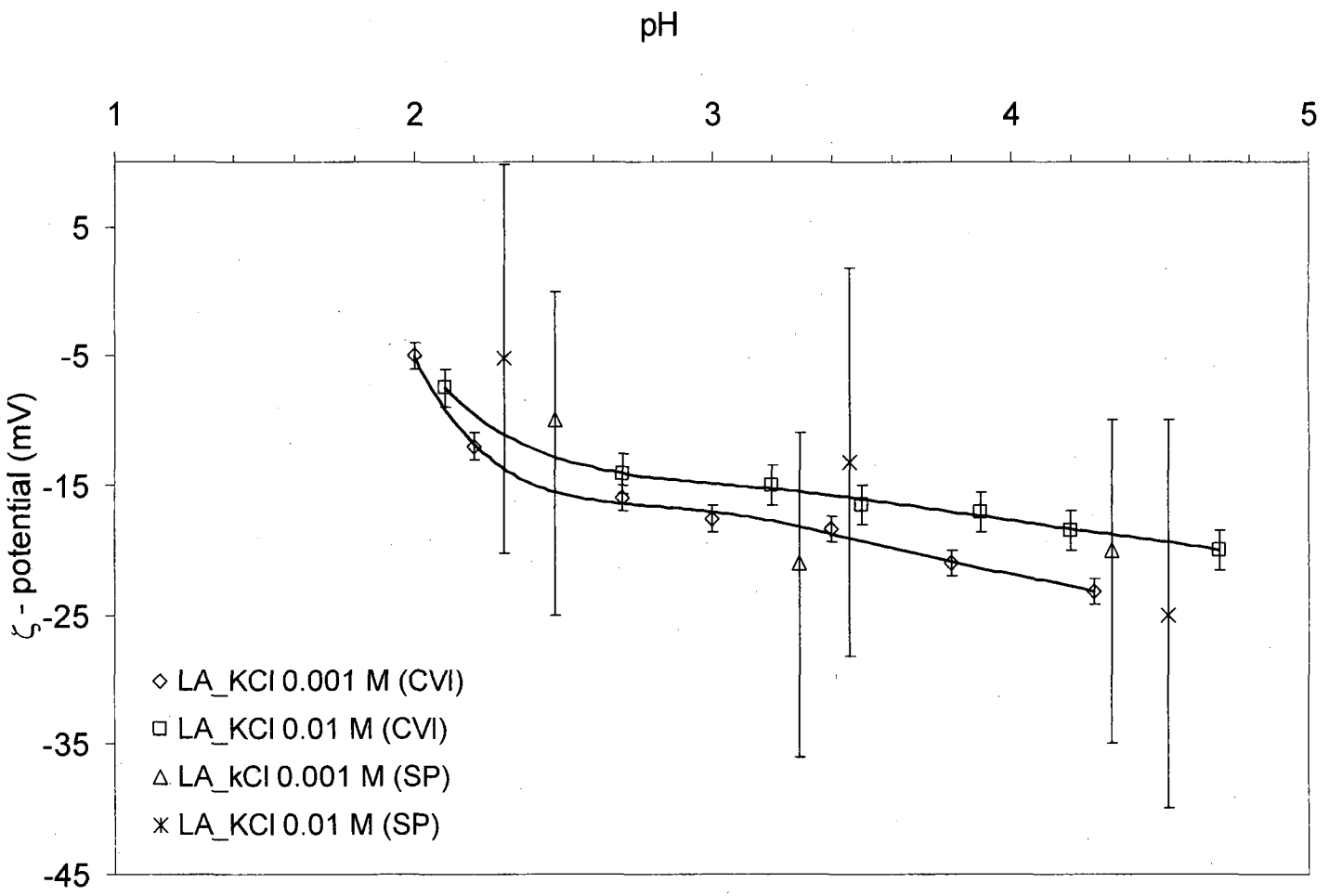

Figure 5-10: Variation of the zeta-potential of LA mine tailings as a function of pH and KCl concentration.

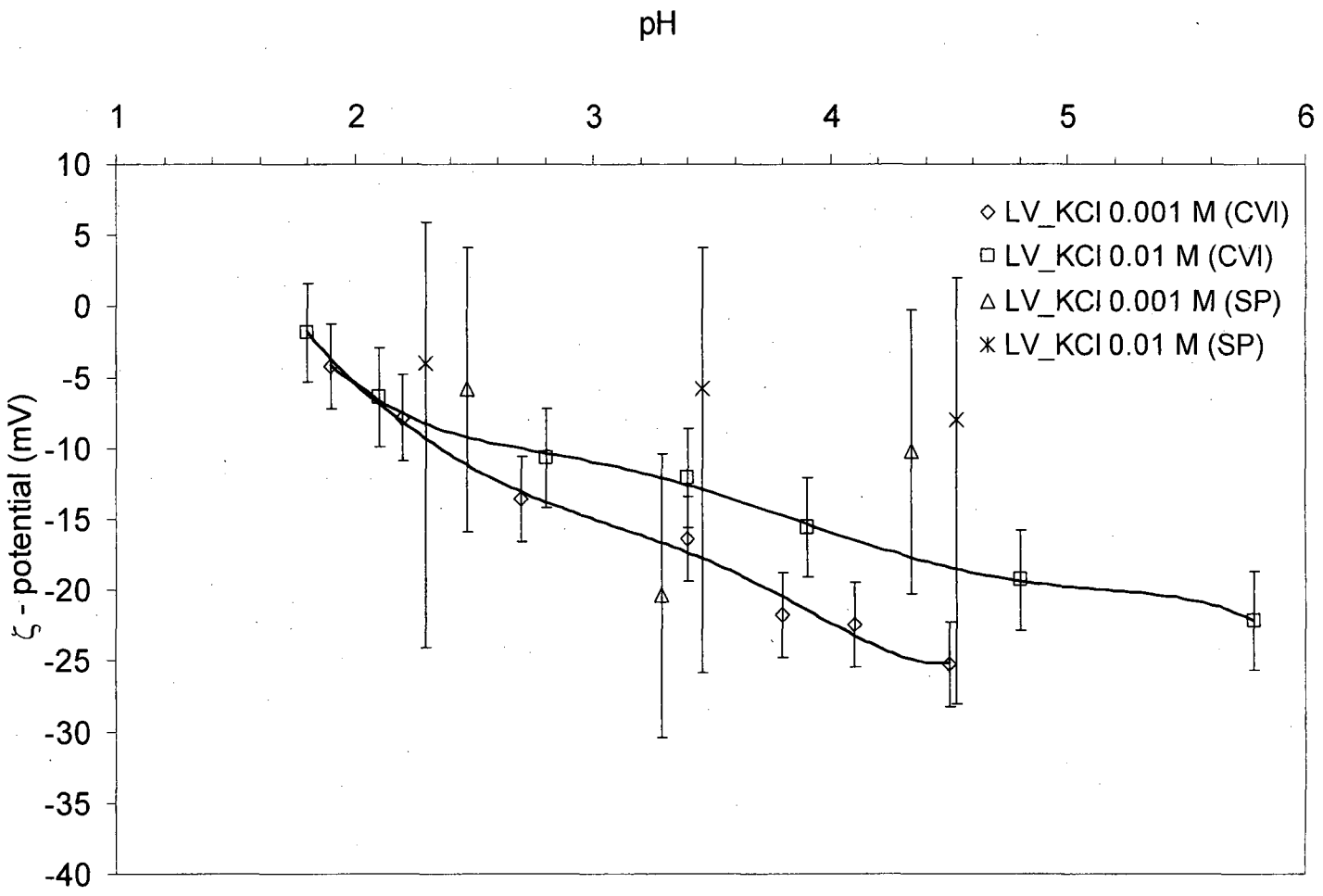

Figure 5-11: Variation of the zeta-potential of LV mine tailings as a function of pH and KCl concentration

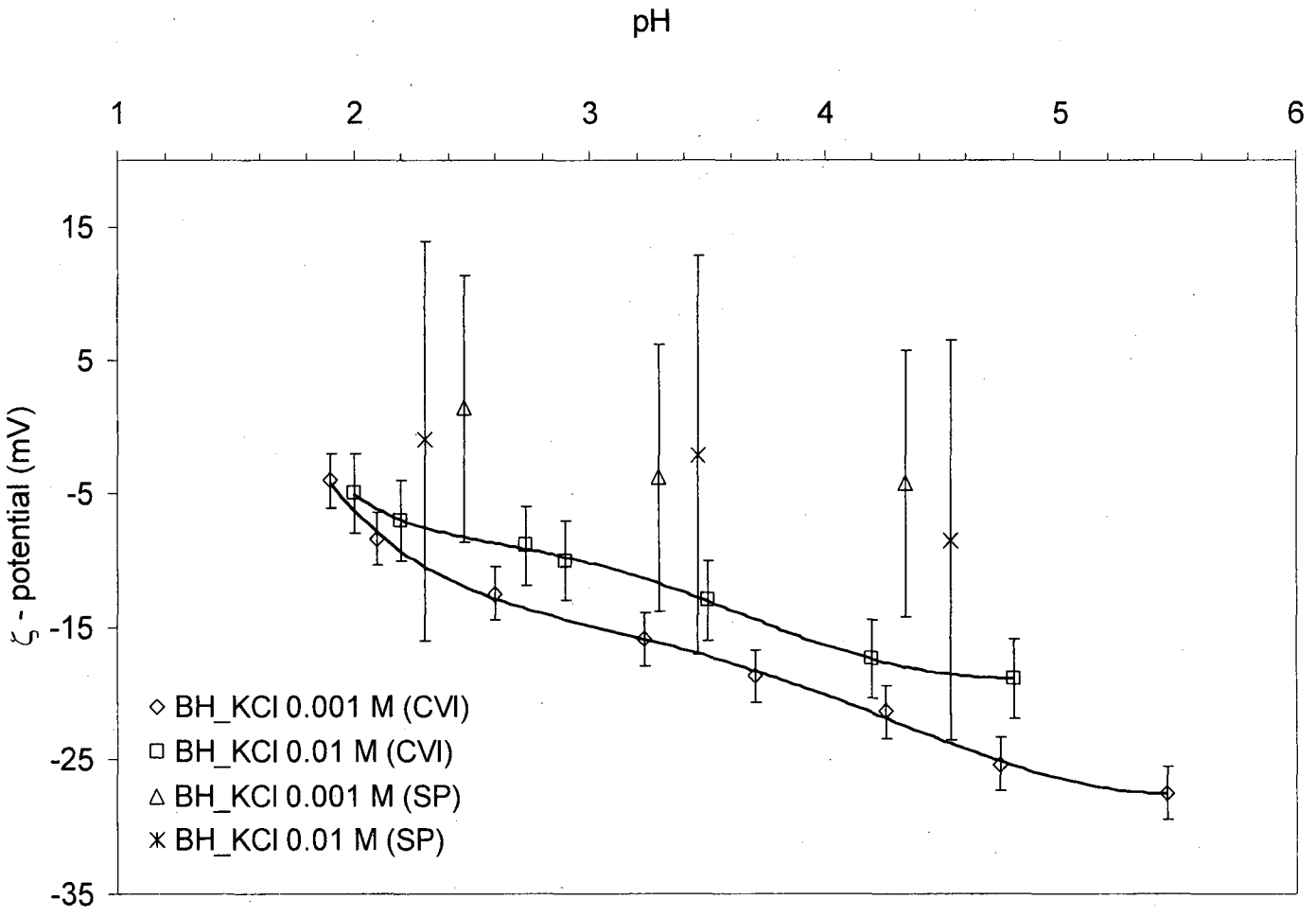

Figure 5-12: Variation of the zeta-potential of BH mine tailings as a function of pH and KCl concentration

CHAPTER : 6 SUMMARY AND CONCLUSIONS AND FUTURE WORK

6.1. SUMMARY AND CONCLUSIONS

In the present fundamental laboratory investigation, the resistivity variation was presented as a function of the loss of fine particles. The zeta potential for sulfide rich tailings inferred from streaming potential and electroacoustic spectroscopy measurements was presented as a function of the pH and electrolyte solution concentration.

A testing program consisting of 96 streaming potential measurements, 108 electroacoustic measurements of the zeta-potential and 108 resistivity measurements was conducted to further the understanding of the streaming potential (SP) in sulfide rich tailings and the influence of the tailings geophysical parameters and fluid properties on the cross-coupling coefficient. The main objectives were to estimate the magnitude of the zeta-potential and its variation with pH and fluid conductivity, and to study the effect of the loss of fine particles on the resistivity.

In addition to the experimental study we discussed the theoretical relationship between the zeta-potential and the water flux. We also discussed the importance of the zeta-potential in the numerical modeling of the streaming potential and its application in embankment dams.

The present experimental results give fundamental information on the zeta-potential of water - sulfide rich tailings systems. Clearly much more laboratory data must be collected before a comprehensive relationship between the zeta-potential and flux can extracted. The measured zeta-potential is affected by several factors, which include:

1. the tendency of sulfide rich tailings to oxidize with time or when the chemistry or pH of the electrolyte solution changes;
2. tailings are polymineralic, the ratio of the different minerals will certainly affect the measured zeta-potential; and

3. the technology used to measure the zeta-potential.

The zeta-potential was found to vary from – 27 mV to -2 mV for the three tested sulfide rich tailings, depending on the pH and the electrolyte concentration. Attempts to compare the results from the different technologies used were not successful, probably due to a difference in chemical composition of the full gradation of the tailings and the coarse fraction, sample density and ionic equilibration.

The tailings resistivity was observed to depend on the percentage of fine particles present in the sample. The laboratory measurements on the study's tailings samples reveal a decrease in resistivity of the full gradation of the tailings compared to the full gradation or coarse fraction. Consequently, this would imply that when an internal erosion problem arises we should expect an increase in resistivity.

From the laboratory resistivity measurements we can conclude that the tailings' resistivity is influenced by the surface conductivity effects of the conductive pyrite grains. Consequently, Archie's law is not applicable since the global resistivity of the sample is not solely a function of the fluid conductivity.

In order for the results of this research to be used in the detection of the seepage paths in sulfide rich tailings dams and in order to estimate an average flow rate for this anomalous seepage, repeated resistivity surveys should be conducted in conjunction with the self-potential surveys in order to establish the resistivity distribution of the subsurface and to detect zones of high resistivity.

The following three-step procedure is suggested;

1. the resistivity survey should locate areas of high resistivity, which could imply an internal erosion problem;
2. the self-potential survey results at this same location should be analysed using numerical modelling;
3. The modelling will give an estimated value for the streaming potential which could be compared with the measured potential. In order to remove unwanted signals, namely

the electrochemical and sedimentation potentials. Measurements can be taken in the areas where no resistivity anomalies are detected.

6.2. FUTURE WORK

In the process of researching a certain topic there are always interesting possibilities that cannot be explored due to constraints such as time or the availability of economic resources. The research work presented in this thesis is a preliminary study that leaves room for further development. More research needs to be carried out in order to elucidate the different parameters affecting the streaming potential in sulfide rich tailings.

The following studies are recommended for future consideration:

- Since preliminary data on the zeta-potential and the resistivity of the sulfide rich tailings is presented in this thesis, it would be reasonable to further the study by (1) conducting field resistivity and streaming potential surveys at the studied tailings ponds; (2) by modeling the flow using one of the available SP numerical modeling software packages; and (3) by using the results from this thesis to interpret the SP anomaly by inputting the right parameters in the model.

- Since the zeta-potential measurements results indicate a strong dependence on the pH and on the electrolyte chemistry, it would be reasonable to further examine the influence of pond water chemistry on the zeta-potential.

- Since the sulfide rich-tailings tend to oxidize with time, it would be interesting to study the effect of oxidation on the zeta-potential values.

- Since the resistivity of the tailings is highly dependent on the chemistry of the pore fluid, the degree of saturation, permeability and porosity, which is dependent on the degree of compaction, it would be reasonable to further the study of the resistivity of the tailings by conducting field surveys as well as laboratory tests similar to the ones performed in this thesis, but using the pond water.

- Since the sulfide rich tailings tend to oxidize and new minerals tend to form with time, it would be interesting to study the longitudinal effect of oxidation on the resistivity of the sulfide rich tailings.

6.3. CONTRIBUTION TO KNOWLEDGE

- The zeta-potential of sulfide rich tailings was measured and the influence of the pH and electrolyte concentration on the magnitude of the zeta-potential was established.
- The electroacoustic measurement of the zeta-potential of sulfide rich tailings was successfully used.
- The influence of particle size on the resistivity of sulfide rich tailings was measured.
- A procedure for detecting and monitoring water seepage from tailings dams using repeated resistivity and streaming potential measurements combined with a numerical analysis is suggested.

REFERENCES

Abu-Hassanein, Z.S.; Benson, C.H.; Blotz, L.R. (1996). Electrical resistivity of compacted clays. Journal of Geotechnical Engineering, 122: 397-406.

Agarwal B.N.P. (1984). Quantitative interpretation of self-potential anomalies. 54th Ann. Internat. Mtg., Soc. Expl. Geophys., Expanded Abstracts, p. 154 – 157.

Ahmad, M.U. (1964). A laboratory study of streaming potentials, Geophysical Prospecting, 12: 49-64.

Al-Saigh N.H., Mohammed Z.S. & Dahham M.S. (1994). Detection of water leakage from dams by self-potential method. Engineering Geology 37, p. 115 – 121.

Arrnbruster H, Brauns J., Mazur W. & Merkler G.P. (1989). Effect of leaks in dams and trials to detect leakages by geophysical means: Lecture notes in earth sciences, Vol. 27, G.P. Merkler et al., eds., Springer-Verlag, Berlin, p. 3 – 17.

ASTM (2006). Standard Test Methods for Specific Gravity of Soil Solids by Water Pycnometer (D854-06). In 2006 Annual Book of ASTM Standards, Vol. 04-08. ASTM, Philadelphia,

Aubert M., Atangana Q.Y. (1996). Self-potential method in hydrogeological exploration of volcanic areas. Ground Water 34, p. 1010 – 1016.

Aubertin M., Bussiere B. & Bernier L. (2002). *Environnement et gestion des rejets miniers*. Presses Internationales Polytechniques.

Aubertin M., Bussière B., and Chapuis R.P. (1996). Hydraulic conductivity of homogenized tailings from hard rock mines. Canadian Geotechnical Journal, 33: 470–482.

Aubertin M., Chapuis R.P., Bussière B., and Aachib M. (1993). Propriétés des résidus miniers utilizés comme matériaux de recouvrement pour limiter le DMA. In Proceedings of the Geoconfine 93, A.A. Balkema, Rotterdam, pp. 299–308.

Bartsch M. (1995). *Filtration processes and internal erosion in dams of broadly graded material*. Technical Report, Royal Institute of Technology, Stockholm

Beattie A.G. (1983). Acoustic Emission, Principles and Instrumentation. Journal of Acoustic Emission, 2, No. 1, p. 95 – 128.

Beck B.F. (1988). Environmental and engineering effects of sinkholes – the processes behind the problems. In: Yuan DX (ed) Karst hydrogeology and karst environment protection. IAH 21st Congress, p. 17–29

Bérubé, A.P. (2004). Investigation the streaming potential phenomenon using electric measurements and numerical modeling with special reference to seepage monitoring in embankment dams. Doctoral Thesis, Lulea University of Technology, Sweden.

Bhattacharya B.B. & Roy N. (1981). A note on the use of a nomogram fro self-potential anomalies. Geophys. Prosp., 29, p. 102 – 107.

Birch F.S. (1993) Testing Fournier's method for finding water table from self-potential. Ground Water 31, p. 50 – 56.

Black W.E. & Corwin R.F. (1984). Application of self-potential measurements to the delineation of groundwater seepage in earth-fill embankments. Fifty fourth SEG Meeting, Atlanta, USA, Expanded abstracts, p. 162 – 164.

Bogoslovsky V.A. & Oglivy A.A. (1970a). Natural potential anomalies as a quantitative index of the role of water seepage from reservoir. Geophysical Prospecting, 18, p. 261 – 268.

Bogoslovsky V.A. & Oglivy A.A. (1970b). Application of geophysical methods for studying the technical status of earth dams. Geophysical Prospecting, 18, p. 758 – 773.

Bogoslovsky V.A. & Oglivy A.A. (1973). Deformation of natural electric fields near drainage structures. Geophysical Prospecting, 21, p. 716 – 723.

Bogoslovsky V.A., Kuzmina E.N., Oglivy A.A. & Strakhova N.A. (1979). Geophysical methods for controlling the seepage regime in earth dams. Bulletin of the International Association Engineering Geology, 20, p. 249 – 251.

Bogoslovsky V.V. & Ogilvy A.A. (1972). The Study of Streaming Potentials on Fissured Media Models. Geophysical Prospecting, 20(4), p. 109 – 117.

Bogoslovsky V.V. & Ogilvy A.A. (1977). Magnetometric and Electrometric Methods for the Investigation of the Dynamics of Landslide Processes. Geophysical Prospecting, 25(3), p. 280 – 291.

Boncompain B., Paré J.J. & Levay J. (1989). Crest sinkholes related to collapse of loose material upon wetting, Vol. 3. Proceedings of the 12th ICSMFE, Rio de Janeiro, 13–18 août. A.A. Balkema, Rotterdam, p. 1797 – 1801.

Bussière B. (1993). Évaluation des propriétés hydrogéologiques des résidus miniers utilizés comme barrières de recouvrement. Master's thesis, École Polytechnique, Montréal, Québec., 171 pp.

Butler D.K. (1984). Geophysical methods for seepage detection, mapping and monitoring, Fifty-fourth SEG Meeting, Atlanta, USA, Expanded abstracts, p. 157 – 160.

Butler D.K., Llopis J.L., Dobecki T.L., Wilt M.J., Corwin R.F. & Olhoeft G. (1990). Comprehensive geophysics investigation of an existing dam foundation : Engineering geophysics research and development, Part 2. The Leading Edge 9, p. 44 – 53.

Campanella, R.G. and Weemees, I. (1990). Development and use of an electrical resistivity cone for groundwater contamination studies. Canadian Geotechnical Journal, 27: 557-567.

Cartwright K. (1968). Thermal prospecting for groundwater, Water Resources Research, 4(2), p. 395 – 401.

Cartwright K. (1974). Tracing shallow groundwater systems by soil temperatures, Water Resources Research, 10(4), p. 847 – 855.

Cedergren H.R. (1997). Seepage, Drainage, and Flow Nets, Wiley-Interscience.

Chapuis R.P. and Aubertin M. (2003). On the use of the Kozeny-Carman equation to predict the hydraulic conductivity of soils. Canadian Geotechnical Journal, 40: 616–628.

Chapuis R.P., and Légaré P.P. (1992). A simple method for determining the surface area of fine aggregates and fillers in bituminous mixtures. In Effects of aggregates and mineral fillers on asphalt mixture performance. American Society for Testing and Materials, ASTM STP Vol. 1147, p. 177 – 186.

Corwin R.F. & Butler D.K. (1989). Geotechnical applications of the self-potential method; Rept. 3: Development of self-potential interpretation techniques for seepage detection: Tech. Rep. REMR-GT-6, U.S. Army Corps of Engineers, Washington DC.

Corwin R.F. & Conti U. (1973). A rugged silver – silver chloride electrode for field use. Review of scientific instruments, 44, p. 708 – 711.

Corwin R.F. & Hoover D.B. (1979). The self-potential method in geothermal exploration. Geophysics 44, p. 226–245.

Corwin R.F. (1989a). Self-potential investigation, Nevada Test Site, Mercury, Nevada: Report UCRL- 21187, January 19 1989, P.O. 719-003, Lawrence Livermore National Laboratory, Livermore, CA.

Corwin R.F. (1989b). Data quality for engineering self-potential surveys. In: Lecture Notes in Earth Sciences, Vol. 27 (ed. G-P. Merkler, H. Militzer, H. Hoetzl, H. Armbruster and J. Brauns), p. 51 – 72. Berlin: Springer-Verlag.

Corwin R.F. (1990a) The self-potential method for environmental and engineering applications, in S.H. Ward, ed., Geotechnical and environmental geophysics, Vol. 1, Soc. of Exploration Geophysicists, Tulsa, OK, p. 127 – 145.

Corwin R.F. (1990b). Self-potential investigation of seepage flow, east embankment, Wells Dam: Report for Douglas County Public Utility District No. 1, Washington.

Corwin R.F. (1990c). Direct-current electrical resistivity investigation, east embankment, Wells Dam: Report for Douglas County Public Utility District No. 1, Washington.

Corwin R.F. (1991). Evaluation of effects of cutoff wall construction on seepage flow using selfpotential data, east embankment, Wells Dam: Report for Douglas County Public Utility District No. 1, Washington.

Corwin R.F., DeMoully G.T. & Morrison H.F. (1981). Interpretation of self-potential survey results from the East Mesa geothermal field. J. Geophys. Res., 86, B3, p. 1841 – 1848.

Dahlin T., Sjödahl P. & Johansson S. (2005). Resistivity monitoring for internal erosion detection at Hällby and Sädva embankment dams. Procs. International

Symposium on Dam Safety and Detection of Hidden Troubles of Dams and Dikes, November 1-3 2005, Xi'an, China, p. 10

Dahlin T., Sjodahl P., Friborg J. & Johansson S. (2004). Defect detection using measurements of resistivity and self potential – Experiences from field test damans large embankment dams in Sweden. *Proceedings – Stability and Breaching of Embankment Dams*, EBL Oslo.

Dahlin T., Sjödahl P., Friborg J., Johansson S. (2001). Resistivity and SP surveying and monitoring at the Sädva embankment dam, Sweden. ISBN 90 5809 196 1, Procs. 5th European ICOLD Symposium, 25-27 June 2001, Geiranger, Norway, p. 107 – 113.

Darnet M. and Marquis G. (2004). Modelling streaming potential (SP) signals induced by water movement in the vadose zone. Journal of Hydrology, Vol. 285, p. 114 – 124.

Davies M.P. & Martin T.E. (2000). Upstream constructed tailings dams – A review of the basics. Proceedings of Tailings and Mine Waste 2000, p. 3 – 15.

DeMoully G. T. & Corwin R.F. (1980). Self-potential survey results from Beowawe KGRA, Nevada. Trans. Geotherm. Resources Council, 4, p. 33 – 36.

Denbigh K.G. (1951). The themodynamics of the steady sate. John Wiley & Sons, Inc.

Dornstadter J. (1997). "Detection of Internal Erosion in Embankment Dams, " ICOLD 19th Congress, 4.73, R.7, Florence 1997.

Dukhin, A.S. and Goetz, P.J. (1996a). Acoustic and electroacoustic spectroscopy. Langmuir, 12: 4336-4344.

Dukhin, A.S. and Goetz, P.J. (1996b). Acoustic spectroscopy for concentrated polydisperse colloids with high density contrast. Langmuir, 12: 4987-4997.

Dukhin, A.S. and Goetz, P.J. (2002). Ultrasound for Characterizing Colloids, Studies in Interface Science, Elsevier, Amsterdam.

Dukhin, A.S., Oshima, H., Shilov, V.N. and Goetz, P.J. (1999a). Electroacoustic for concentrated dispersions. Langmuir, 15: 3445-3451.

Dukhin, A.S., Shilov, V.N., Oshima, H., and Goetz, P.J. (1999b). Electroacoustic phenomena in concentrated dispersions: New theory and CVI experiment. Langmuir, 15: 6692-6706.

Elimelech, M., Gregory, J., Jia, X. and Williams, R.A. (1998). Particle Deposition and Aggregation - Measurement, Modelling and Simulation. Butterworth-Heinemann. Engineer's Viewpoint. Tailings Disposal Today, Proceedings of the First International Tailings Symposium, Tucson, Arizona.

Emstson K. & Scherer H.U. (1986). Self-potential variations with time and their relation to hydrogeologic and meteorological parameters: Geophysics, v. 5 1, p. 1967 – 1977.

Erchul R.A. & Slifer D.W. (1987) The use of spontaneous potential in the detection of groundwater flow patterns and flow rate in karst areas. In: Beck BF (ed) 2nd

Multidisciplinary Conf on Sinkholes and the Environmental Impacts of Karst, Orlando, Florida, p. 217 – 226.

Ernston K. & Scherer H.U. (1986). Self-potential variations with time and their relation to hydrogeologic and meteorological parameters. Geophysics 51, p. 1967 – 1977.

Ewing S. (1939). The copper-copper sulfate half-cell for measuring potentials in the earth. Tech. Section, American Gas Association Proc.

Fagerlund F. & Heinson G. (2003). Detecting subsurface groundwater flow in fractured rock using self-potential (SP) methods. Environmental Geology 43 (7), p. 782 – 794.

Fitterman D.V. & Corwin R.F. (1982). Inversion of self-potential data from the Cerro Prieto geothermal field, Mexico. Geophysics, 47, p. 938 – 945 .

Fitterman D.V. (1978). Electrokinetic and magnetic anomalies associated with dilatant regions in a layered earth. Journal of Geophysical Research, 83, p. 5923–5928.

Fitterman D.V. (1979). Calculations of self-potential anomalies near vertical contacts. Geophysics, 44, p. 195 – 205.

Fitterman D.V. (1982). Computer program SPDIKE for calculation of self-potential anomalies near vertical dikes. U.S. Geol. Surv. Open file rept., p. 82 – 470.

Fitterman D.V. (1983). Modeling of self-potential anomalies near vertical dikes. Geophysics, 48, p. 171 – 180.

Fitterman D.V. (1984). Thermoelectrical self-potential anomalies and their relationship to the solid angle subtended by the source region. Geophysics, 49, p. 165 – 170.

Foster M., Fell R. & Spannagle M. (2000). "The statistics of embankment dam failures and accidents." *Canadian Geotechnical Journal*, Vol. 37, p. 1000 – 1024.

Foster M., Fell R. & Spannagle M. (2000a). The statistics of embankment dam failures and accidents, Canadian Geotechnical Journal, Vol.37, No.5, National Research Council Canada, Ottawa, p. 1000 – 1024.

Foster M., Fell R. & Spannagle M. (2000b). A method for assessing the relative likelihood of failure of embankment dams by piping. Canadian Geotechnical Journal, 37, p. 1025 – 1061.

Gex P. (1980). Electrofiltration phenomena associated with several dam sites. Bulletin of the Society Vaud Science and Nature No 357, issue 75, p. 39 – 50.

Godfrey K.A. (1984), New tools help find flaws. Civil Engineering, ASCE, Sept., p. 39 – 42.

Gribble C.D. (1992). Optical mineralogy: principles and practice, London, UCL Press.

Hadley L.M. (1983). A geophysical method for evaluating existing earth embankments. Bulletin of the International Association of Engineering Geology 20, p. 289 – 295.

Haile J.P. (1997). Discussion on the Failure of the Omai Tailings Dam. *Geotechnical News*, Vol. 15, No 1, p. 44 – 49.

Haines B.M. (1978). The detection of water leakage from dams using streaming potentials. Soc. Prof. Well Log. Analysts 19th Ann. Logging Sympos.

Head K.H. (1992). Manual of Soil Laboratory Testing, New York, John Wiley & Sons Inc.

Holtz R.D. and Kovax W.D. (1981). An introduction to geotechnical engineering, Prentice-Hall.

Hunter, R.J. (1998). Recent development in the electroacoustic characterization of colloidal suspension and emulsions. Colloids and Surfaces, 141, 37-65.

Hunter, R.J. (2001). Foundations of Colloid Science. Oxford University Press, New York.

Huntley, D. (1986). "Relations between permeability and electrical resistivity in granular aquifers." Ground Water, 24(4), 466-474.

ICOLD (1983). *Deterioration of Dams and Reservoirs*, International Commission on Large Dams.

ICOLD (1994). Embankment Dams Granular Filters and Drains, Review and Recommendations, Bulletin 95, International Commission on Large Dams.

ICOLD (1995). *Dam Failures Statistical Analysis*, Bulletin 99, International Commission on Large Dams.

ICOLD (2001). Tailings Dam Risk of Dangerous Occurrences. Lessons Learnt from Practical Experiences, Bulletin 121, International Commission on Large Dams.

Ishido T. & Mizutani H. (1981). Experimental and theoretical basis of electrokinetic phenomena in rock–water systems and its applications to geophysics. Journal of Geophysical Research, 86: p. 1763–1775.

Ishido T. & Pritchett J.W. (1999). Numerical simulation of electrokinetic potentials associated with subsurface fluid flow. Journal of Geophysical Research, 104, p. 15247 – 15259.

Ives D.J.G. & Janz G.J. (1961). Reference electrodes, theory and practice. New York: Academic Press Inc.

Johansson S. & Farhadiroushan M. (1999). Fibre-optic System for Temperature measurements at the Lovon Dam. Elforsk Rapport 99:36, Stockholm, p. 25.

Johansson S. (1991). Localization and quantification of water leakage in ageing embankment dams by regular temperature measurements. Q 65, R54, ICOLD 17th Congress in Vienna, p. 991 – 1005.

Johansson S. (1997). *Seepage Monitoring in Embankment Dams*. Doctoral Thesis. Royal Institute of Technolog, Stockholm.

Johansson S. (1997). Seepage Monitoring in Embankment Dams. Doctorial Thesis at The Royal Institute of Technology (KTH), Div. of Hydraulic Engineering, Dep. of Civil and Environmental Engineering. Stockholm, Sweden.

Johansson S. (2007). Detection of internal erosion in embankment dams using temperature, resistivity and SP measurements. *Internal Erosion of Dams and their Foundations* – Fell & Fry (eds), London

Johansson S., Dahlin T. & Friborg J. (2000b). Seepage monitoring by resistivity and streaming potential measurements at Hallby embankment dam, 1996-1999: Elforsk Report 00: 15, Elforsk AB, Stockholm, Sweden.

Johansson S., Dahlin T. & Friborg J. (2000c). Seepage monitoring by continuous measurements of resistivity and streaming potential in Hallby and Sadva embankment dams, Sweden: Proc., Commission Internationale des Grand Barrages, Vingtieme Congres des Grands Barrages, Beijing, 2000, p. 1099 – 1123.

Johansson S., Friborg J., Dahlin T. & Sjödahl P. (2003) Long term resistivity and self-potential monitoring of embankment dams – Experiences from Hällby and Sädva dams,Sweden. Elforsk report 05:15, p. 123.

Johansson S., Friborg J., Farhaidoushan M. & Dahlin T. (2000a). New and improved monitoring systems for embankment dams [Sadva Dam - Ed.]: Elforsk Report 00:14, Elforsk AB, Stockholm, Sweden.

Jouniaux L. & Pozzi J.P. (1995a). Permeability dependence of streaming potential in rocks for various fluid conductivities. Geophysical Res Lett, 22, p. 485 – 488.

Jouniaux L. & Pozzi J.P. (1995b). Streaming potential and permeability of saturated sandstones under triaxial stress: consequences for electrotelluric anomalies prior to earthquakes. Journal of Geophysical Research, 100, p. 10197 – 10209.

Jouniaux L. & Pozzi J.P. (1997). Laboratory measurements anomalous 0.1– 0.5 Hz streaming potential under geochemical changes: Implications for electrotelluric precursors to earthquakes, Journal of Geophysical Research, 102, p. 15 335 – 15 343.

Kaiser J. (1950). Untersuchungen uber das auftreten gerausen bein zugersuch. Ph.D. Thesis. Technische Huchschule, Munich.

Kakuturu S. & Reddi L.N. (2006b). Mechanistic Model for Self-Healing of Core Cracks in Earth Dams. *Journal of Geotechnical and Geoenvironmental. Engineering*, Vol. 132, No. 7, p. 890 – 901.

Kakuturu S. & Reddi, L.N. (2006a). Evaluation of the parameters influencing self-healing in earth dams. *Journal of Geotechnical and Geoenvironmental. Engineering*, Vol. 132, No. 7, p. 879 – 889.

Kamon M., and Katsumi T. (1994). Potential utilization of waste rock powder. Proceedings, 1st International Congress on Environmental Geotechnics, Edmonton, p. 281 – 292.

Kappelmeyer O. (1957). The Use of Near Surface Temperature Measurements for Discovering Anomalies due to Causes at Depths. Geophysical Prospecting, Vol. 3, p. 239 – 258, The Hague, 1957.

Kassel A., Faber S. & Merkler G-P. (1989). Laboratory studies on the characteristics of electrodes used for streaming potential measurements. In: Lecture Notes in Earth Sciences, Vol. 27 (ed. G-P. Merkler, H. Militzer, H. Hoetzl, H. Armbruster and J. Brauns), p. 157 – 170. Berlin: Springer-Verlag.

Keller G.V. and Frischknecht F.C. (1966). Electrical methods in geophysical prospecting, In: *International Series of Monographs in Electromagnetic Waves* **Vol. 10**, Pergamon, New York.

Keller, G. & Frischknecht. F. (1966). Electrical methods in geophysical prospecting, Pergamon Press, New York, N.Y.

Kenney T.C. & Lau D. (1985). Internal stability of granular filters. *Canadian Geotechnical Journal*, Vol. 22, p. 215 – 225.

Kenney T.C., Chanal R., Chin E., Ofoeghu G.I., Omange G.N. & Ume C.A. (1985). Controlling constriction size of granular filters. *Canadian Geotechnical Journal*, Vol. 22, p. 32 – 43.

Kilty KT, Lange AL (1991). Electrochemistry of natural potential processes in karst. In: Proc 3rd Conf on Hydrogeology, Ecology, Monitoring & Management of Groundwater in Karst Terranes, 4–6 Dec 1991, Maxwell House, Clarison, Nashville, Tennessee. P. 163 – 177.

Kilty, K.T. (1984). On the origin and interpretation of self-potential anomalies.Geophysical Prospecting 32, p. 51 – 62.

Koerner R.M., Lord A.E. Jr. and McCabe W.M. (1976). Acoustic emission (Microseismic) monitoring of earth dams. Proceedings, Conference on Evaluating Dam Safety, Nov. 28 – Dec. 3, p. 274 – 291.

Koerner R.M., McCabe W.M. and Baldivieso L.F. (1981). Acoustic emission monitoring of seepage. Journal of the Geotechnical Engineering Division, ASCE, Vol. 107, No. GT7, Technical Notes, p. 521 – 526.

Koester, J.P., Butler, D.K., Coper, S.S. & Llopis, J.L. (1984). Geophysical investigation in support of Clearwater Dam comprehensive seepage analysis: U.S. Army Corps of Engineers Waterways Experiment Station Misc. Paper GL-84-3.

L'Écuyer M., Chapuis R.P., and Aubertin M. (1992). Propriétés hydro-géotechniques des résidus miniers de Solbec et Cupra, Québec. In Proceedings of the 45th Canadian Geotechnical Conference, Toronto, Ont., pp. 79.1–11

Lamb, H. (1945). Hydrodynamics. 6th ed. New York: Dover.

Lange A.L. & Barner W.L. (1995). Application of the natural electrical field for detecting karst conduits on Guam. In: Beck BF (ed) Karst geohazards. Balkema, Rotterdam, p. 425 – 441.

Lange A.L. & Kilty K.T. (1991). Natural-potential response of karst systems at the ground surface. In: Proc 3rd Conf on Hydrogeology, Ecology, Monitoring, and Management of Groundwater in Karst Terranes, 4–6 Dec 1991, Maxwell House, Nashville, Tennessee, p. 179 – 197.

Loke M.H. (2000). Electrical imaging surveys for environmental and engineering studies, A practical guide to 2-D and 3-D surveys, Dr. M.H.Loke, Internet site:http://www.geoelectrical.com.

Loke M.H., (2004). Tutorial : 2-D and 3-D electrical imaging surveys, Dr. M.H.Loke, Internet site:http://www.geoelectrical.com.

Lorne B., Perrier F. & Avouac J.-P. (1999). Streaming potential measurements. 1. Properties of the electrical double layer from crushed rock samples. Journal of Geophysical Research, 104, p. 17857 – 17877.

Lykelema, J. (1995). Fundamentals of Interface and Colloid Science: Volume II, Academic Press, London.

Mabes D.L., James H.H., and Williams R.E. (1977). Physical properties of Pb-Zn mine-process wastes. *Proceedings, Conference on Geotechnical Practice for Disposal of Solid Waste Materials*, ASCE, p. 103 – 117.

MacInnes D.A. (1961). *The principles of electrochemistry*, Dover, New York.

Matyas E.L., Welch D.E., and Reades D.W. (1984). Geotechnical parameters and behaviour of uranium tailings. *Canadian Geotechnical Journal*, Vol. 21, p. 489 – 504.

Mbonimpa M., Aubertin M., Chapuis R.P., and Bussière B. (2002). Practical pedotransfer functions for estimating the hydraulic conductivity. Geotechnical and Geological Engineering, Vol. 20, p. 235 – 259.

Merkler G.P., Blinde A., Armbruster H. & Döscher H.D. (1985). Field investigations for the assessment of permeability and ident ification of leakage in dams and dam foundations, Proc. ICOLD 15th Congress, Q58, R7, Lausanne, Switzerland.

Merkler G.P., Militzer H., Hötzl H., Armbruster H., & Brauns J. (1989). Lecture Notes in Earth Sciences, Vol 27, Detection of Subsurface Flow Phenomena, Springer Verlag Berlin, Heidelberg.

Mitchell J.K. (1976). Fundamentals of soil behavior. John Wiley & Sons, Inc.

Mitchell J.K. (1976). *Fundamentals of soil behaviour*, John Wiley & Sons, New York.

Mittal H.K., and Morgenstern N.R. (1976). Seepage control in tailings dams. *Canadian Geotechnical Journal*, Vol. 13, p. 277 – 293.

Monzon M. (1998). Étude en laboratoire des propriétés hydrogéotechniques des résidus miniers utilizés comme barrière de recouvrement. Mémoire de M.Sc.A., Ecole Polytechnique, Montréal, Québec.

Morgan F. D., Williams E. R. & Madden T. R. (1989). Streaming potential properties of Westerly granite with applications, Journal of Geophysical Research, 94: p. 12449 – 12461.

Morgan F.D. (1989). Fundamentals of streaming potentials in geophysics: Laboratory methods, *Lecture notes in earth sciences*, Vol. 27, G.P. Merkler et al., eds, Springer-Verlag, Berlin, p. 133 – 144.

Morgan F.D., Williams E.R. & Madden T.R. (1989). Streaming potential properties of Westerly granite with applications, *Journal of Geophysical Research*, Vol. 94, p. 12449 – 12461.

Murty B.V.S. & Haricharan P. (1985). Nomogram for the complete interpretation of spontaneous polarization profiles over sheet-like and cylindrical two dimensional sources. Geophysics, 50, p. 1127 – 1135.

Nesse W.D. (2004). Introduction to optical mineralogy, New York, Oxford University Press.

Nordstrom, D.K., 1982. Aqueous pyrite oxidation and the consequent formation of secondary iron minerals. In: Kitrick, J.A., Fanning, D.S., Hossner, L.R. (Eds.), Acid Sulfate Weathering, vol. 10. Soil Sci. Soc. Am. Madison, WI, p. 37– 56.

Nourbehecht B. (1963). Irreversible thermodynamic effects in inhomogeneous media and their application in certain geoelectrical problems. PhD thesis, Massachusetts Institute of Technology.

Nowatzki E.A., and Robertson A.M. (1988). Cement stabilization of dewatered mine tailings and its effect on vehicle mobility. In Hydraulic Fill Structures, ASCE, p. 795 – 8 15.

O'Brien, R.W., Cannon, D.W. and Rowlands, W.N. (1995). Electroacoustic determination of particle size and zeta potential. Journal of Colloid and Interface Science, 173, 406-418.

Oglivy A.A., Ayed M.A. & Bogoslovsky V.A. (1969). Geophysical studies for water leakages from reservoirs. Geophysical Prospecting, Vol. 17, p. 36 – 62.

Onsager L. (1931). Reciprocal relations in irreversible processes I. Phys. Rev., 37, p. 405 – 426.

Oshima, H. (1998). Sedimentation potential in a concentrated suspension of spherical colloidal particles. Journal of Colloid and Interface Science, 208, 295-301.

Oshima, H. and Dukhin, A.S. (1999). Colloid vibration potential in a concentrated suspension of spherical colloidal particles. Journal of Colloid and Interface Science, 212, 449-452.

Overbeek JThG (1952). IV. Electrochemistry of the double layer and V. Electrokinetic phenomena. In: Kruyt HR (ed) Colloid science, vol I, irreversible systems. Elsevier, Amsterdam, 115–243.

Panthulu T.V., Krishnaiah C. & Shirke J.M. (2000). Detection of seepage paths in earth dams using self-potential and electrical resistivity methods. Engineering Geology, 59, p. 281 – 295.

Parasnis D.S. (1997). Principles of applied geophysics. 5th ed. London: Chapman and Hall.

Perrier F., Petiau G., Clerc G., Bogorodsky V., Erkul E., Journiaux L., Lesmes D., Macnae J., Meunier J., Morgan D., Nascimento D., Oettinger G., Schwartz G., Toh H., Vailiant M., Vozoff K. & Yazici-Cakin O. (1997). A one-year systematic

study of electrodes for long period measurement of the electric field in geophysical environments: Journal of Geomagnetism and Geoelectricity, v. 49, p. 1677 – 1696.

Petiau G. & Dupis A. (1980). Noise temperature coefficient, and long-time stability of electrodes for telluric observations. Geophysical Prospecting, 28, p. 792 – 804.

Pettibone H.C., and Kealy C.D. (1971). Engineering properties of mine tailings. Journal of the Soil Mechanics and Foundations Division, ASCE, Vol. 97, p. 1207 – 1225.

Pourbaix M.J.N. (1949). Themodynamics of dilute aqueous solutions. E. Arnold and Co.

Powers M.C. (1953). A new roundness scale for sedimentary particles. Journal of Sedimentary Petrology, Vol 23, No. 2, p. 117 – 119.

Prigogine I. (1955). Thermodynamics of irreversible processes. Charles C. Thomas, Publisher.

Raj B. & Jha B.B. (1994). Fundamentals of acoustic emission. British Journal of NDT, 36, No. 1, p. 16 – 23.

Rao B.S.R., Murthy I.V.R. & Reddy S.J. (1970). Interpretation of self-potential anomalies of some geometric bodies. Pure Appl. Geophys., 78, p. 66 – 77.

Reddi L.N. & Kakuturu S.P. (2004). Self-healing of concentrated leaks at core-filter interfaces in earth dams. *Geotechnical Testing Journal*, Vol. 27, No. 1, p. 89 – 98.

Revil A., Pezard P.A. and Glover P.W. (1999a). Streaming potential in porous media 1. Theory of the zeta potential. Journal of Geophysical Research, 104:20021–20031.

Revil A., Schwaeger H., Cathles L.M., Manhardt P.D. (1999b). Streaming potential in porous media, 2. Theory and application to geothermal systems. Journal of Geophysical Research, 104: 20033–20048.

Rozycki, A.,Ruiz Fonticiella, J.M., Cuadra, A. (2006). Detection and evaluation of horizontal fractures in earth dams using the self-potential method. Engineering Geology, 82, 145– 153.

Sasitharan S., Sheffer M. & Gaffran P. (2001). An investigation of streaming potential and its application to earthfill dams. Proceedings – Canadian Dam Association 2001 Annual Conference, Fredericton, Canada, p. 135 – 142.

Sato M. & Mooney H.M. (1960). The electrochemical mechanism of sulphide selfpotentials. Geophysics 25, p. 226 – 249.

Schiffman R.L., Vick S.G., and Gibson R.E. (1988). Behavior and properties of hydraulic fills. In Hydraulic Fill Structures, ASCE, p. 166 – 202.

Sharma P.V. (1997). Environmental and engineering geophysics. Cambridge University Press.

Sheffer M. & Howie J.A. (2001). Imaging subsurface seepage conditions through the modelling of streaming potential. Proceedings of 54th Canadian Geotechnical Conference, Calgary, p. 1094 – 1101.

Sheffer M. & Howie J.A. (2003). A numerical modelling procedure for the study of the streaming potential phenomenon in embankment dams. Proceedings – Symposium on the Application od Geophysics to Engineering and Environmental Problems, San Antonio, p. 475 – 487.

Sheffer M. (2002). Response of the self-potential method to changing seepage conditions in embankment dams (M. Sc. Thesis). Department of Civil Engineering, University of British Colombia.

Sherard J.L. & Dunnigan L.P. (1985). L.P. filters and leakage control, in Seepage and Leakage from Dams and Impoundments. ASCE Geotechnical Engineering Division.

Sherard J.L., Dunnigan L.P. & Talbot R.T. (1984a). Basic properties of sand and gravel filters. *JASCE Geotechnical Engineering,* Vol. 110, No. 6.

Sherard J.L., Dunnigan L.P. & Talbot R.T. (1984b). Filters for silts and clays. *JASCE Geotechnical Engineering*, Vol. 10, No. 6.

Sherard J.L., Dunnigan L.P., & Talbot J.R. (1984). "Filters for Silts and Clays," *ASCE Journal of Geotechnical Engineering,* Vol. 110, No. 6, p.701 – 718.

Sherard, J.L. & Dunnigan, L.P., (1989). "Critical Filters for Impervious Soils," *ASCE Journal of Geotechnical Engineering*, Vol. 115, No. 7, p. 927 – 947.

Shuey R. (1975). Developments in Economic Geology, 4, Semiconducting Ore Minerals, Elsevier, Amsterdam, 145 and 251.

Sill R.W. (1983). Self-potential modeling from primary flows. Geophysics, 48: p 76–86.

Sill W.R. & Killpack T.J. (1982). SPXCPL: Two-dimensional modelling program of self-potential effects from cross-coupled fluid and heat flow (User's guide and documentation for version 1.0). Report DOE/ID/12079-60 ESL-74. Earth Sciences Laboratory, University of Utah.

Sjödahl P. (2006). Resistivity investigation and monitoring for detection of internal erosion and anomalous seepage in embankment dams. Doctorial Thesis at Lund University, Sweden.

Sjödahl P., Dahlin T. & Johansson S. (2003). Resistivity monitoring for leakage detection at Hällby embankment dam. Procs. 9th Meeting Environmental and Engineering Geophysics, 31 August-4 September 2003, Prague, Czech Republic, p 4

Sjödahl P., Dahlin T. & Johansson S. (2004). Resistivity monitoring for internal erosion detection at Hällby embankment dam. Procs. International Conference on Environment and Engineering Geophysics, June 6-11 2004, Wuhan, China: p. 310 – 316.

Stern W. (1945). Relation between spontaneous polarization curves and depth, size, and dip of ore bodies. Trans. Am. Inst. Min., Metallurg., Petr. Eng., 164, p. 189 – 196.

Stewart M. & Parker J. (1992). Localization and seasonal variation of recharge in a covered karst aquifer system, Florida, USA. In: Back W, Herman JS, Paloc H

(eds) Hydrogeology of selected karst regions. Int Assoc Hydrogeol 13, p. 443 – 460.

Stewart R.A. & Watts B.D. (2000). The WAC Bennett Dam sinkhole incident. Proceedings of the 53rd Canadian Geotechnical Conference, Montreal, Quebec, Canada.

Stumm W. (1992). Chemistry of the solid-water interface: processes at the mineral water and particle-water interface in natural systems. New York: Wiley Interscience.

Stumm, W., Morgan, J.J., 1981. Aquatic Chemistry: An Introduction Emphasizing Chemical Equilibria in Natural Waters. John Wiley & Sons, New York.

Telford W.M., Geldart L.P., Sheriff R.E. & Keys D.A. (1976). Applied geophysics. Cambridge University Press.

Terzaghi K. (1922). "Der Grundbruch an Stauwerken und seine Verhutung (The Failure of Dams by Piping and Its Prevention)," Die Wasserkraft, Vol. 17, p. 445 – 449.

Timm, F. & Möller, P. (2001). The relation between electric and redox potential: Evidence from laboratory and field measurements. Journal of Geochemical exploration, 72, p. 115 – 128.

Titov K., Loukhmanov V. & Potapov A. (2000). Monitoring of water seepage from a reservoir using resistivity and self polarization methods: case history of the Petergoph fountain water supply system. First Break, 18.10, p. 431 – 435.

Truesdail SE, Westermann-Clark GB, Shah DO (1998). Apparatus for streaming potential measurements on granular filter media. Journal of Environmental Engineerin, 124: 1228–1232.

UNEP (1996). "United Nations Environment Programme. – *Tailings Dam Incidents 1980-1996*," a report by Mining Journal Research Services, UK, May.

USBR (1994). "Protective Filters," *Design Standards – Embankment Dams*, No. 13, Chapter 5, U.S. Bureau of Reclamation.

USCOLD (1994). *Tailings dam incidents*. U.S. Committee on Large Dams.

USSCS (1994). "Gradient Design of Sand and Gravel Filters," National Engineering Handbook, Part 633, Chapter 26, U.S. Soil Conservation Service.

Vagshal, D.S., and Belyaev, S.D. (2001). Self-potential anomalies in Cerro de Pasco and Hualgayoc areas (Peru) revisited, Geophysical Prospecting Vol. 49 (1), p. 151 – 154.

Vaughan P. R. & Soares H. F. (1982). "Design of Filters for Clay Cores of Dams," *ASCE Journal of Geotechnical Engineering Division*, Vol. 108, No. 1, p. 17 – 31.

Vick S.G. (1983). Planning, Design and Analysis of Tailings Dams. BiTech Publishers Ltd.

Vick S.G. (1997). Failure of the Omai tailings dam. *Geotechnical News*, Vol. 14, No 3, p. 34 – 40.

Vick S.G. (1997). Failure of the Omai tailings dam: closure. *Geotechnical News*, Vol. 15, No 1, p. 49 – 55.

Volpe R.L. (1979). Physical and engineering properties of copper tailings. In Current Geotechnical Practice in Mine Waste Disposal, ASCE, p. 242 – 260.

Wanfang Z., Beck B.F. & Stephenson J.B. (1999). Investigation of groundwater flow in karst areas using component separation if natural potential measurements. Environmental Geology 37 (1), p. 19 – 25.

Ward, S. (1990). "Resistivity and induced-polarization methods." Geotechnical and Environmental Geophysics, Vol. I , S. Ward, ed., 147-190.

Wilt M.J. & Convin R.F. (1989). Numerical modeling of self-potential anomalies due to leaky dams: model and field examples: Lecture notes in earth sciences, Vol. 27, G.P. Merkler et al., eds., Springer-Verlag, Berlin, p. 73 – 89.

WISE (2006). "Chronology of Major Tailings Dam Failures" WISE Uranium Project, internet access.

Wurmstich B. & Morgan F.D. (1994). Modeling of streaming potential responses caused by oil well pumping: Geophysics, v. 59, no. 1, p. 46 – 56.

Wurmstich B. (1995). 3-D self-consistent modeling of streaming potential responses: theory andfeasibility of applications in earth sciences: Ph.D. thesis, Texas A&M University.

Wurrnstich B., Morgan F.D., Merkler G.P. & Lytton R.L. (1991). Finite element modeling of streaming potentials due to seepage: study of a dam: Expanded techcal program abstracts, Soc. Explor. Geophysicists annual meeting.

Yeung, A. T. (1990). Coupled flow equations for water, electricity and ionic contaminants through clayey soils under hydraulic, electrical and chemical gradients, Journal of Non-Equilibrium Thermodynamics, Vol.15, No.3, 247-267.

Yeung, A.T. and Mitchell, J.K. (1993). Coupled fluid, electrical and chemical flows in soil. Géotechnique, 43: 121–134.